Drivers of the marine CO_2 system in the High Arctic

- from the deep basins to the shallow fjords

Ylva Ericson

Thesis for the Degree of Philosophiae Doctor (PhD)
University of Bergen, Norway
2019

UNIVERSITY OF BERGEN

Drivers of the marine CO_2 system in the High Arctic

- from the deep basins to the shallow fjords

Ylva Ericson

Thesis for the Degree of Philosophiae Doctor (PhD)
at the University of Bergen

Date of defence: 20.02 2019

Year: 2019

Title: Drivers of the marine CO_2 system in the High Arctic

Name: Ylva Ericson

Print: Skipnes Kommunikasjon / University of Bergen

Drivers of the marine CO_2 system in the High Arctic - from the deep basins to the shallow fjords

Ylva Ericson

Geophysical Institute, Faculty of Mathematics and Natural Sciences, University of Bergen, Bergen, Norway

in cooperation with

UNIS

Department of Arctic Geophysics, The University Centre in Svalbard, Longyearbyen, Norway

Acknowledgements

None of this would be without my family, friends, colleagues, and course mates that have brought me so much joy, but also help, throughout this time. There are no words to cover the gratitude that I feel and there are more of you than I can write down on a few pages.

Like a fly drawn to the light, I have been drawn to CO_2 and the isolated areas of the North and South, for as long as I can remember. My deepest thanks go to Eva Falck and Melissa Chierici, for this beyond amazing opportunity, for your kindness and your patience, and for all the wise guidance and help you have given me on the way. A very big thank you to Agneta Fransson for help with the Isfjorden papers! Following up on these papers, a thank you also goes to Svein Kristianssen and Elizabeth Jones.

The Arctic adventure started many years ago, when Leif G. Anderson took a leap of faith and sent me on a long journey north. Leif, I will be for ever grateful for this and everything else that followed. Thank you also to the wonderful marine chemistry people that at least once worked at the University of Gothenburg.

One of the greatest joys over these years has been to work at sea where I have met so many amazing people, on the big boats (Polarstern, Oden, Helmer Hansen, Håkon Mosby, and Lance), as well as on the small boats (UNIS Polaris and Viking Explorer). Thank you ALL of you for all the help and all the fun!

A special thank you, for help with the fieldwork in Svalbard, to: Lars Frode Stangeland, Marcos Porcires, Helene Lødemel Hodal, Ragnheid Skogseth, Katie Herlingshaw, Pål Gunnar Ellingsen, Agnieszka Kalinowska, Carmen Clausbruckner, Anna Vader, Tove Gabrielsen, Janne Søreide, Stuart Thomson, Lene Lund, Maja Hattleback, Lauris Boissonnot, the staff at the Tech and Logistics department, and students at the AGF-214 and AGF-352/852 courses.

The always changing AGF department at UNIS must be the friendliest working place a human being can find in this world. I will miss ALL of you and I feel very lucky to have enjoyed your company over these years. Thank you so much for just being you and also for all the help you have given along the way. Special thanks to Marika for reading the draft in the last minutes. Also, lots of thank yous to Siiri and Eli Anne for being my ACSI-family here on Svalbard.

When the Svalbard days are filled with heavy clouds, the sun always shines somewhere within the UNIS walls, so thank you to all my colleagues at UNIS for brightening my days (like playing guitar with you Lena), and all other amazing people that walk the hallways of Forskningsparken (like having tea with you Cecilia). A special thank you to Idun, for hundreds of walks filled with beautiful dreams and talks.

I also wish to send lots of love and gratitude to Christina, Elin & Jörgen, Hanna & Thomas + Flora & Hedvig (yes, you kept my spirit up just by being you), Håkan & Åsa, Josefin, and Kajsa.

How come I have such a lovely family, so far beyond what I could ever imagine? What can I say? I cannot thank you enough.

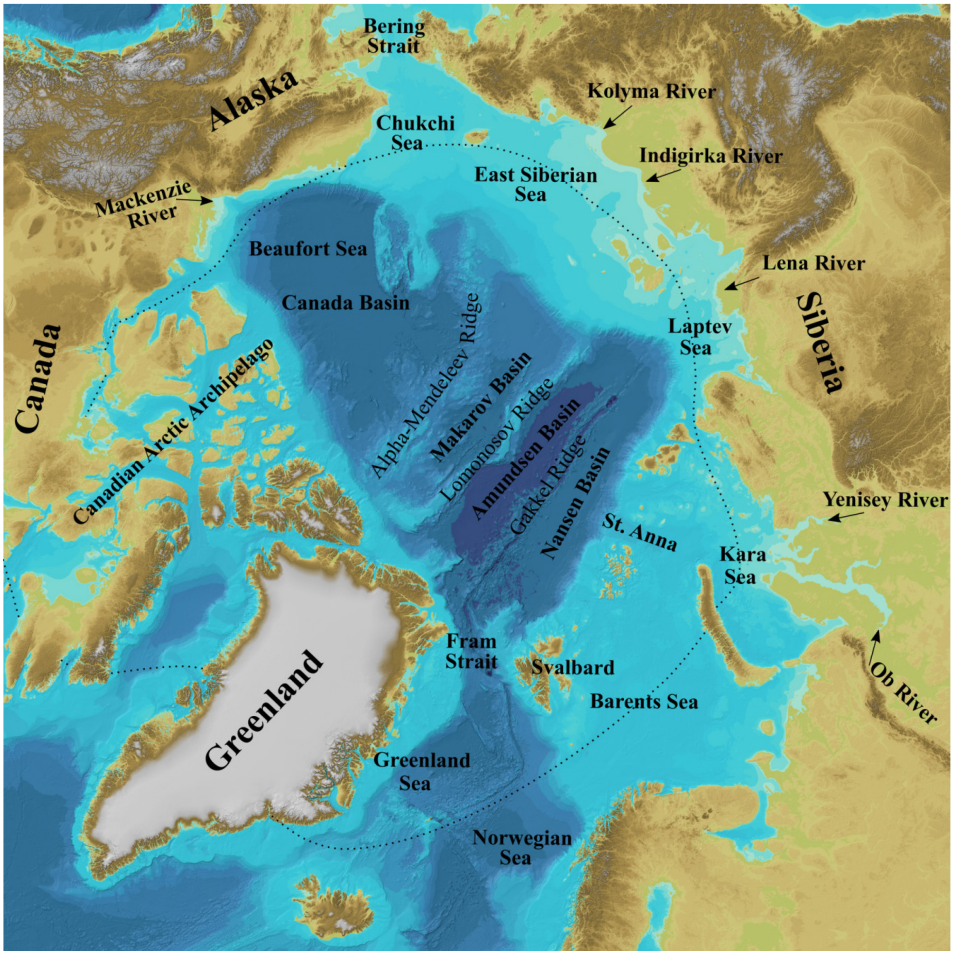

Fig. 1. The area north of the dotted line is the High Arctic (following AMAP, 2018; IBCAO version 3.0, Jakobsson et al., 2012)

Introduction

This story started some years ago, further north in what we call the central Arctic Ocean, during a crossing of the deep Arctic basins that were once predominantly covered in multiyear sea ice, passing over the huge ridges of Gakkel, Lomonosov, and Alpha-Mendeleev (Fig. 1). Far below the surface, at depths of hundreds of meters where we find water masses that are of Atlantic origin, we could see a peak in the total dissolved inorganic carbon profiles, which was not there 20 years earlier. How could such a remote and largely ice-covered place provide such an effective storage of carbon? Where did the carbon come from and why did the accumulation of carbon differ between the Arctic basins? Finally, what will happen in the coming years as the Arctic Ocean continues its transformation from an ice-capped ocean to a seasonally open one?

Some of the answers to these questions relate to the journey that the Atlantic Water takes on before it becomes part of the High Arctic where anthropogenic CO_2 has been absorbed at its surface. Some answers reflect the circulation and ventilation of the Arctic Ocean, whereas others relate to the biogeochemical factories that the Arctic shelf seas and their coastal extensions are. Some answers focus on how the Arctic carbon cycle will respond to progressing climate change and ocean acidification.

The longing to better comprehend this type of carbon mysteries has been the motivation for this thesis. The setting above became the foundation of Paper I, but this is also a journey that travels down the scale both in time and space, from the big deep Arctic basins to the shallow micro-versions of the Arctic Ocean that Arctic fjords to some extent are. While Paper II traces biogeochemically transformed waters from one of the Arctic shelf seas into the deep Arctic Ocean and out through Fram Strait, Papers III-V investigate seasonal drivers of the marine carbon cycle in a High Arctic fjord system (Isfjorden, Svalbard).

Abstract

The High Arctic is largely undersampled in terms of marine CO_2 system data due to the cold dark season and often an extensive sea ice cover. The current understanding of the Arctic carbon cycle is thus vulnerable to both the spatial distribution and the timing of the data that so far exist. The fact that the Arctic is in transition due to the Arctic Amplification of climate change, makes it the more important to fill the knowledge gaps on the carbon cycle that prevail. This thesis is not only an attempt to add data to the existing pool of measurements, but also an investigation of processes that drive changes in the marine CO_2 system. The uptake of anthropogenic carbon (C_{ant}) from the atmosphere and the subsequent storage thereof, do not always occur in the same region. The C_{ant} load in the Atlantic Water that flows into the central Arctic Ocean likely explains observed trends of increasing total dissolved inorganic carbon of 0.4-0.9 μmol kg^{-1} yr^{-1} at the intermediate depths of the deep Arctic basins. Further up in the water column at depths between 50 to150 m, the signature of organic decay products that originates from the bottom of the river-influenced East Siberian Sea can be traced all the way to the Fram Strait. This rather fresh water type is undersaturated in the calcium carbonate minerals aragonite and calcite and can therefore have negative consequences for shell-building calcifying marine organisms. In Adventfjorden, a fjord branch of the Isfjorden system that is situated on the West Spitsbergen coast, the thermodynamic driving force of the air-sea CO_2 flux was mainly governed by biological processes and temperature changes. This likely reflects the absence of sea ice that has prevailed over the last couple of years. The air-sea CO_2 uptake of 31-36 g C m^{-2} yr^{-1} largely balanced the combined effects of primary production and respiration over the annual cycle. Also, the saturation state of aragonite was controlled by biological activity. In the glacier-influenced neighbouring fjord branch, Tempelfjorden, the freshwater discharge accounted for about 25% of the air-sea CO_2 uptake over the melt season. The freshwater discharge decreased the aragonite saturation state, but at least a freshwater fraction larger than 50% (lower range of uncertainty) was needed for the water to become undersaturated in the mineral.

List of publications

Ericson, Y., Ulfsbo, U., van Heuven, S., Kattner, G., & Anderson, L.G. (2014), Increasing carbon inventory of the intermediate layers of the Arctic Ocean, *J. Geophys. Res. Oceans*, 119, 2312-2326. doi:10.1002/2013JC009514

Anderson, L.G., Ek, J., Ericson, Y., Humborg, C., Semiletov, I., Sundbom, M., & Ulfsbo, A. (2017), Export of calcium carbonate corrosive waters from the East Siberian Sea, *Biogeosciences*, 14, 1811-1823. doi:10.5194/bg-14-1811-2017

Ericson, Y., Falck, E., Chierici, M., Fransson, A., Kristiansen, S., Platt, S.M., Hermansen, O., & Myhre, C.L. (2018), Temporal variability in surface water pCO_2 in Adventfjorden (West Spitsbergen) with emphasis on physical and biogeochemical drivers, *J. Geophys. Res. Oceans*, 123. https://doi.org/10.1029/2018JC014073

Ericson, Y., Chierici, M., Falck, E., Fransson, A., Jones, E., & Kristiansen, S. (2018), Seasonal dynamics of the marine CO_2 system in Adventfjorden, a West Spitsbergen fjord, revised for *Polar Research*.

Ericson, Y., Falck, E., Chierici, M., Fransson, A., & Kristiansen, S. (2018), Marine CO_2 system variability in a high Arctic tidewater-glacier fjord system, Tempelfjorden, Svalbard, submitted to *Continental Shelf Research*.

Contents

1. Aim of the study

The overarching driving force behind this thesis has been to 1) investigate the current state of the marine CO_2 system in different parts of the High Arctic, and 2) to determine key drivers of the system in these areas. To achieve this goal, a fundamental part of the project has been to collect data in areas that are rarely sampled, at least not in a high enough spatiotemporal resolution to reveal the natural variability in the Arctic marine systems or the variability that result from environmental and climate change.

A special attention is given to different aspects of the air-sea CO_2 exchange. Both basin-scale decadal changes in the dissolved inorganic carbon due to anthropogenic CO_2 uptake (Paper I) as well as local-scale seasonal and annual air-sea CO_2 fluxes are covered (Papers III-V). In line with this follow evaluations of processes that control the surface water partial pressure of CO_2 (pCO_2, Papers III and V), which will reveal the local drivers of the thermodynamic driving potential of the air-sea CO_2 exchange.

The uptake of anthropogenic CO_2 has resulted in shifts in the seawater acid-base systems, commonly referred to as ocean acidification (OA). OA has not only reduced the oceanic pH, but also the saturation states of the calcium carbonate minerals aragonite (Ω_{Ar}) and calcite (Ω_{Ca}). The natural variability in Ω is investigated in Papers II, IV, and V to elucidate the sensitivity of the High Arctic to ongoing and future OA and other environmental changes.

Central processes in all papers are the production and decay of organic matter, and also in Papers II-V the effects of freshwater discharges on the marine CO_2 system.

2. Background

CO_2 has become the most notorious gas in modern times. While it contributes with only 0.04% of the gases in the atmosphere compared to the 78% and 21% of nitrogen and oxygen, respectively (i.e. for dry air), its rising star as a news magnet is a result of essentially three things: 1) its increase in the atmosphere by 45% since 1750, from about 277 to more than 403 ppm as of today, due to especially fossil fuel combustion (67%), land-use changes (31%) and cement production (less than 3%, Global Carbon Project, 2018), 2) its ability to absorb and emit infrared light thereby increasing the heat content in the troposphere, which has consequences for the heat balance and climate of this planet, and 3) its extraordinary capability to dissolve in seawater due to a series of equilibrium reactions, with resultant changes in the global ocean's pH and consequently the chemical environment of all marine organisms.

To put the amount of released CO_2 from the human-induced, i.e. anthropogenic, sources, into a context. Between 1750 and 2011 approximately 555 Pg of anthropogenic carbon was emitted (IPCC, 2013). This is close to the amount of carbon that was stored in the pre-industrial atmosphere of about 590 Pg (Sarmiento & Gruber, 2006). The atmospheric CO_2 concentration has however far from doubled, which is a result of CO_2 uptake by terrestrial ecosystems (about 160 PgC) and CO_2 uptake by the ocean (about 155 PgC) (IPCC, 2013). Still, the fraction of anthropogenic CO_2 that has accumulated in the atmosphere has increased the global surface temperature by 1°C compared to pre-industrial levels (IPCC, 2018). The warming has been especially pronounced in the Arctic (e.g. Overland et al., 2016), a phenomenon known as the Arctic Amplification, with subsequent changes in several aspects of the Arctic environmental systems including sea ice loss (Vaughan et al., 2013). The sink that is provided by the ocean mitigates the effects of anthropogenic CO_2 on the climate, but it has also resulted in a decreased surface ocean pH by 0.1 units (Rhein et al., 2013). The changes in the marine acid-base systems that result from the absorption of anthropogenic CO_2 (i.e. denoted as C_{ant}) are referred to as ocean acidification (OA, e.g. Doney et al., 2009). Model projections suggest that the

oceanic surface pH will decrease by another 0.1 to 0.3 units by the end of this century, with the severest changes expected to occur in the Arctic (Ciais et al., 2013).

To say it the least, CO_2 is an interesting gas that plays a fundamental part in the global carbon cycle and climate as it is transformed within and exchanged between the three key carbon reservoirs, i.e. the atmosphere, the terrestrial biosphere, and the ocean, that have exchange rates that are fast enough to fluctuate considerably over the human life span (Sabine & Tanhua, 2010). Still, to comprehend the consequences of our human-induced changes on the global carbon cycle and its coupling to the climate system with complex feedback loops, there are several knowledge gaps to be filled. One of these gaps relates to the carbon cycle of the Arctic and the High Arctic is therefore the setting of this thesis. The protagonist of this story is a complex chemical system, known as the marine CO_2 system also referred to as the marine carbonate system.

2.1 The Arctic carbon cycle

Carbon is a ubiquitous element on the planet that is transformed over a wide range of oxidation states (from +IV to –IV) through various chemical reactions. This allows for unceasing fluxes of carbon between the atmosphere, the terrestrial biosphere, the hydrosphere (i.e. mainly the ocean), and the lithosphere, that together make up the system that we know as the carbon cycle. The area that contributes to the Arctic carbon cycle is vast and includes not only the Arctic Ocean with its marginal seas in itself, but also the surrounding catchment and permafrost areas on land (McGuire et al., 2009). The key actors in the Arctic carbon cycle are the Arctic terrestrial and oceanic carbon stocks and the exchanges of CO_2, methane (CH_4), dissolved inorganic carbon (DIC), dissolved organic carbon (DOC), particulate inorganic carbon (PIC), and particulate organic carbon (POC) between the Arctic land, ocean, and atmosphere including the exchanges with the adjacent Pacific and Atlantic Oceans (Fig. 2, McGuire et al., 2009).

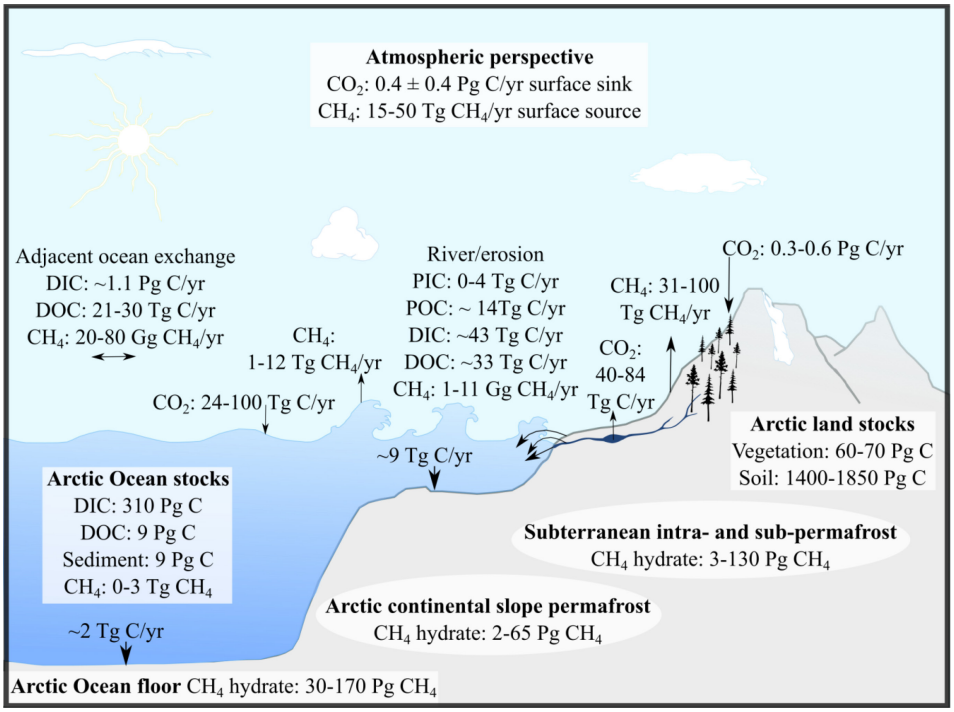

Fig. 2. The Arctic carbon cycle. Source: redrawn after McGuire et al. (2009). Be aware that these values are dependent on how the Arctic is defined and not necessarily directly comparable to other estimates.

From an oceanic perspective, the cycling is governed by the exchanges of carbon with the surrounding seas, but substantial amounts of carbon are also released from coastal areas through fluvial transports and coastal erosion (McGuire et al., 2009). Despite its 1% of the world's ocean volume, the Arctic Ocean receives 11% and 10% of the global runoff and terrigenous DOC load, respectively (McGuire et al., 2009). The ongoing environmental and climate change have resulted in increased runoff (Peterson et al., 2002; Haine et al., 2015), as well as in increased coastal erosion at different sites in the Arctic (e.g. Mars & Houseknecht, 2007; Barnhart et al., 2014; Günther et al., 2015) in recent years.

In general, the Arctic Ocean is considered to be a net sink of atmospheric CO_2 (Fig. 2). It is especially the shelf seas and coastal areas that have significantly large fluxes, although the magnitude and direction of these fluxes vary considerably both

seasonally as well as spatially (e.g. Semiletov et al., 2007; Pipko et al., 2011; Else et al., 2011; Evans et al., 2015; Yasunaka et al., 2016; Pipko et al., 2017). The air-sea CO_2 exchange is largely affected by the sea ice that covers about 6 to $15x10^6$ km^2 of the Arctic over the annual cycle (Vaughan et al., 2013). In the past, the sea ice was considered to block the air-sea gas transfer, but several investigations over the last decades have shown that the sea ice is involved in the transfer to some degree (e.g. Rysgaard et al., 2011; Butterworth & Else, 2018). The annual Arctic sea ice extent decreased between 1979 and 2012 by around 4% per decade and the thickness decreased by 1 to 2 m (i.e. between 1980 and 2008, Vaughan et al., 2013). If the greenhouse gas emissions continue to be high in the coming years, the Arctic Ocean is projected to become an open sea in September already by the mid-century or even earlier (i.e. for the representative concentration pathway scenario 8.5, Kirtman et al., 2013). This will have consequences for the air-sea CO_2 exchange as the surface waters become more exposed to the atmosphere. The oceanic absorption of CO_2 may increase since the surface waters of the central Arctic Ocean are largely undersaturated in CO_2 (e.g. Bates & Mathis, 2009; Jutterström & Anderson, 2010; Yasunaka et al., 2016), but the future size of this potentially increased sink is debated.

2.2 The marine CO_2 system

The marine CO_2 system is the key buffer system that regulates the oceans pH (Zeebe & Gladrow, 2001). It has been thoroughly explained in several contributions including those of Zeebe and Wolf-Gladrow (2001), Sarmiento and Gruber (2006), and Dickson et al. (2007). Although, its components may be few, its behaviour is complex and governed by a series of equilibrium reactions (Fig. 3).

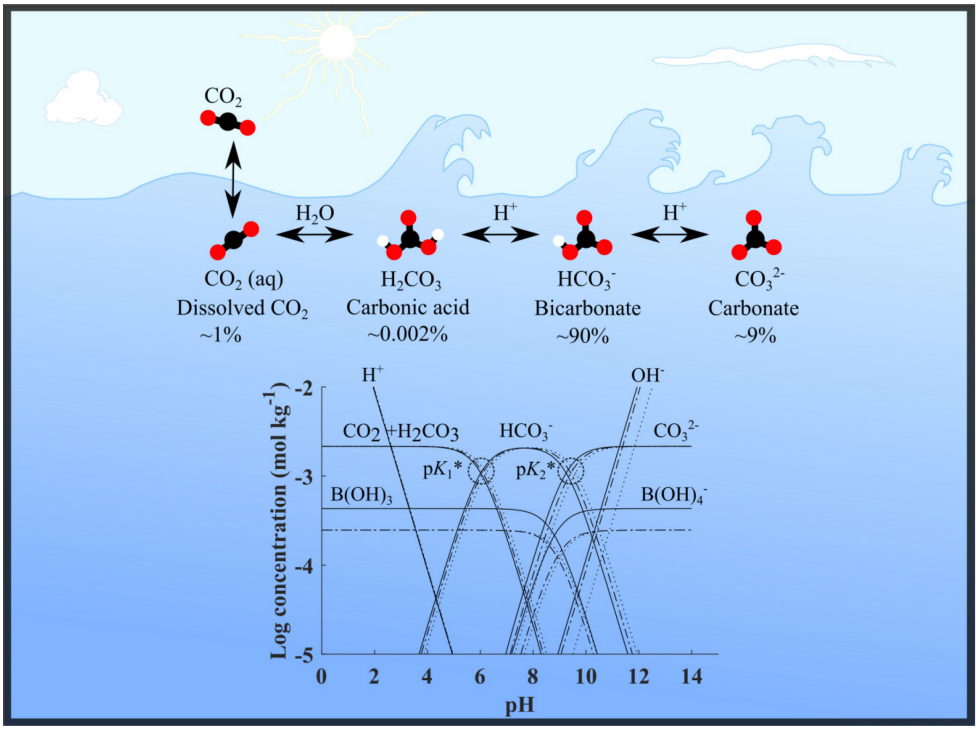

Fig. 3. Illustration of the marine CO_2 system. Air-sea CO_2 exchange is controlled by the equilibration between the atmospheric and oceanic CO_2 pools. In seawater, dissolved CO_2 is governed by a series of equilibrium reactions that determine the speciation between dissolved CO_2, carbonic acid, bicarbonate and carbonate ions. Relative contributions are from van Heuven (2013). The Bjerrum plot shows the speciation of the marine CO_2 system for DIC = 2160 µmol kg^{-1}. The solid line is calculated for a salinity = 34.9 and a temperature = 8°C, i.e. values of warm Atlantic Water in the Svalbard area in the summer. The dashed line shows how a decreased salinity (S = 20), i.e. due to melt water discharge, shifts the negative logarithms of the dissociation constants of carbonic acid, pK_1^* and pK_2^*, to higher values. Note that this example excludes the effect of dilution on DIC. The dotted line shows for the freshened water (i.e. S = 20) how pK_1^* and pK_2^* also are shifted to higher values when the water is cooled to -1°C. Be aware, it is pH that depends on the relative proportions of the dissolved inorganic carbon species and not the other way round, as pointed out by Zeebe and Gladrow (2001). Source: modified to Svalbard conditions and redrawn after Zeebe and Gladrow (2001).

First of all, the gaseous CO_2 equilibrates thermodynamically with the dissolved CO_2 in the ocean:

$$CO_2(g) \leftrightarrow CO_2(aq) \quad (1)$$

It takes about a year for the equilibration of this exchange between the global surface ocean and atmosphere to be achieved (Sabine & Tanhua, 2010). Hence, the annual CO_2 increase rate in the global surface ocean largely follows that of the atmosphere (Takahashi et al., 2009). The equilibration can, however, be achieved at a quicker pace locally. For a 20 m mixed layer depth in an Arctic fjord, the equilibration timescale, which for a non-reactive gas is equal to the mixed layer depth divided by the air-sea gas transfer velocity, would be nearly half a year (i.e. about 174 days for a gas transfer velocity of 9.6 cm hr^{-1} for 8°C according to Wanninkhof, 2014, using the global mean wind speed of 7.3 m s^{-1}). Still, this is a very long time in comparison to the corresponding timescale for oxygen of about 8 days (same conditions as for CO_2 but with a gas transfer velocity of 10.3 cm hr^{-1} according to Wanninkhof, 2014). The reason for this difference is that within the ocean, the dissolved pool of CO_2 is governed by the equilibrium reactions of the acid-base system of carbonic acid (H_2CO_3), which include the bicarbonate (HCO_3^-), carbonate (CO_3^{2-}), and hydrogen (H^+) ions:

$$CO_2(aq) + H_2O(l) \leftrightarrow H_2CO_3(aq) \leftrightarrow H^+(aq) + HCO_3^-(aq) \leftrightarrow 2H^+(aq) + CO_3^{2-}(aq) \quad (2)$$

The equilibria show how aqueous CO_2 reacts with water and forms H_2CO_3, which firstly dissociates into HCO_3^-, and secondly dissociates into CO_3^{2-}. However, be aware that these equilibria, which are governed by the energy of the system, are not equivalent to the actual reaction pathways that occur in the ocean (Zeebe & Wolf-Gladrow, 2001). More importantly, they govern the concentrations of the different forms of dissolved inorganic carbon. The sum of these concentrations is referred to as total dissolved inorganic carbon:

$$DIC \equiv [CO_2(aq)] + [H_2CO_3] + [HCO_3^-] + [CO_3^{2-}] \quad (3)$$

Here denoted as DIC, but also the denotations: TCO_2, C_T, and $\sum CO_2$ can be found in the literature (Zeebe & Wolf-Gladrow, 2001). The $[H_2CO_3]$ constitutes a very small fraction of the DIC (i.e. about 0.002%, van Heuven, 2013). Since it is also hard to

analytically separate between the [H_2CO_3] and the [CO_2(aq)] (Dickson et al., 2007), of which the latter constitutes about 1% (van Heuven, 2013) or less of the DIC, the two concentrations are typically combined to the concentration of the imaginary species CO_2*(aq). Roughly 1 of 20 molecules that dissolve in seawater will remain as CO_2*, which explains the comparatively long equilibration timescale for air-sea CO_2 exchange (Sarmiento & Gruber, 2006). Using CO_2* instead, the equilibrium reactions in Eq. 2 are simplified to:

$$CO_2^*(aq) + H_2O(l) \overset{K_1}{\leftrightarrow} H^+(aq) + HCO_3^-(aq) \overset{K_2}{\leftrightarrow} 2H^+(aq) + CO_3^{2-}(aq) \quad (4)$$

where K_1 and K_2 are the first and second dissociation constants of H_2CO_3, respectively. Additionally, the formation and dissolution of metal carbonate complexes, such as calcium carbonate ($CaCO_3$), affect the equilibria:

$$Ca^{2+}(aq) + CO_3^{2-}(aq) \leftrightarrow CaCO_3(s) \quad (5)$$

where Ca^{2+} is the calcium ion. Through the equilibrium relationships above a set of equations can be used to describe the marine CO_2 system. These equations are for practical reasons based on total concentrations (denoted by square brackets) and stoichiometric equilibrium constants (denoted by the *) instead of 'effective concentrations' (or activities). For water in equilibrium with gaseous CO_2, the [CO_2*] is determined by Henry's law:

$$[CO_2^*] = K_0 fCO_2 \quad (6)$$

where K_0 is the solubility coefficient of CO_2 in seawater and fCO_2 is the fugacity of CO_2. K_0 is typically estimated from salinity and temperature data (e.g. according to Weiss, 1974). The fugacity is closely related to the partial pressure of CO_2 (pCO_2, i.e. the product of the mole fraction of CO_2, xCO_2, and the total pressure of the gas mixture, p, at equilibrium), but takes into account the non-ideal behaviour of CO_2. For water masses found along the West Spitsbergen coast, the difference between the two is small, about 1 µatm.

The dissociation constants, K_1^* and K_2^*, are equal to the concentrations according to:

$$K_1^* = \frac{[\mathrm{HCO_3^-}][\mathrm{H^+}]}{[\mathrm{CO_2^*}]} \quad (7)$$

$$K_2^* = \frac{[\mathrm{CO_3^{2-}}][\mathrm{H^+}]}{[\mathrm{HCO_3^-}]} \quad (8)$$

The solubility product for water saturated in $CaCO_3$ (K_{sp}^*) is given by:

$$K_{sp}^* = [\mathrm{Ca^{2+}}][\mathrm{CO_3^{2-}}] \quad (9)$$

The stoichiometric constants above, which are dependent on the ionic strength, temperature, and pressure, can be calculated from salinity, temperature, and pressure data using empirical formulas (e.g. K_1^*, and K_2^* from Mehrbach et al., 1973 as refitted by Dickson & Millero, 1987; K_{sp}^* from Mucci, 1983; with additional pressure corrections).

Historically, it was not possible to measure either the $[HCO_3^-]$ or the $[CO_3^{2-}]$ directly, but both pH, which gives the $[H^+]$, and the xCO_2 of a gas in equilibrium with a seawater sample, were frequently measured. From the latter quantity, fCO_2 could be calculated and converted to $[CO_2^*]$ using Henry's law. With some additional information, however, any pair of the measurable parameters: DIC, total alkalinity (TA), fCO_2, and pH, were enough to calculate the concentrations of all the dissolved inorganic carbon species. Since the combination of pH and fCO_2 resulted in rather large uncertainties in the calculated quantities, other combinations of the four parameters were usually preferred. Nowadays, thanks to new procedures also the $[CO_3^{2-}]$ can be measured (e.g. Byrne & Yao, 2008; Patsavas et al., 2015), and combined with any of the other four quantities.

TA is an important parameter that is closely related to the marine CO_2 system. In essence it is a result of the charge imbalance between the conservative ions in seawater (Wolf-Gladrow et al., 2007). It has, however, typically been defined from an acid-base perspective that agrees with the titrimetric methods that have been used historically to determine TA (Dickson, 1981). The most precise definition was provided by Dickson in 1981 who expressed TA as a proton (H^+) deficit of seawater in relation to a chosen zero level of protons:

"*The total alkalinity of a natural water is thus defined as the number of moles of hydrogen ion equivalent to the excess of proton acceptors (bases formed from weak acids with a dissocation constant K ≤$10^{-4.5}$ at 25°C and zero ionic strength) over proton donors (acids with K >$10^{-4.5}$) in one kilogram of sample.*"

This definition results in the following mass balance equation (e.g. Dickson et al., 2007):

$$\mathrm{TA} = [\mathrm{HCO_3^-}] + 2[\mathrm{CO_3^{2-}}] + [\mathrm{B(OH)_4^-}] + [\mathrm{OH^-}] + [\mathrm{HPO_4^{2-}}] + 2[\mathrm{PO_4^{3-}}] + [\mathrm{SiO(OH)_3^-}] + [\mathrm{NH_3}] + [\mathrm{HS^-}] + \ldots - [\mathrm{H^+}]_\mathrm{F} - [\mathrm{HSO_4^-}] - [\mathrm{HF}] - [\mathrm{H_3PO_4}] - \ldots \approx [\mathrm{HCO_3^-}] + 2[\mathrm{CO_3^{2-}}] + [\mathrm{B(OH)_4^-}] + [\mathrm{OH^-}] - [\mathrm{H^+}] \quad (10)$$

which shows that it is especially HCO_3^- and CO_3^{2-} that contribute to the TA and hence the buffer capacity of seawater, with additional contributions also from borate ($B(OH)_4^-$) and hydroxide (OH^-). Equation 10 also shows that if TA is used to determine the marine CO_2 system, at least $[B(OH)_4^-]$ and $[OH^-]$ need to be accounted for. The contributions of the other bases in seawater (pH~8) are usually very small in comparison, but the contributions of the phosphate and silicate species, i.e. HPO_4^{2-}, PO_4^{3-} and $SiO(OH)_3^-$, are occasionally considered as well.

To fully solve the marine CO_2 system with the simplified version of TA, one more mass balance equation for the total boron concentration (TB, can be determined from salinity data according to Lee et al., 2010) is needed together with the dissociation constants of boric acid (K_B^*, e.g. after Dickson, 1990) and water (K_W^*, e.g. after Millero, 1995):

$$\mathrm{TB} = [\mathrm{B(OH)_3}] + [\mathrm{B(OH)_4^-}] \quad (11)$$

$$K_\mathrm{B}^* = [\mathrm{B(OH)_4^-}][\mathrm{H^+}]/[\mathrm{B(OH)_3}] \quad (12)$$

$$K_\mathrm{W}^* = [\mathrm{H^+}][\mathrm{OH^-}] \quad (13)$$

Of DIC, TA, fCO_2, pH, and CO_3^{2-} it is only the former two that obey linear mixing relationships. That makes them the ultimate pair to comprehend how different

processes will affect the speciation within the marine CO_2 system. As they vary the carbonate species and pH will be altered in accordance with the equilibrium conditions (Zeebe & Wolf-Gladrow, 2001). There are, however, processes that do affect the marine CO_2 system, without necessarily changing either DIC or TA. These processes typically affect the pressure and temperature dependent stability constants.

A final remark, the hydrogen ion concentration $[H^+]_F$ in Eq. 10 refers to the free hydrogen ion concentration. This is essentially the contribution from hydrate complexes, such as the hydronium ion (H_3O^+) and hydronium ions linked to other water molecules (e.g. the $H_9O_4^+$ unit), rather than the contribution from free H^+ (Zeebe & Wolf-Gladrow, 2001). $[H^+]$ on the other hand, which is used in many of the presented equations, represents in this thesis the pH scale dependent hydrogen ion concentration. Theoretically, pH is defined as the negative logarithm of the effective concentration, i.e. the activity (a), of hydrogen ions (or H_3O^+ and $H_9O_4^+$).

$$p\mathrm{H} = -\log a_{H^+} \tag{14}$$

It is, however, not possible to measure this quantity in seawater. Therefore, there are three commonly used pH scales: the free scale (F), the total scale (T), and the seawater scale (SWS):

$$\mathrm{pH_F} = -\log[\mathrm{H^+}]_\mathrm{F} \tag{15}$$

$$\mathrm{pH_T} = -\log([\mathrm{H^+}]_\mathrm{F} + [\mathrm{HSO_4^-}]) = -\log[\mathrm{H^+}]_\mathrm{T} \tag{16}$$

$$\mathrm{pH_{SWS}} = -\log([\mathrm{H^+}]_\mathrm{F} + [\mathrm{HSO_4^-}] + [\mathrm{HF}]) = -\log[\mathrm{H^+}]_\mathrm{SWS} \tag{17}$$

Note that the empirical formulas used to determine the different dissociation constants are derived for one of these pH scales. To convert between the scales, the mass balance equations for the total fluoride concentration (TF) and the total sulfate concentration (TS) have to be determined, together with the dissociation constants for hydrogen fluoride (K_F^*) and bisulfate (K_S^*):

$$\mathrm{TF} = [\mathrm{HF}] + [\mathrm{F^-}] \tag{18}$$

$$TS = [HSO_4^-] + [SO_4^{2-}] \quad (19)$$

$$K_F^* = [H^+]_F[F^-]/[HF] \quad (20)$$

$$K_S^* = [H^+]_F[SO_4^{2-}]/[HSO_4^-] \quad (21)$$

Through the hard work of marine chemists over the last 50 years (and earlier), also these quantities can be determined from empirical formulas. Even better, several software options exist, such as CO2SYS (Lewis & Wallace, 1998; van Heuven et al., 2011), that have incorporated not only the empirical formulas for the determination of the different stability constants and mass balance equations, but also functions to solve the marine CO_2 system as a whole for any chosen pair of DIC, TA, fCO_2 and pH. Still, it is important to keep in mind that these calculations assume that all existing acid-base species in seawater that contribute significantly to the seawater TA are accounted for. This assumption is not necessarily valid, at least not in some coastal environments that receive considerable amounts of terrestrial humic substances. Therefore, it is quite useful to measure at least three of the parameters: DIC, TA, fCO_2, pH, or $[CO_3^{2-}]$, to compare between measured and calculated quantities.

2.3 Analytical methods

This thesis is based on papers and manuscripts, which in turn are based on data that have been collected during thousands of hours spent at sea and in the laboratory. Seawater samples for the marine CO_2 system parameters (all papers), nutrients (all papers) and oxygen (Papers I and II) were generally collected from discrete depths using Niskin bottles. Sampling always included continuous water column conductivity, temperature, and depth (CTD)-measurements from which salinity can be derived.

Especially pH and TA (Papers I, III-V), but also DIC (Paper I) were measured by the author. The methods behind these measurements are briefly presented below. For

Papers II-V also nutrients were measured by the author to some extent. Details for these procedures can be found in the respective papers.

2.3.1 Determination of pH

Spectrophotometric measurements of seawater samples containing the pH-sensitive sulfonephthalein indicator *m*-cresol purple (*m*CP) were used to determine pH (Clayton & Byrne, 1993). The indicator exists in three forms – H_2I, HI^-, and I^{2-} – of which only the latter two have significant contributions at seawater pH. Therefore, the following equilibrium reaction dominates:

$$I^{2-} + H^+ \overset{K_1}{\leftrightarrow} HI^- \tag{22}$$

where K_1 is the formation constant and can be determined from temperature and salinity (Clayton & Byrne, 1993). The ratio of the indicator absorbance (A) at the two wavelengths of maximum absorption, i.e. 434 and 578 nm for HI^- and I^{2-}, respectively ($R = {}_{578}A/{}_{434}A$), and the molar absorptivity (ε) ratios of the two indicator species can be used together with K_1 to determine the pH:

$$\mathrm{pH} = logK_1 + log\left(\frac{R - e_1}{e_2 - Re_3}\right) \tag{23}$$

where $e_1 = {}_{578}\varepsilon_{HI}/{}_{434}\varepsilon_{HI}$, $e_2 = {}_{578}\varepsilon_{I}/{}_{434}\varepsilon_{HI}$, and $e_3 = {}_{434}\varepsilon_{I}/{}_{434}\varepsilon_{HI}$. The R value is corrected for the background absorbance measured at 730 nm. The obtained pH when using the method of Clayton and Byrne (1993) is given on the total scale. The addition of the indicator solution perturbs the sample pH slightly and this effect needs to be accounted for. This can be done in several ways, for instance according to Chierici et al. (1999). The precision of the method has typically been determined as the mean absolute difference for all duplicate analyses, which is about ±0.001. For a purified indicator batch, the accuracy of the method should reflect the accuracy of the empirical formula used to determine K_1. In this thesis, however, non-purified *m*CP batches have been used, which can introduce additional uncertainties in the data through impurities (e.g. Liu et al., 2011; Patsavas et al., 2013). Fortunately, for paper I the marine CO_2 system was overdetermined and the internal consistency of the data

set was evaluated. The two batches of *m*CP used for Papers III-V were tested on an inter-laboratory comparison in 2017 provided by the laboratory of A.G. Dickson, Scripps Institution of Oceanography, La Jolla, CA, USA. For both batches used, the measured pH was 0.005 units higher than the certified value of the inter-laboratory comparison samples, i.e. for the unknown samples with ambient pCO_2.

2.3.2 Determination of total alkalinity

TA was determined from non-purged open cell potentiometric titrations using dilute hydrochloric acid (0.05 M) with an ionic strength comparable to seawater. The potential of each sample was monitored using a pH sensitive electrode. Paper I used a non-modified Gran evaluation with a method described by Haraldsson et al. (1997). Papers III-V on the other hand, disregarding the open titration system, used a non-linear least square optimisation as outlined in DOE (1994). The precision, determined in the same way as for pH, is typically about 2 μmol kg^{-1}. The accuracy is ensured by routine measurements of Certified Reference Materials (CRM, purchased from A. Dickson, Scripps Institution of Oceanography, USA). The TA system used for papers III-V was also tested in the inter-laboratory comparison in 2017. The measured TA at the laboratory at the University Centre in Svalbard was less than 1 μmol kg^{-1} from the certified TA values of the inter-laboratory comparison samples.

2.3.3 Determination of total dissolved inorganic carbon

DIC was determined by a coulometric titration according to Johnson et al. (1985). A seawater sample with a known volume is acidified by phosphoric acid addition and purged by an inert carrier gas (N_2) to release all the dissolved inorganic carbon species in the form of CO_2. The gas is stripped from water vapour and brought to an electrochemical titration cell. The cathode compartment of the cell is filled with a solution of dimethylsulfoxide that contains ethanolamine and thymolphthalein. The CO_2 reacts with the ethanolamine thereby producing hydroxyethylcarbamic acid:

$$2CO_2 + 2NH_2(CH_2)_2OH \rightarrow 2HO(CH_2)_2NHCOOH \quad (24)$$

The dissociation of the hydroxyethylcarbamic acid causes a change in the pH of the solution and subsequently in the colour of the thymolphthalein indicator, from blue to

transparent, which raises the transmittance of the solution. This change is detected by an optical sensor, which triggers a coulometric titration where hydroxide ions are produced at the platinum cathode by reduction of H_2O:

$$2H_2O + 2e^- \rightarrow H_2 + 2OH^- \quad (25)$$

Simultaneously, at the anode compartment silver ions are produced through oxidation of the silver anode:

$$2Ag^0(s) \rightarrow 2Ag^+ + 2e^- \quad (26)$$

The hydroxide ions neutralize the produced acid:

$$2HO(CH_2)_2NHCOOH + 2OH^- \rightarrow 2H_2O + 2HO(CH_2)_2NHCOO^- \quad (27)$$

whereas the silver ions form complexes with iodide ions of the potassium iodide saturated anode compartment solution:

$$2Ag^+ + 4I^- \rightarrow 2AgI_2^- \quad (28)$$

The charge in coulombs needed to neutralize the acid produced, through the production of OH^-, is related to the amount of CO_2 in the seawater sample, which consequently gives the DIC of the sample.

The precision was determined by duplicate analysis, i.e. for Paper I about 4 μmol kg^{-1} or better, and the accuracy was set by the analysis of CRM.

3. Drivers of the marine CO_2 system

3.1 Physical processes

Advection and mixing

The advection of water parcels, including convection, and the mixing between different water types due to diffusive, concentration-gradient-dependent processes (the slow molecular diffusion and the speedier turbulence-driven eddy diffusion) and turbulence-driven entrainment, redistributes the chemical constituents of seawater and ventilates the ocean.

Temperature variability

As seawater is transported northwards to the Arctic, it is cooled. The cooling results in an increase in the solubility coefficient K_0. For a decrease in temperature of 1°C, the fCO_2 will decrease by approximately 4-5% (e.g. 4.23% in Takahashi et al., 1993; 4.54-4.59% in Paper III). Since it is the difference between the atmospheric fCO_2 and surface water fCO_2 that is the thermodynamic driving potential of air-sea CO_2 exchange, cooling will also affect this flux. The feature, where the surface water is transported into the high latitudes and subsequently cooled with resultant absorption of atmospheric CO_2, is referred to as the "solubility pump" (Sabine & Tanhua, 2010). The cooling of the water not only drives an uptake of CO_2, but it also increases the density of the water so that it may sink down into the ocean interior.

The dissociation constants, K_1^* and K_2^*, decrease for a decrease in temperature. This effect can be seen in the Bjerrum plot in Fig. 3, where the negative logarithms of K_1^* and K_2^*, i.e. pK_1^* and pK_2^*, respectively, are shifted to higher values. For West Spitsbergen conditions a cooling from 8°C to -1 will decrease the $[CO_2^*]$ and $[CO_3^{2-}]$ by a few μmol kg^{-1} in favour for the $[HCO_3^-]$. The decrease in temperature also increases the pH. This effect on pH can be approximated to $dpH/dT \approx -0.016°C^{-1}$ for smaller changes in temperature (i.e. <10°C, Millero, 2007).

Changes in freshwater content

Freshwater addition (precipitation, river runoff, glacial melt, or sea ice melt) or removal (evaporation or sea ice growth), dilutes or concentrates the salinity, DIC, and TA. Changes in the salinity, and consequently the ionic strength of the water, have a direct impact on the stability constants. A 1% decrease in salinity will decrease the fCO_2 by approximately 0.9% due to an increase in K_0 (i.e. for water masses found on the West Spitsbergen coast, Paper III). K_1^* and K_2^*, on the other hand, will decrease when salinity decreases (see Bjerrum plot in Fig. 3). As a result, the pH will increase (by about 0.01 for a change in salinity of 1 for typical Arctic or Atlantic Water) and the relative fractions of the dissolved inorganic carbon forms are shifted in favour for CO_3^{2-} (the increase is minor i.e. <0.5 µmol kg^{-1}). This, of course, only accounts for the change in salinity.

The changes in DIC and TA, which are simultaneous with the changes in salinity, will also affect the speciation of the marine CO_2 system. The extent of this effect depends on how the balance between DIC and TA is shifted, which ultimately depends on the contribution of DIC and TA of the freshwater source. Sea ice is a special case, which provides the ocean with rather fresh water as it melts and concentrated seawater as it is produced through the expulsion of brine (Rysgaard et al., 2007). The brine typically contains low TA:DIC ratios, which could reflect a net heterotrophic system within the brine pockets (Rysgaard et al., 2007) and/or the precipitation of the calcium carbonate mineral ikaite (Dieckmann et al., 2010). The sea ice melt on the other hand contains comparatively high TA:DIC ratios, which may result from a net autotrophic system before the melt and/or the dissolution of the ikaite crystals at the onset of melting (Rysgaard et al., 2007).

Air-sea CO_2 exchange

The difference between the fCO_2 in the atmosphere and surface ocean is the thermodynamic driving force of air-sea CO_2 exchange (Wanninkhof et al., 2009). The rate of the transfer is controlled by the surface ocean boundary layer dynamics and the flux (F) can therefore be defined as (Wanninkhof et al., 2009):

$$F = k(C_w - C_0) \tag{29}$$

where k is the gas transfer velocity, C_0 is the concentration at the top of the boundary layer and C_w is the concentration at the bottom of the boundary layer (i.e. equal to the concentration of the well mixed water below the boundary layer). If the chemical potential is assumed to be equivalent across the air-water phase boundary the flux can, as is common, be expressed from the air-sea fCO_2 gradient, i.e. difference between the atmospheric fCO_2 (fCO_{2a}) and the well mixed water fCO_2 (fCO_{2w}, Wanninkhof et al., 2009):

$$F = kK_0(fCO_{2w} - fCO_{2a}) \tag{30}$$

where K_0 is the solubility coefficient. From this definition, it is clear that negative fluxes result in an oceanic uptake of CO_2 from the atmosphere. The marine CO_2 system buffers against the absorption of CO_2 according the following reaction:

$$[CO_2^*] + [CO_3^{2-}] + [H_2O] \leftrightarrow 2[HCO_3^-] \tag{31}$$

where a small part of the produced HCO_3^- protolyzes and thereby increases the $[H^+]$ (Zeebe & Wolf-Gladrow, 2001).

The thermodynamic driving force of the flux is mainly governed by the processes that control the surface water fCO_2, since the atmospheric fCO_2 variability is small in comparison, at least for shorter timescales such as years. The quantitative change in fCO_2 when CO_2 is absorbed from the atmosphere is not easily understood from Eq. 31 due to the minor dissociation of $[HCO_3^-]$. This sensitivity of fCO_2 to changes in DIC can however be expressed by the Revelle factor:

$$\text{Revelle factor} = \frac{\text{DIC}}{fCO_2}\frac{\partial fCO_2}{\partial \text{DIC}} \tag{32}$$

Off the West Spitsbergen coast, the Revelle factor ranges between 10.7 and 17.3. This means that for a 1% increase in DIC the fCO_2 will increase by 11-17%. Note that one of the consequences of anthropogenic CO_2 uptake is that it increases the Revelle factor, which therefore reduces the ocean's capacity to take up more in the future. Similar sensitivities can be derived for temperature and salinity, as already

mentioned in the Sections 3.1 and 3.2, but also for TA. These are all presented with values observed along the West Spitsbergen coast in Table 1.

Table 1. fCO_2 sensitivities with typical ranges for the West Spitsbergen region (adapted from Sarmiento & Gruber, 2006).

Parameter	Definition	Range
Temperature	$\frac{1}{fCO_2}\frac{\partial fCO_2}{\partial T}$	0.0454 to 0.0459°C^{-1}
Salinity	$\frac{S}{fCO_2}\frac{\partial fCO_2}{\partial S}$	0.73 to 0.96
DIC	$\frac{DIC}{fCO_2}\frac{\partial fCO_2}{\partial DIC}$	10.7 to 17.3
TA	$\frac{TA}{fCO_2}\frac{\partial fCO_2}{\partial TA}$	-16.6 to -10.1

Note. The fCO_2 sensitivity to temperature was modelled using CO2SYS as outlined in Paper III. The other fCO_2 sensitivities have been calculated using CO2SYS (van Heuven et al., 2011) where the calculations for the salinity and TA factors have been added to the script using a similar procedure as the existing calculation of the Revelle factor.

Note that processes that drive comparable changes in DIC and TA will have little influence on the fCO_2. This is true because the Revelle factor and TA factor are of similar magnitudes, i.e. they differ by 0.59-0.70, but have opposite signs.

The kinetic forcing that drives air-sea gas exchange is expressed by the gas transfer velocity, k. This property depends on many variables including different aspects of the wind forcing on the sea surface, surfactants, bubbles, and microbreaking (Wanninkhof et al., 2009). If the air-sea flux cannot be measured directly, as is often the case, the gas transfer velocity can be estimated from different types of parameterizations, for instance using wind speed. Since it is not the wind alone that controls the kinetic forcing of the flux, such an approach will introduce some uncertainties. For instance, the cold Arctic surface ocean is affected by intense convection in the winter (Andersson et al., 2017). Yet, there are currently no wind

speed parameterizations that account for this effect properly. The present thesis, i.e. Papers III-V, has used the wind speed parameterization of Wanninkhof (2014), which is based on the bomb ^{14}C inventory and the Cross Calibrated Multi-Platform (CCMP) wind product. The parameterization agrees well with several other formulas, including that of Nightingale et al. (2000), which is based on dual-tracer data from the North Sea, and the hybrid formula of Wanninkhof et al. (2009). This is promising, in the sense that the different approaches are based on data from different spatiotemporal scales. Still, calculations of the air-sea CO_2 flux based on local wind measurements may not necessarily work well with any of these parameterizations. Therefore, it is clear that there is a need for more studies on the gas transfer velocity that can provide wind speed parameterizations for the different environments and seasons of the Arctic.

3.2 Biological processes

Organic matter formation and remineralisation

The primary producers (autotrophs) within the ocean fixate carbon into organic matter, i.e. carbohydrates, lipids, proteins, and nucleic acids, using nutrients, CO_2, and energy from either sunlight, i.e. photosynthesis, or from reduced inorganic compounds. Marine phytoplankton have a composition that is fairly general in terms of their stoichiometric ratios of C:N:P:O_2. Redfield et al. (1963) was the first to determine these ratios of C:N:P:O_2 to 106:16:1:-138, the so-called Redfield ratio. The aerobic production of organic matter can therefore be summarized as follows:

$$106\ CO_2 + 16\ HNO_3 + H_3PO_4 + 122\ H_2O \leftrightarrow (CH_2O)_{106}(NH_3)_{16}(H_3PO_4) + 138\ O_2 \quad (33)$$

Variability in the Redfield ratio do however exist both spatially as well as temporally depending on the dominant phytoplankton groups and the nutrient availability. The largest uncertainty lies in the C to O_2 ratio (Sarmiento & Gruber, 2006). Several investigations have aimed to improve the C:N:P:O_2 ratios (e.g. Sterner et al., 2008), or provided regional ratios instead (e.g. Frigstad et al., 2014).

The effect of aerobic production of organic matter on the marine CO_2 system is for DIC a decrease and TA an increase (i.e. due to the assumed consumption of a proton for each assimilated NO_3^-, Wolf-Gladrow et al. 2007), which consequently result in a speciation-shift of the dissolved inorganic carbon forms toward more CO_3^{2-} and a higher pH. Therefore the fCO_2 will decrease, which may enhance the oceanic potential to absorb more atmospheric CO_2 as shown in Paper III. The assimilation of HPO_4^{2-}, which dominates among the dissolved phosphate species at seawater pH, has only a minor impact on TA since the concentration in the Arctic typically is about 1-2 μmol kg^{-1} or less.

The metabolic process where organisms oxidize organic matter for energy is referred to as respiration. The reverse of Eq. 33 is therefore aerobic respiration and the process when organic matter is transformed into its inorganic constituents is termed remineralisation. The difference between the gross primary production and the autotrophic and heterotrophic respiration is referred to as the Net Community Production (NCP, investigated in Paper IV). In the surface ocean, it is consequently the NCP that will dominate the effects of biological processes on the marine CO_2 system, i.e. if the $CaCO_3$ production is minimal.

A fraction of the organic matter that is produced within the surface layer will sediment to the ocean interior where it is either broken down or eventually settled on the sea floor. At the bottom it is either buried or transformed through diagenetic processes. This removal of carbon from the surface to the deep is referred to as the soft-tissue pump (Sarmiento & Gruber, 2006) and the flux of organic carbon out of the so-called euphotic zone is referred to as export production. The export production is dependent on the NCP and they are equal for a system that is in steady state.

Production and dissolution of $CaCO_3$

$CaCO_3$ do generally not precipitate naturally in the ocean because of nucleation barriers that likely result from interactions with magnesium ions, phosphate, or organic compounds (Sarmiento & Gruber, 2006). Marine organisms, on the other hand, can facilitate the reaction internally to use the mineral, in the form of calcite,

aragonite, or even magnesium calcite, to construct shells or skeletons. Of these, calcite is the most stable form. A fourth mineral form, ikaite, can also precipitate naturally in brine pockets of sea ice (Dieckmann et al., 2010). The production of $CaCO_3$ can be described by the following reaction:

$$Ca^{2+} + 2\,HCO_3^- \leftrightarrow CaCO_3(s) + CO_2 + H_2O \quad (34)$$

Note that the production of $CaCO_3$ result in a decrease in TA of 2 moles for each mole of $CaCO_3$ formed. DIC on the other hand is decreased by only 1 mole. For dissolution of $CaCO_3$ the reverse is true. The production of $CaCO_3$ in the surface ocean, including the subsequent sedimentation of the mineral to deeper layers, is referred to as the "carbonate pump" (Sarmiento & Gruber, 2006). The saturation state of $CaCO_3$ (Ω) is defined as:

$$\Omega = \frac{[Ca^{2+}][CO_3^{2-}]}{K_{sp}^*} \quad (35)$$

where the solubility product, K_{sp}^*, is defined in Eq. 9. Waters with Ω less than 1 are undersaturated in $CaCO_3$, as observed in Paper II, and the $CaCO_3$ crystals may therefore dissolve. If Ω is larger than 1 the water is supersaturated in the mineral as observed in Papers II, IV, and V.

The absorption of anthropogenic CO_2 by the ocean, results in the production of protons and the consumption of CO_3^{2-} (Eq. 31). Therefore both the oceanic pH and the $[CO_3^{2-}]$ have decreased since the industrial revolution. Consequently, through its proportional relation to the $[CO_3^{2-}]$, also the Ω has decreased. The high solubility of CO_2 in the High Arctic surface waters, due to the cold temperatures and the high freshwater content, makes this region especially sensitive to OA.

4. The study area

In short, this thesis takes off in the Atlantic and intermediate layers of the deep Nansen, Amundsen, and Makarov Basins (Paper I). These waters enter the central Arctic Ocean, either directly through Fram Strait, i.e. Fram Strait Branch Water (FSBW) that is a weaker continuation of the West Spitsbergen Current (WSC), or at the Saint Anna Through after a crossing over the Barents Sea, i.e. the cooled, freshened, and biogeochemically transformed Barents Sea Branch Water (BSBW).

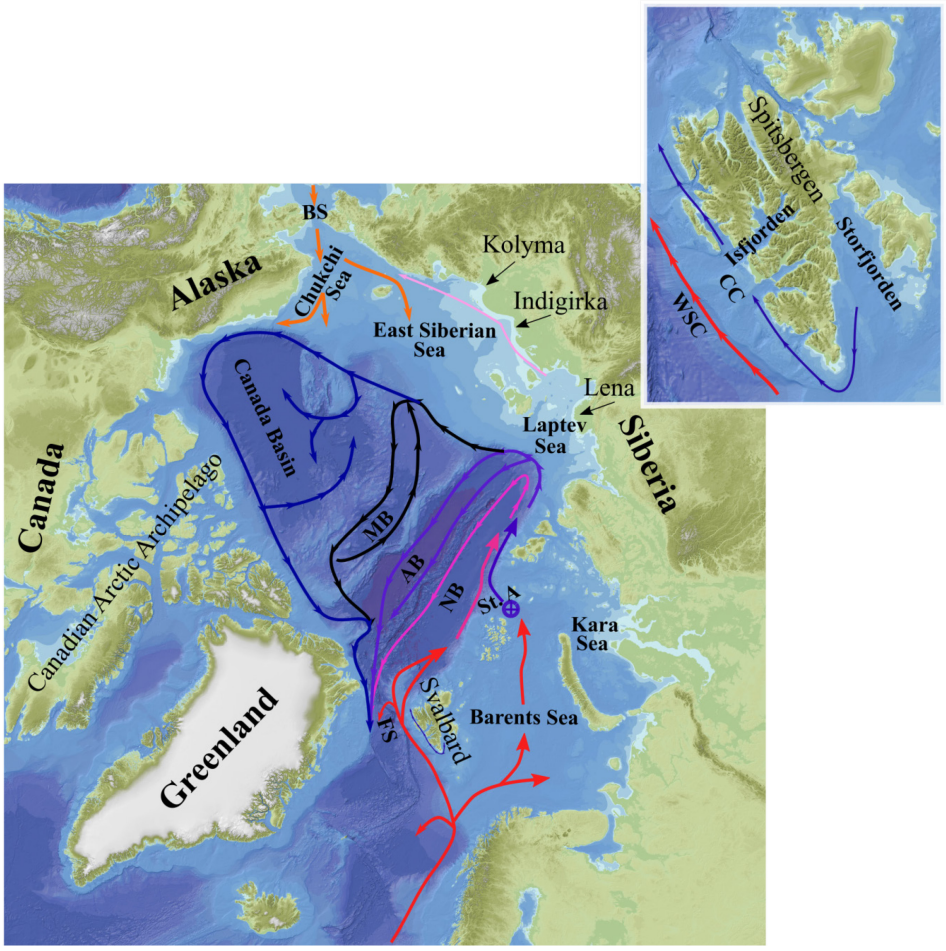

Fig. 4. The circulation in the study areas. The circulation of the Atlantic and intermediate layers of the Arctic Ocean is redrawn after Rudels et al. (2012). The annotations NB, AB, and MB refer to the

Nansen, Amundsen, and Makarov Basins, respectively. FS and BS denote the Fram and Bering Straits, respectively. The West Spitsbergen Current is denoted as WSC and the Coastal Current as CC. St. A refers to the Saint Anna Through. (IBCAO version 3.0, Jakobsson et al., 2012)

The two branches form a cyclonic boundary current that splits at each of the Arctic mid-ocean ridges. Additional ventilation results from sinking plumes of cold, high-salinity water at the continental slope (Rudels et al., 2012). This type of water is produced, typically in polynyas, on the Arctic shelf seas (Rudels et al., 2012). One of these seas that harbour a polynya in wintertime is also the setting for Paper II, namely the East Siberian Sea. The Arctic shelf seas have areas of intensive CO_2 drawdown such as the Barents Sea, but also areas where riverine organic decay products result in seasonal CO_2 efflux. The shallow East Siberian Sea (mean depth: 58 m, Jakobsson, 2002) is of the latter type. This sea not only receives the freshwater discharges from the Indigirka and Kolyma rivers in the summer, but also the organic matter-loaded freshwater of the Lena River that is released into the neighbouring Laptev Sea. That is if the atmospheric pressure field allows for the eastward flowing coastal current. The East Siberian Sea is also influenced by Pacific Water from the Chukchi Sea in the east.

The story ends in the glacier-influenced coastal waters of West Spitsbergen (Svalbard, Papers III-V), or to be more specific in Isfjorden (Fig. 5), a fjord system with several side-branches. This is a region that is influenced by the same type of Atlantic Water that likely harbours the solution to the scientific riddle that was addressed in Paper I. The temporal and spatial scales in Papers III-V are, however, different and therefore the research themes as well. Of importance to the Isfjorden system is the WSC that carries Atlantic Water northwards along the continental slope and the Coastal Current (CC) that brings cold and rather fresh Arctic Water that originates from Storfjorden and the northern parts of the Barents Sea. The sea ice cover in this area has decreased significantly in recent years (Muckenhuber et al., 2016), likely due to increased intrusions of Atlantic Water (Nilsen et al., 2016), which also have become warmer (Pavlov et al., 2013).

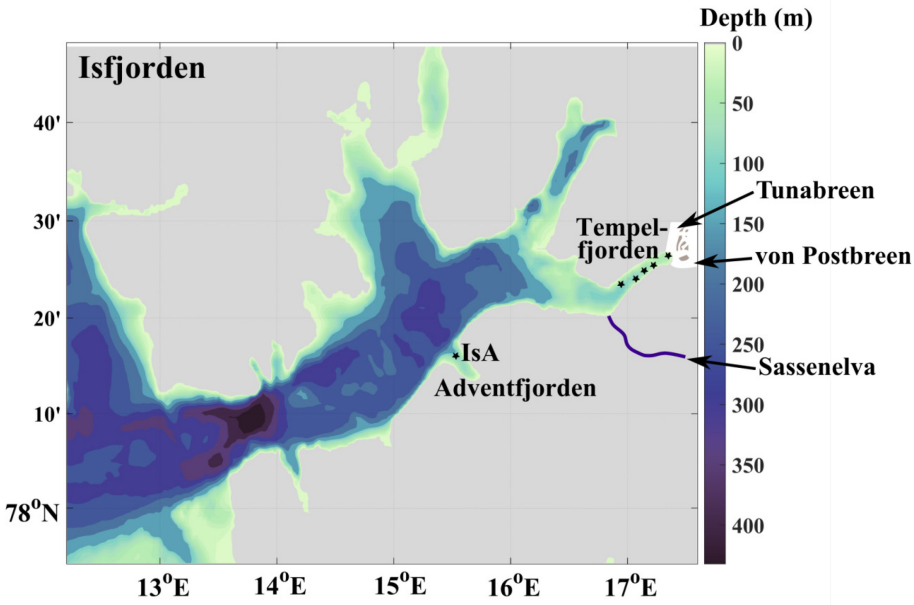

Fig. 5. Map over Isfjorden showing the locations of Adventfjorden (with the IsA Station as a black star) and Tempelfjorden (black stars show station locations).

Adventfjorden is the area under investigation in Papers III and IV, that is to say the IsA Station, which is situated close to the opening. The fjord is a very small (area: 22 km^2) and shallow (mean depth around 50 m) branch of the Isfjorden system. With no sill, it is easily ventilated by a boundary current that flows counter clockwise along the walls of the main part of Isfjorden. The sea ice has essentially been absent in recent winters. In the summers, the freshwater discharges of snow and glacial melt from the surrounding catchment area result in seasonal changes in salinity of about 4 at the IsA Station (i.e. at 2 m depth).

Last but not least, the slightly larger Tempelfjorden (area: 57 km^2, Forwick et al., 2010), the easternmost side-branch of the Isfjorden system, is the scope of Paper V. The tide-water glacier Tunabreen and the land-terminating von Postbreen at the head of the fjord, largely influence the freshwater dynamics here, that is together with the runoff from the river Sassenelva that is located just outside the fjord entrance. The seasonal changes in salinity are close to three times as large as the corresponding

changes that were observed at the opening of the neighbouring Adventfjorden. Apart from a freshening impact, the glaciers also have a cooling effect on the fjord and sea ice is sporadically produced every winter, i.e. in recent years sometime between February and May (Paper V).

5. Summary

Air-sea CO_2 exchange in the Arctic is a hot topic, not only due to the warming of the region with subsequent decreased sea ice extent and increased exposure of the surface waters to the atmosphere, but also in regards to the sequestration of atmospheric CO_2 to the ocean interior.

The findings in Paper I can be regarded as a consequence of the latter phenomenon, where atmospheric CO_2 is absorbed by the Atlantic Water, that flows north towards the Arctic Ocean, as it is cooled down. A fraction of this CO_2 is of anthropogenic origin and will contribute to the storage of C_{ant} in the deep basins of the central Arctic Ocean. This can be seen in the evolution of DIC in the Atlantic layers of the Nansen, Amundsen, and Makarov Basins. The DIC has increased by 0.6-0.9 μmol kg^{-1} yr^{-1} over a period of two decades (between 1991 and 2011), whereas there have been no coinciding changes in the nutrient concentrations (i.e. no changes in the rate of decay of organic matter) nor in the TA (i.e. no changes in the $CaCO_3$ dissolution).

Svalbard is an area where the sea ice cover has decreased over the last decades. Zooming in to the shallow Adventfjorden, where the sea ice has been more or less absent in recent years, the oceanic sink for atmospheric CO_2 was estimated to 31-36 g C m^{-2} yr^{-1} (Paper III). For the current state of the fjord, the key processes that seasonally controlled the thermodynamic driving force of the air-sea CO_2 flux through its relation to the surface pCO_2, were primary production/respiration and to a lesser extent warming/cooling. The moderate freshening of the surface layer over the melt season had only a small impact on the surface pCO_2 and consequently on the air-sea CO_2 flux. A little further to the east, on the other hand, in the tidewater-glacier fjord, Tempelfjorden, an extensive freshening of the surface layer accounted for about 25% of the oceanic CO_2 uptake over the melt season (Paper V).

The natural variability in Ω in different Arctic environments is substantial, that is from values as low as 0.5-1.5 for the mineral form aragonite in the river-influenced East Siberian Sea (as observed in July-September 2014, Paper II) to values between

1.3 and 2.4 in the glacier-influenced coastal waters of West Spitsbergen (as observed on a close to monthly basis between 2015 and 2017, Papers IV and V). The especially low values in the East Siberian Sea coincide with high pCO_2, as well as high nutrient and low oxygen concentrations, typical for waters that are affected by remineralisation of terrestrial and/or marine organic matter. These geochemical fingerprints, that could have severe implications for calcifying marine organisms, can be traced all the way from the shelf to the Fram Strait at depths of 50-150 m. Biological processes were also the seasonal key driver of Ω in Adventfjorden (Paper IV), as well as in Tempelfjorden (Paper V), but for these waters the effect of primary production on Ω exceeded that of respiration over the annual cycle.

Freshwater discharges are important in both the East Siberian Sea and the Svalbard region. Mixing with freshwater decreases Ω in both regions (Papers II, IV, and V), but to a lesser degree in the West Spitsbergen fjords (Papers IV and V) compared to the situation in the East Siberian Sea (Paper II), due to differences in the chemical properties of the freshwater sources.

6. Future Perspectives

A dream to determine local and seasonal wind speed parameterisations for the CO_2 gas transfer velocity took shape as this PhD project developed over time. This would greatly benefit estimates of the air-sea CO_2 flux in the Arctic, where seasonally important processes, such as convection and sea ice production in the winter and freshwater discharges in the summer, are likely to impact the transfer rate. Also, the transition of the Arctic, from an ice-capped sea to a seasonally open one, points to the necessity of better constraining the air-sea CO_2 flux. A first, although unsuccessful, attempt to realize the dream took place over a two weeks period in June 2017, using a CO_2 sensor in the surface water and an eddy covariance mast on the shore.

Another important issue in the Arctic, where the surface water at least regionally is extensively freshened, which also is related to the air-sea CO_2 flux, is realistic estimates of the depth to which the absorbed CO_2 may be mixed down. The classical methods that are used to determine the mixed layer depth, e.g. using a density threshold, can be difficult to apply in the summer due to the lack of a well constrained surface layer in the upper water column. This also makes it difficult to accurately assess effects of vertical eddy diffusion on the marine CO_2 system. Especially, since the turbulence-dependent eddy diffusivity coefficient is highly variable by several orders of magnitude in itself. A higher spatiotemporal resolution of DIC and TA measurements from sea ice, glacier ice, and river runoff would also be beneficial for our understanding of the effects of freshwater on the marine CO_2 system.

Whereas different aspects of the air-sea CO_2 exchange have been considered in this thesis, the ocean-sea floor exchange has largely been ignored. Recent attention on methane releases from the bottom has provided flux estimates for the marine CO_2 system in specific areas. Such information for different environments in the Arctic will be valuable to better constrain the Arctic carbon cycle.

This thesis is done in a changing Arctic, with no baseline for what it used to be. It is therefore clear that environmental monitoring of the marine CO_2 system is crucial for us to not only understand the current state of the system, but also to comprehend how the system will respond to the changes that are currently happening in the region, or will happen in the future.

References

AMAP (2018), *AMAP Assessment 2018: Arctic Ocean Acidification*, Arctic Monitoring and Assessment Programme (AMAP), Tromsø, Norway, vi+187pp.

Andersson, A., Falck, E., Sjöblom, A., Kljun, N., Sahlée, E., Omar, A.M., & Rutgersson, A. (2017), Air-sea gas transfer in high Arctic fjords, *Geophys. Res. Lett.,* 44, 2519-2526. https://doi.org/10.1002/2016GL072373

Barnhart, K.R., Overeem, I., & Anderson, R.S. (2014), The effect of changing sea ice on the physical vulnerability of Arctic coasts, *The Cryosphere,* 8, 1777-1799. doi: 10.5194/tc-8-1777-2014

Bates, N.R., & Mathis, J.T. (2009), The Arctic Ocean marine carbon cycle: evaluation of air-sea CO_2 exchanges, ocean acidification impacts and potential feedbacks, *Biogeosciences,* 6, 2433-2459.

Butterworth, B.J., & Else, B.G.T. (2018), *Atmos. Meas. Tech*., 11, 6075-6090. https:/doi.org/10.5194/amt-11-6075-2018

Byrne, R.H., & Yao, W. (2008), Procedures for measurement of carbonate ion concentrations in seawater by direct spectrophotometric observations of Pb(II) complexation, *Mar. Chem*., 112, 128-135. doi:10.1016/j.marchem.2008.07.009

Chierici, M., Fransson, A., & Anderson, L.G. (1999), Influence of *m*-cresol purple indicator additions on the pH of seawater samples: correction factors evaluated from a chemical speciation model, *Mar. Chem.,* 65, 281-290. https://doi.org/10.1016/S0304-4203(99)00020-1

Ciais, P., Sabine, C., Bala, G., Bopp, L., Brovkin, V., Canadell, J. Chhabra, A., DeFries, R., Galloway, J., Heimann, M, Jones, C., Le Quéré, C., Myneni, R.B., Piao, S., & Thornton, P. (2013), Carbon and Other Biogeochemical Cycles, In: *Climate Change 2013: The Physical Science Basis. Contribution of Working Group I to the Fifth Assessment Report of the Intergovernmental Panel on Climate Change*, Stocker, T.F., Qin, D., Plattner, G.-K., Tignor, M., Allen, S.K., Boschung, J., Nauels, A., Xia, Y., Bex, V., & Midgley, P.M. (Eds), Cambridge University Press, Cambridge, United Kingdom and New York, NY, USA.

Clayton, T.D., & Byrne, R.H. (1993), Spectrophotometric seawater pH measurements: total hydrogen ion concentration scale calibration of *m*-cresol purple and at-sea results, *Deep Sea Res. I, 40*(10)*,* 2115–2129. https://doi.org/10.1016/0967-0637(93)90048-8

Dickson. A.G. (1981), An exact definition of total alkalinity and a procedure for the estimation of alkalinity and total inorganic carbon from titration data, *Deep Sea Res., 28A*(6), 609-623.

Dickson, A.G., (1990), Thermodynamics of the dissociation of boric acid in synthetic seawater from 273.15 to 318.15 K, *Deep Sea Res., 37*(5), 755-766.

Dickson, A.G., & Millero, F.J. (1987), A comparison of the equilibrium constants for the dissociation of carbonic acid in seawater media, *Deep Sea Res., 34*(10), 1733–1743. https://doi.org/10.1016/0198-0149(87)90021-5

Dickson, A.G., Sabine, C.L., & Christian, J.R. (Eds) (2007), *Guide to best practices for ocean CO_2 measurement,* PICES Special Publication, 3, 191 pp.

Dieckmann, G.S., Nehrke, G., Uhlig, C., Göttlicher, J., Gerland, S., Granskog, M.A., & Thomas, D.N. (2010), Brief communication: ikaite ($CaCO_3 * 6H_2O$) discovered in Arctic sea ice, *The Cryosphere,* 4, 227–230.

DOE (U.S. Department of Energy) (1994), *Handbook of methods for the analysis of the various parameters of the carbon dioxide system in sea water*, version 2. Dickson, A.G., Goyet, C. (Eds.), ORNL/CDIAC-74.

Doney, S.C., Balch, W.M., Fabry, V.J., & Feely, R.A. (2009), Ocean acidification: A critical emerging problem for the ocean sciences, *Oceanography, 22*(4), 16-25.

Else, B.G.T., Papakyriakou, T.N., Galley, R.J., Drennan, W.M., Miller, L.A., & Thomas, H. (2011), Wintertime CO_2 fluxes in an Arctic polynya using eddy covariance: Evidence for enhanced air-sea gas transfer during ice formation, *J. Geophys. Res*. 116, C00G03. doi:10.1029/2010JC006760

Evans, W., Mathis, J.T., Cross, J.N., Bates, N.R., Frey, K.E., Else, B.G.T., et al. (2015), Sea-air CO_2 exchange in the western Arctic coastal ocean, *Global Biogeochem. Cycles*, 29, 1190-1209. https://doi.org/10.1002/2015GB005153

Forwick, M., Vorren, T.O., Hald, M., Korsun, S., Roh, Y., Vogt, C., & Yoo, K.-C. (2010), Spatial and temporal influence of glaciers and rivers on the sedimentary environment in Sassenfjorden and Tempelfjorden, Spitsbergen, In: *Fjord Systems and Archives*, Howe, J.A., Austin, W.E.N., Forwick, M., & Paetzel, M. (Eds), Geological Society, London, Special Publications, 344, 163–193. http://doi.org/10.1144/SP344.13

Frigstad, H., Andersen, T., Bellerby, R.G.J. Silyakova, A. & Hessen, D.O. (2014), Variation in the seston C:N ratio of the Arctic Ocean and pan-Arctic shelves, *J. Mar. Syst.,* 129, 214-223. http://dx.doi.org/10.1016/j.jmarsys.2013.06.004

Global Carbon Project (2018), *Carbon budget and trends 2017*, www.globalcarbonproject.org/carbonbudget

Günther, F., Overduin, P.P., Yakshina, I.A., Opel, T., Baranskaya, A.V., & Grigoriev, M.N. (2015), Observing Muostakh disappear: permafrost thaw subsidence and erosion of a ground-ice-rich island in response to arctic summer warming and sea ice reduction, *The Cryosphere,* 9, 151-178. doi:10.5194/tc-9-151-2015

Haine, T.W.N., Curry, B., Gerdes, R., Hansen, E., Karcher, M, Lee, C., Rudels, B., Spreen, G., de Steur, L., Stewart, K.D., & Woodgate, R. (2015), Arctic freshwater export: Status, mechanisms, and prospects*, Global and Planetary Change,* 125*,* 13-35.

Haraldsson, C., Anderson, L.G., Hassellöv, M., Hulth, S., & Olsson, K. (1997), Rapid, high-precision potentiometric titration of alkalinity in ocean and sediment pore waters, *Deep Sea Res. I, 44*(12), 2031–2044.

IPCC (2013), Summary for Policymakers, In: *Climate Change 2013: The Physical Science Basis. Contribution of Working Group I to the Fifth Assessment Report of the Intergovernmental Panel on Climate Change*, Stocker, T.F., Qin, D., Plattner, G.-K., Tignor, M., Allen, S.K., Boschung, J., Nauels, A., Xia, Y., Bex, V., & Midgley, P.M. (Eds), Cambridge University Press, Cambridge, United Kingdom and New York, NY, USA.

IPCC (2018), Summary for Policymakers, In: *Global warming of 1.5°C. An IPCC Special Report on the impacts of global warming of 1.5°C above pre-industrial levels and related global greenhouse gas emission pathways, in the context of strengthening the global response to the threat of climate change, sustainable development, and efforts to eradicate poverty*, Masson-Delmotte, V., Zhai, P., Pörtner, H.O., Roberts, D., Skea, J., Shukla, P.R., Pirani, A., Moufouma-Okia, W., Péan, C., Pidcock, R., Connors, S., Matthews, J.B.R., Chen, Y., Zhou, X., Gomis, M.I., Lonnoy, E., Maycock, T., Tignor, M., Waterfield, T. (Eds), World Meteorological Organization, Geneva, Switzerland, 32 pp.

Jakobsson, M. (2002), Hypsometry and volume of the Arctic Ocean and its constituent seas, *Geochem. Geophys. Geosyst., 3*(5). doi:10.1029/2001GC000302

Jakobsson, M., Mayer, L., Coakley, B., Dowdeswell, J.A., Forbes, S., Fridman, B., Hodnesdal, H., Noormets, R., Pedersen, R., Rebesco, M., Schenke, H.W., Zarayskaya, Y., Accettella, D., Armstrong, A., Anderson, R.M., Bienhoff, P., Camerlenghi, A., Church, I., Edwards, M., Gardner, J.V., Hall, J.K., Hell, B., Hestvik, O., Kristoffersen, Y., Marcussen, C., Mohammad, R., Mosher, D., Nghiem, S.V., Pedrosa, M.T., Travaglini, P.G., & Weatherall, P. (2012), The international bathymetric chart of the Arctic Ocean (IBCAO) version 3.0, *Geophys. Res. Lett.,*39, L12609. doi:10.1029/2012GL052219

Johnson, K.M., King, A.E., & Sieburth, J.M. (1985), Coulometric TCO_2 analyses for marine studies; an introduction, *Mar. Chem*., 16, 61-82.

Jutterström, S., & Anderson, L.G. (2010), Uptake of CO_2 by the Arctic Ocean in a changing climate, *Mar. Chem.,* 122, 96-104. doi:10.1016/j.marchem.2010.07.002

Kirtman, B., Power, S.B., Adedoyin, J.A., Boer, G.J., Bojariu, R., Camilloni, I., Doblas-Reyes, F.J., Fiore, A.M., Kimoto, M, Meehl, G.A., Prather, M., Sarr, A., Schär, C., Sutton, R., van Oldenborgh, G.J., Vecchi, G., & Wang, H.J. (2013), Near-term Climate Change: Projections and Predictability, In: *Climate Change 2013: The Physical Science Basis. Contribution of Working Group I to the Fifth Assessment Report of the Intergovernmental Panel on Climate Change*, Stocker, T.F., Qin, D., Plattner, G.-K., Tignor, M., Allen, S.K., Boschung, J., Nauels, A., Xia, Y., Bex, V., & Midgley, P.M. (Eds), Cambridge University Press, Cambridge, United Kingdom and New York, NY, USA.

Lee, K., Kim, T.-W., Byrne, R.H., Millero, F.J., Feely, R.A., & Liu, Y.-M. (2010), The universal ratio of boron to chlorinity for the North Pacific and North Atlantic oceans, *Geochimica et Cosmochimica Acta, 74*, 1801-1811.

Lewis, E., & Wallace, D.W.R. (1998), *Program developed for CO_2 system calculations,* ORNL/CDIAC-105, Carbon Dioxide Information Analysis Center, Oak Ridge National Laboratory, Oak Ridge, Tennessee.

Liu, X., Patsavas, M.C., & Byrne, R.H. (2011), Purification and characterization of meta-Cresol purple for spectrophotometric seawater pH measurements, *Environ. Sci. Technol*., 45, 4862-4868. dx.doi.org/10.1021/es200665d

Mars, J.C., & Houseknecht, D.W. (2007), Quantitative remote sensing study indicates doubling of coastal erosion rate in past 50 yr along a segment of the Arctic coast of Alaska, *Geology,* 35, 583-586.

McGuire, A.D., Anderson, L.G., Christensen, T.R., Dallimore, S., Guo, L., Hayes, D.J., Heimann, M, Lorenson, T.D., Macdonald, R.W., & Roulet, N. (2009), Sensitivity of the carbon cycle in the Arctic to climate change, *Ecological Monographs*, 79(4), 523-555.

Mehrbach, C., Culberson, C.H., Hawley, J.E., & Pytkowicz, R.M. (1973), Measurement of the apparent dissociation constants of carbonic acid in seawater at atmospheric pressure, *Limnol. Oceanogr*., 18, 897–907. https://doi.org/10.4319/lo.1973.18.6.0897

Millero, F.J. (1995), Thermodynamics of the carbon dioxide system in the oceans, *Geochimica et Cosmochimica Acta, 59*(4), 661-677.

Millero, F.J. (2007), The marine inorganic carbon cycle. *Chem. Rev.,* 107, 308-341.

Mucci, A. (1983), The solubility of calcite and aragonite in seawater at various salinities, temperatures, and one atmosphere total pressure, *American Journal of Science,* 283, 780-799.

Muckenhuber, S., Nilsen, F., Korosov, A., & Sandven, S. (2016), Sea ice cover in Isfjorden and Hornsund, Svalbard (2000-2014) from remote sensing data, *The Cryosphere,* 10*,* 149-158. https://doi.org/10.5194/tc-10-149-2016

Nightingale, P.D., Malin, G., Law, C.S., Watson, A.J., Liss, P.S., Liddicoat, M.I., et al. (2000), In situ evaluation of air–sea gas exchange parameterizations using novel conservative and volatile tracers, *Global Biogeochem. Cycles, 14*(1), 373-387. https://doi.org/10.1029/1999GB900091

Nilsen, F., Cottier, F., Skogseth, R., & Mattsson, S. (2008), Fjord-shelf exchanges controlled by ice and brine production: The interannual variation of Atlantic Water in Isfjorden, Svalbard, *Continental Shelf Research,* 28, 1838-1853. https://doi.org/10.1016/j.csr.2008.04.015

Nilsen, F., Skogseth, R., Vaardal-Lunde, J., & Inall, M. (2016), A simple shelf circulation model: Intrusion of Atlantic Water on the West Spitsbergen Shelf, *J. Phys. Oceanogr*., *46*(4), 1209–1230. https://doi.org/10.1175/JPO-D-15-0058.1

Overland, J., Hanna, E., Hanssen-Bauer, I., Kim, S.-J., Walsh, J.E., Wang, M., Bhatt, U.S., & Thoman, R.L. (2016), *Surface air temperature.* Arctic report card: update for 2016. Available at: http://www.arctic.noaa.gov/Report-Card/Report-Card-2016/ArtMID/5022/ArticleID/271/Surface-Air-Temperature

Patsavas, M.C., Byrne, R.H., & Liu, X. (2013), Purification of meta-cresol purple and cresol red by flash chromatography: Procedures for ensuring accurate spectrophotometric seawater pH measurements, *Mar. Chem*., 150, 19-24. http://dx.doi.org/10.1016/j.marchem.2013.01.004

Patsavas, M.C., Byrne, R.H., Yang, B., Easley, R.A., Wanninkhof, R., & Liu, X. (2015), Procedures for direct spectrophotometric determination of carbonate ion concentrations: Measurements in US Gulf of Mexico and East Coast waters, *Mar. Chem*., 168, 80-85. http://dx.doi.org/10.1016/j.marchem.2014.10.015

Pavlov, A.K., Tverberg, V., Ivanov, B.V., Nilsen, F., Falk-Petersen, S., & Granskog, M.A. (2013), Warming of Atlantic Water in two west Spitsbergen fjords over the last century (1912-2009), *Polar Research,* 32, 11206. https://dx.doi.org/10.3402/polar.v32i0.11206

Peterson, B.J., Holmes, R.M., McClelland, J.W., Vörösmarty, C.J., Lammers, R.B., Shiklomanov, A.I., Shiklomanov, I.A., & Rahmstorf, S. (2002), Increasing river discharge to the Arctic Ocean, *Science,* 298, 2171-2173.

Pipko, I.I., Pugach, S.P., Semiletov, I.P., Anderson, L.G., Shakova, N.E., Gustafsson, Ö., Repina, I.A., Spivak, E.A., Charkin, A.N., Salyuk, A.N., Shcherbakova, K.P., Panova, E.V., & Dudarev, O.V. (2017), The spatial and interannual dynamics of the surface water carbonate system and air-sea CO_2 fluxes in the outer shelf and slope of the Eurasian Arctic Ocean, *Ocean Sci*., 13, 997-1016. https://doi.org/10.5194/os-13-997-2017

Pipko, I.I., Semiletov, I.P., Pugach, S.P., Wåhlström, I., & Anderson, L.G. (2011), Interannual variability of air-sea CO_2 fluxes and carbon system in the East Siberian Sea, *Biogeosciences,* 8, 1987-2007. https://doi.org/10.5194/bg-8-1987-2011

Redfield, A.C., Ketchum, B.H., & Richards, F.A. (1963), The influence of organisms on the composition of sea-water, In: *The Sea: Ideas and Observations on the Progress in the Study of the Seas*, vol. 2, Hill, M.N., (Ed), Interscience, New York.

Rhein, M., Rintoul, S.R., Aoki, S., Campos, E., Chambers, D., Feely, R.A., Gulev, S., Johnson, G.C., Josey, S.A., Kostianoy, A., Mauritzen, C., Roemmich, D., Talley, L.D., & Wang, F. (2013), Observations: Ocean, In: *Climate Change 2013: The Physical Science Basis. Contribution of Working Group I to the Fifth Assessment Report of the Intergovernmental Panel on Climate Change*, Stocker, T.F., Qin, D., Plattner, G.-K., Tignor, M., Allen, S.K., Boschung, J., Nauels, A., Xia, Y., Bex, V., & Midgley, P.M. (Eds), Cambridge University Press, Cambridge, United Kingdom and New York, NY, USA.

Rudels, B., Anderson, L., Eriksson, P., Fahrback, E., Jakobsson, M., Jones, E.P., Melling, H., Prinsenberg, S., Schauer, U., & Yao, T. (2012), Observations in the ocean, In: *Arctic Climate Change: The ACSYS Decade and Beyond*, Lemke, P., & Jacobi, H.-W. (Eds), Atmos. Oceanogr. Sci. Libr., vol. 43, pp. 117–198. doi:10.1007/978-94-007–2027-5_4. © Springer Science+Business Media B.V.

Rysgaard, S., Bendtsen, J., Delille, B., Dieckmann, G.S., Glud, R.N., Kennedy, H., Mortensen, J., Papadimitriou, S., Thomas, D.N., & Tison, J.-L. (2011), Sea ice contribution to the air-sea CO_2 exchange in the Arctic and Southern Oceans, *Tellus,* 63B, 823-830.

Rysgaard, S., Glud, R.N., Sejr, M.K., Bendtsen, J., & Christensen, P.B. (2007), Inorganic carbon transport during sea ice growth and decay: A carbon pump in polar seas, *J. Geophys. Res*.,112, C03016. doi:10.1029/2006JC003572

Sabine, C.L., & Tanhua, T. (2010), Estimation of Anthropogenic CO_2 Inventories in the Ocean*, Annu. Rev. Mar. Sci*., 2, 175-198.

Sarmiento, J.L., & Gruber, N. (2006), *Ocean biogeochemical dynamics,* Princeton, NJ: Princeton University Press.

Semiletov, I.P., Pipko, I.I., Repina, I., & Shakhova, N.E. (2007), Carbonate chemistry dynamics and carbon dioxide fluxes across the atmosphere-ice-water interfaces in the Arctic Ocean: Pacific sector of the Arctic, *J. Mar. Syst.,* 66, 204–226. https://doi.org/10.1016/j.jmarsys.2006.05.012

Sterner, R.W., Andersen, T., Elser, J.J., Hessen, D.O., Hood, J.M., McCauley, E., & Urabe, J. (2008), Scale-dependent carbon : nitrogen : phosphorus seston stoichiometry in marine and freshwaters, *Limnol. Oceanogr., 53*(3), 1169-1180.

Takahashi, T., Olafsson, J., Goddard, J.G., Chipman, D.W., & Sutherland, S.C. (1993), Seasonal variation of CO_2 and nutrients in the high-latitude surface oceans: A comparative study, *Global Biogeochem. Cycles, 7*(4), 843–878. https://doi.org/10.1029/93GB02263

Takahashi, T., Sutherland, S.C., Wanninkhof, R., Sweeney, C., Feely, R.A., Chipman, D.W., Hales, B., Friederich, G., Chavez, F., Sabine, C., Watson, A., Bakker, D.C.E., Schuster, U., Metzl, N, Yoshikawa-Inoue, H., Ishii, M., Midorikawa, T., Nojiri, Y., Körtzinger, A., Steinhoff, T., Hoppema, M., Olafsson, J., Arnarson, T.S., Tilbrook, B., Johannessen, T., Olsen, A., Bellerby, R., Wong, C.S., Delille, B., Bates, N.R., & de Baar, H.J.W. (2009), Climatological mean and decadal change in surface ocean pCO_2, and net air-sea CO_2 flux over the global oceans, *Deep Sea Res. II,* 56, 554-577.

van Heuven, S. (2013), *Determination of the rate of oceanic storage of anthropogenic CO_2 from measurements in the ocean interior: the South Atlantic Ocean*, Doctoral thesis, Rijksuniversiteit Groningen, Groningen, The Netherlands.

van Heuven, S., Pierrot D., Rae, J.W.B., Lewis, E., & Wallace, D.W.R. (2011), *MATLAB program developed for CO_2 system calculations,* ORNL/CDIAC-105b, Carbon Dioxide Information Analysis Center, Oak Ridge National Laboratory, Oak Ridge, Tennessee. doi: 10.3334/CDIAC/otg.CO2SYS_MATLAB_v1.1

Vaughan, D.G., Comiso, J.C., Allison, I., Carrasco, J., Kaser, G., Kwok, R., Mote, P., Murray, T., Paul, F., Ren, J., Rignot, E., Solomina, O., Steffen, K., & Zhang, T. (2013), Observations: Cryosphere, In: *Climate Change 2013: The Physical Science Basis. Contribution of Working Group I to the Fifth Assessment Report of the Intergovernmental Panel on Climate Change*, Stocker, T.F., Qin, D., Plattner, G.-K., Tignor, M., Allen, S.K., Boschung, J., Nauels, A., Xia, Y., Bex, V., & Midgley, P.M. (Eds), Cambridge University Press, Cambridge, United Kingdom and New York, NY, USA.

Wanninkhof, R., (2014), Relationship between wind speed and gas exchange over the ocean revisited, *Limnol. Oceanogr. Methods,* 12, 351–362. https://doi.org/10.4319/lom.2014.12.351

Wanninkhof, R., Asher, W.E., Ho, D.T., Sweeney, C., & McGillis, W.R. (2009), Advances in quantifying air-sea gas exchange and environmental forcing, *Annu. Rev. Mar. Sci.*, 1, 213-244. doi:10.1146/annurev.marine.010908.163742

Weiss, R. F. (1974), Carbon dioxide in water and seawater: the solubility of a non-ideal gas, *Mar. Chem.,* 2, 203–215. https://doi.org/10.1016/0304-4203(74)90015-2

Wolf-Gladrow, D.A., Zeebe, R.E., Klaas, C., Körtzinger, A., & Dickson, A.G. (2007), Total alkalinity: The explicit conservative expression and its application to biogeochemical processes, *Mar. Chem*., 106, 287-300. doi:10.1016/j.marchem.2007.01.006

Yasunaka, S., Murata, A., Watanabe, E., Chierici, M., Fransson, A., van Heuven, S., et al. (2016), Mapping of the air-sea CO_2 flux in the Arctic Ocean and its adjacent seas: Basin-wide distribution and seasonal to interannual variability, *Polar Sci.,* 10, 323–334. https://doi.org/10.1016/j.polar.2016.03.006

Zeebe, R.E., & Wolf-Gladrow, D.A. (2001), *CO_2 in seawater: Equilibrium, kinetics, isotopes*, Elsevier Oceanography Series 65, *pp*. 1-84.

I

AGU PUBLICATIONS

JGR

Journal of Geophysical Research: Oceans

RESEARCH ARTICLE

10.1002/2013JC009514

Increasing carbon inventory of the intermediate layers of the Arctic Ocean

Ylva Ericson[1], Adam Ulfsbo[1], Steven van Heuven[2], Gerhard Kattner[3], and Leif G. Anderson[1]

[1]Department of Chemistry and Molecular Biology, University of Gothenburg, Gothenburg, Sweden, [2]Centre for Isotope Research, University of Groningen, Groningen, Netherlands, [3]Alfred-Wegener-Institut Helmholtz-Zentrum für Polar und Meeresforschung, Bremerhaven, Germany

Key Points:
- Inorganic carbon concentration increase in intermediate water layers of the Arctic Ocean
- No significant trend in nutrient or oxygen concentrations was found
- Inflow of anthropogenic carbon to intermediate layers is the likely cause

Correspondence to:
L. G. Anderson,
leifand@chem.gu.se

Citation:
Ericson, Y., A. Ulfsbo, S. van Heuven, G. Kattner, and L. G. Anderson (2014), Increasing carbon inventory of the intermediate layers of the Arctic Ocean, *J. Geophys. Res. Oceans*, *119*, 2312–2326, doi:10.1002/2013JC009514.

Received 21 OCT 2013
Accepted 15 MAR 2014
Accepted article online 20 MAR 2014
Published online 14 APR 2014

Abstract Concentrations of dissolved inorganic carbon (DIC), total alkalinity (TA), nutrients, and oxygen in subsurface waters of the central Arctic Ocean have been investigated for conceivable time trends over the last two decades. Data from six cruises (1991–2011) that cover the Nansen, Amundsen, and Makarov Basins were included in this analysis. In waters deeper than 2000 m, no statistically significant trend could be observed for DIC, TA, phosphate, or nitrate, but a small rate of increase in apparent oxygen utilization (AOU) was noticeable. For the individual stations, differences in concentration of each property were computed between the mean concentrations in the Arctic Atlantic Water (AAW) or the upper Polar Deep Water (uPDW), i.e., between about 150 and 1400 m depth, and in the deep water (assumed invariable over time). In these shallower water layers, we observe significant above-zero time trends for DIC, in the range of 0.6–0.9 μmol kg^{-1} yr^{-1} (for AAW) and 0.4–0.6 μmol kg^{-1} yr^{-1} (for uPDW). No time trend in nutrients could be observed, indicating no change in the rate of organic matter mineralization within this depth range. Consequently, the buildup of DIC is attributed to increasing concentrations of anthropogenic carbon in the waters flowing into these depth layers of the Arctic Ocean. The resulting rate of increase of the column inventory of anthropogenic CO_2 is estimated to be between 0.6 and 0.9 mol C m^{-2} yr^{-1}, with distinct differences between basins.

1. Introduction

The impact on climate, by accelerating fossil fuel burning, is mitigated by oceanic CO_2 uptake and storage [e.g., *Ballantyne et al.*, 2012]. Roughly 25% of the present annual anthropogenic CO_2 (C_{ant}) emissions are stored in the oceans [e.g., *Le Quéré et al.*, 2009]. However, as a consequence of the resulting decrease of the oceanic buffer capacity [*Revelle*, 1983], this fraction will decline with time and there are already signs of a reduced absorption rate in several oceanic regions [e.g., *Schuster et al.*, 2009; *Lenton et al.*, 2012]. Despite its remoteness, the Arctic Ocean not only plays an integral role in the global heat balance, but it also contains nearly 2 times the global mean concentration of anthropogenic CO_2 [*Tanhua et al.*, 2009], a feature related to the intense ventilation of subsurface layers.

In the Arctic Ocean, the renewal of Atlantic layer, intermediate, and deep Arctic waters is driven by: (i) inflow of Atlantic water through Fram Strait, (ii) Atlantic water that crosses over the Barents Sea where it cools down, and (iii) dense water formation by brine released during sea ice production, especially in polynyas along the Arctic shelf seas [*Rudels et al.*, 2012a], with subsequent descent of high-salinity bottom waters down the continental slope [*Anderson et al.*, 1999]. Cooling of the inflowing surface waters increases gas solubility and thus promotes uptake of CO_2 from the atmosphere. Furthermore, brine production has been suggested to facilitate uptake of CO_2 from the atmosphere both by promoting water transport from the surface to the deep [e.g., *Anderson et al.*, 2004; *Omar et al.*, 2005; *Else et al.*, 2011] as well as by calcium carbonate formation in the brine channels that changes the pCO_2 levels in both the brine and the sea ice melt [*Rysgaard et al.*, 2011]. The ventilation of the subsurface waters transports C_{ant} to the deep ocean. Downward transport of C_{ant} may be further enhanced by the hypothesized increasing strength of the biological pump [e.g., *Riebesell et al.*, 2007]. The Atlantic layer and intermediate water masses of the Arctic Ocean flow in an cyclonic pattern along topographic boundaries before exiting through Fram Strait and, beyond that, over the Scotland-Greenland Ridge to the Atlantic Ocean thereby linking the Arctic to the global thermohaline circulation [e.g., *Mauritzen*, 1996; *Anderson et al.*, 1999].

The rate of warming of the Arctic atmosphere exceeds the global mean [*Serreze and Francis*, 2006] and coincides with a significant decrease of summer sea ice extent and volume [e.g., *Stroeve et al.*, 2007, 2012; *Laxon*

Table 1. List of Cruises, International Arctic Ocean Expedition 1991 (IAOE 91), Arctic Ocean Section 1994 (IAS 94), Arctic Climate System Study 1996 (ACSYS 96), Beringia 2005, Trans-Arctic Survey of the Arctic Ocean in Transition (TransArc) From Which the C-System Data Were Collected

Survey (Vessel)	Date	Parameters	Source (doi)	Comment
IAOE 91 (I/B Oden)	26 Jul 1991 to 3 Sep 1991	S, T, O_2, DIC*, TA*, nutrients	10.3334/CDIAC/otg. CARINA_77DN19910726	*No CRMs. CARINA data product
AOS 94 (I/B L. St Laurent)	24 Jul 1994 to 1 Sep 1994	S, T, O_2, DIC, TA, nutrients	10.3334/CDIAC/otg. CARINA_18SN19940724	CARINA data product
ACSYS 96 (R/V Polarstern)	Jul 12 1996 to 6 Sep 1996	S, T, O_2, DIC, TA, pH, nutrients	10.3334/CDIAC/otg. CARINA_06AQ19960712	CARINA data product
Beringia 2005 (I/B Oden)	19 Aug 2005 to 25 Sep 2005	S, T, O_2, DIC, TA, pH, nutrients	10.3334/CDIAC/otg. CLIVAR_77DN20050819	
ARK-XXII/2(R/V Polarstern)	28 Jul 2007 to 10 Oct 2007	S, T, O_2*, DIC, TA, nutrients		*Calibrated CTD-oxygen
TransArc/ARK-XXVI/3 (R/V Polarstern)	5 Aug 2011 to 7 Oct 2011	S, T, O_2*, DIC, TA, pH, nutrients	doi.pangaea.de/10.1594/ PANGAEA.775817	*Calibrated CTD-oxygen

et al., 2013]. The presence of sea ice restricts further sea ice growth through its insulating effect. More open water thus facilitates increased sea ice production and brine formation during the winter season, with the prospect of increased deep water formation adding to the surface-to-deep ocean anthropogenic carbon transport [*Anderson et al*., 2004; *Else et al*., 2011]. On the other hand, excessive heat in the inflowing Atlantic water is likely to have the opposite impact in previously seasonally ice-covered areas like the Barents Sea [*Harms*, 1997; *Årthun et al*., 2011].

More open water in the Arctic Ocean also allows for a substantial uptake of atmospheric CO_2 because of less impediment of air-sea gas exchange [*Bates and Mathis*, 2009; *Jutterström and Anderson*, 2010]. Such changes in sea ice conditions, together with rising temperature and the effects thereof on stratification, mixing, and upwelling, are likely to affect primary production [*Tremblay and Gagnon*, 2009]. To what magnitude is not currently possible to conclude, because the changes of these processes could act both negatively and positively. Satellite monitoring suggests that net primary production (NPP) has increased by 20% between 1998 and 2009, largely as a result of the shrinking sea ice cover [*Arrigo and van Dijken*, 2011; *Arrigo et al*., 2011]. Whether this increased productivity will enhance the biological pump remains uncertain. Nevertheless, sea ice-related shifts in Arctic ecosystems are likely to alter carbon fluxes to subsurface layers [*Li et al*., 2009]. Lastly, there is a potential for more production by, and sedimentation of, sea ice algae because more first-year sea ice will lead to better light and thus growth conditions [*Boetius et al*., 2013]. Important unknowns are the amount of the organic matter that sinks and the depth at which it remineralizes.

Historic observations of nutrients in the central Arctic Ocean show very constant concentrations from about 2000 m to the bottom of around 14 μmol kg^{-1} in nitrate and 1 μmol kg^{-1} in phosphate [e.g., *Codispoti et al*., 2013]. Observations of oxygen and dissolved inorganic carbon (DIC) also show very constant concentrations with depth, but below an even shallower depth for the latter. Together with the very low organic matter content of sediments [e.g., *Jakobsson et al*., 2003] and the long residence times of the bottom water (hundreds of years) [e.g., *Tanhua et al*., 2009; *Rudels et al*., 2012a], this strongly supports the notion that the rate of organic carbon export to below 2000 m is very low.

In order to assess conceivable changes in DIC concentrations in subsurface waters of the Arctic Ocean resulting from anthropogenic CO_2 uptake and alterations in the biological carbon pump during the last decades when the sea ice concentration and thickness have decreased, we evaluate the evolution of measured concentrations of the carbon system, oxygen, and nutrients.

2. Methods

2.1. Data Provenance

The cruises during which the data were collected are listed in Table 1, and their station locations are presented in Figure 1. The data from the 1990s are included in the Arctic Ocean data compilation [*Jutterström et al*., 2010] within the carbon dioxide in the Atlantic Ocean (CARINA) data synthesis project [*Key et al*., 2010]. Table 2 provides a detailed description of station positions and data availability. Properties

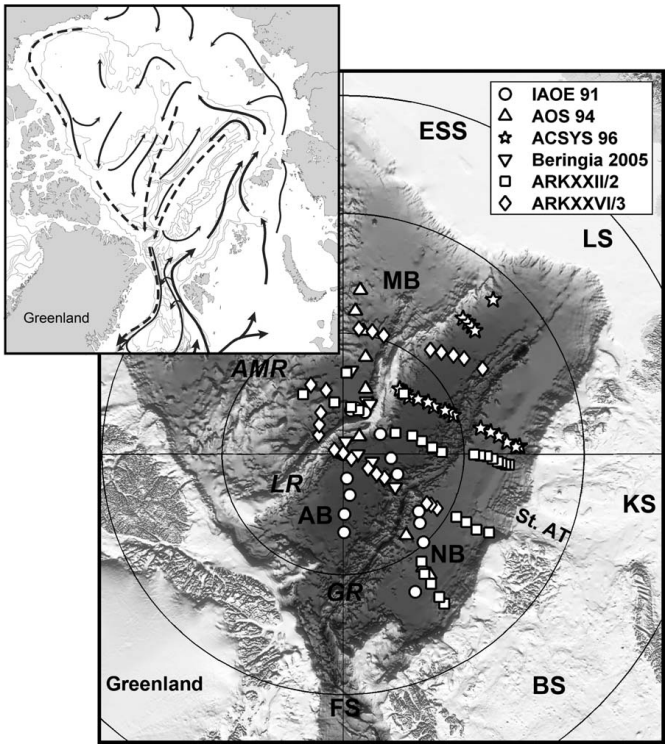

Figure 1. Map of the Arctic Ocean with station locations for carbon system data and an insert showing the main circulation pattern. The abbreviations note the basins, Nansen (NB), Amundsen (AB), Makarov (MB), and Canada (CB), the three ridges, Alpha-Mendeleev (*AMR*), Lomonosov (*LR*), and Gakkel (*GR*) as well as Fram Strait (FS), Barents Sea (BS), Kara Sea (KS), Laptev Sea (LS), and East Siberian Sea (ESS). St. Anna trough is denoted as St. AT.

considered in this contribution are DIC, total alkalinity (TA), pH, oxygen (expressed as apparent oxygen utilization, AOU), nutrients (phosphate and nitrate), all from discrete water samples, and temperature and salinity from the conductivity-temperature-depth (CTD) records.

During all cruises, DIC was determined using coulometric titration according to *Johnson et al*. [1987], following the standard operating procedure outlined in *Dickson et al*. [2007]. The precision (here reported as the standard deviation of differences between duplicate sample runs, except for the Beringia 2005 and ARK-XXVI/3 cruises where the precision is reported as the mean absolute difference) was 1–2 μmol kg^{-1} for all but the ARK-XXVI/3 cruise, which had a precision of 4 μmol kg^{-1}. TA was determined by open cell potentiometric titration according to *Haraldsson et al*. [1997] and, for ARK-XXII/2, *Mintrop et al*. [2000], except for the IAOE 91 cruise where a closed cell potentiometric titration was used [*Johansson and Wedborg*, 1982]. The precision was ~2 μmol kg^{-1} for all but the IAOE 91, which had a precision of 4 μmol kg^{-1}. For both DIC and TA determinations, the accuracy was assured by the use of Certified Reference Materials (CRM) supplied by A. Dickson, Scripps Institution of Oceanography (USA), with the exception for the IAOE 91 cruise during which CRM was not yet available. A spectrophotometric method was used for the pH determination [*Clayton and Byrne*, 1993], with a precision around 0.001 pH units. The total pH scale is used throughout this work. Oxygen was determined with automated Winkler titration systems, with a relative precision of better than 1%. During the 2007 and 2011 TransArc cruises oxygen are from an oxygen sensor mounted on the CTD package, with the data calibrated by Winkler titrations. Thus, the precision should be comparable to

Table 2. Year and Positions of the Stations as Well as Parameters Used in This Evaluation[a]

Year	Stn	Latitude (°N)	Longitude (°E)	DIC	TA	O_2	NUT
1991	5	83.56	27.63	*	*	*	*
1991	9	85.07	42.30	*	*	*	*
1991	10	85.73	48.05	*		*	*
1991	11	86.07	52.79	*	*	*	*
1991	16	87.61	69.70	[b]	[b]	[b]	[b]
1991	17	88.01	85.06		[c]	*	*
1991	19	88.25	118.50	*	*	*	*
1991	25	88.04	152.81			*	*
1991	26	88.02	163.60		*	*	*
1991	27	88.16	169.69		*	*	*
1991	29	90	0		*	*	*
1991	30	88.99	8.94	*	*	*	*
1991	31	88.28	9.34	*	*	*	*
1991	32	87.51	1.44		*	*	*
1991	33	86.76	0.75	*	*	*	*
1994	25	83.173	173.935	*	*	*	*
1994	26	84.063	175.072	*	*	*	*
1994	27	84.852	170.693	*	*	*	*
1994	28	85.892	166.703	*	*	*	*
1994	29	87.155	160.708	*	*	*	*
1994	34	89.017	137.152	*	*	*	*
1994	35	89.998	66.992	*	*	*	*
1994	36	85.733	37.748	*	*	*	*
1994	37	84.245	35.008	*	*	*	*
1994	38	83.845	35.690	*	*	*	*
1996	38	82.68	92.52	*	[d]	*	*
1996	39	82.84	92.32			*	*
1996	40	83.20	94.04	*	[d]	*	*
1996	41	83.50	96.58	*	[d]	*	*
1996	42	83.83	98.40	*	[d]	*	*
1996	43	84.20	100.53	*	[d]	*	*
1996	50	85.17	109.29			*	*
1996	51	85.28	111.59	*	[d]	*	*
1996	52	85.41	113.01	*	[d]	*	*
1996	54	85.76	117.47			*	*
1996	55	85.88	121.24	*	[d]	*	*
1996	56	86.15	125.95		*	*	*
1996	57	86.40	130.63	[c]	[c]	*	*
1996	58	86.39	134.19		*	*	*
1996	59	86.43	136.04	*	*	*	*
1996	60	86.44	138.89	[d]	*	*	*
1996	79	82.50	138.47			*	*
1996	80	82.50	136.41	*	*	*	*
1996	81	82.50	134.61			*	*
1996	82	82.52	132.95	*	*	*	*
1996	87	81.08	135.69	*	[d]	*	*
2005	26	86.538	174.153	*	*	*	*
2005	30	87.614	156.073	*	*	*	*
2005	31	87.640	151.610	*	*	*	*
2005	42	89.473	167.492	*	*	*	*
2005	44	89.380	89.087	*	*	*	*
2005	46	88.762	75.128	*	*	*	*
2005	47	88.045	58.437	*	*	*	*
2005	49	87.444	57.686	*	*	*	*
2007	255	82.503	33.952			*	*
2007	256	82.858	33.877			*	*
2007	257	83.498	34.043	*	*	*	*
2007	258	83.999	34.014	[b]	*	*	*
2007	260	84.489	36.139	[e]	[e]	*	*
2007	261	84.645	60.934	*	*	*	*
2007	263	84.172	60.998			*	*
2007	264	83.642	60.429			*	*
2007	266	83.138	61.741	[f]	*	*	*
2007	294	83.115	86.246			*	*
2007	295	83.272	86.284	*	*	*	*
2007	296	83.435	86.746			*	*
2007	297	83.588	87.237			*	*
2007	298	83.807	88.098	*		*	*

Table 2. (continued)

Year	Stn	Latitude (°N)	Longitude (°E)	DIC	TA	O_2	NUT
2007	299	84.051	89.043	*	*	*	*
2007	300	84.337	89.292			*	*
2007	301	84.580	89.837	[g]	*	*	*
2007	306	85.923	91.122	*	*	*	*
2007	307	86.303	94.287			*	*
2007	308	86.706	99.283			*	*
2007	309	87.046	104.79			*	*
2007	310	87.658	112.04	*	*	*	*
2007	324	88.075	160.63			*	*
2007	326	88.028	170.08	*	*	*	*
2007	328	87.830	189.44	*	*	*	*
2007	333	87.028	213.60	[f]	[f]	*	*
2007	352	86.638	177.56	[b]	[b]	*	*
2007	363	86.459	135.02	[f]	[f]	*	*
2011	201	85.509	59.885	[d]		*	*
2011	202	85.803	59.932	[d]		*	*
2011	203	85.974	59.423	[d]		*	*
2011	212	88.018	59.952	[d]	*	*	*
2011	213	88.385	59.138			*	[f]
2011	214	88.794	60.215	[d]	*	*	*
2011	216	89.600	60.746	[d]	*	*	*
2011	218	89.964	146.631	[d]	*	*	*
2011	219	89.615	−115.228	[d]	*	*	*
2011	222	88.736	−128.249	[d]	*	*	*
2011	223	88.452	−141.171	[d]	*	*	*
2011	224	88.060	−152.054	[d]	*		*
2011	226	87.284	−165.269	[d]	*	*	*
2011	227	86.861	−155.045	[d]	*	*	*
2011	244	84.779	172.747	[d]	*	*	*
2011	245	84.795	166.415	[d]	*	*	*
2011	246	84.814	160.996	[d]	*	*	*
2011	250	84.385	139.910	[d]	*	*	*
2011	251	84.154	135.882	[d]	*	*	*
2011	252	83.879	131.696	[d]	*	*	*
2011	253	83.626	128.295	[d]	*	*	*
2011	258	83.237	121.359	[d]	*	*	*

[a]As denoted by an asterisk, data are available for all water masses.
[b]No measurements within the AAW.
[c]No measurements within the uPDW.
[d]Calculated using CO2SYS version 1.1 [*van Heuven et al.*, 2011] with the carbonate dissociation constants (K_1 and K_2) of *Mehrbach et al.* [1973] as refit by *Dickson and Millero* [1987].
[e]Only measurements within the dAAW.
[f]No measurements within the dAAW.
[g]Only measurements within the uPDW.

the precision of the latter. Nutrients were measured by an autoanalyzer according to standard procedures (e.g., following the World Ocean Circulation Experiment (WOCE) protocol) [*Gordon et al.*, 1994], with a relative precision better than 2%. The nutrients of the ARK-XXVI/3 cruise were converted to μmol kg^{-1} at an assumed analysis temperature of 20°C.

The carbonate system was overdetermined during the ACSYS 96, Beringia 2005, and ARK-XXVI/3 2011 cruises. Within the CARINA data set (see Tables 1 and 2), the alkalinity of the ACSYS 96 cruise was partially calculated from DIC and pH using the carbonate dissociation constants (K_1 and K_2) of *Mehrbach et al.* [1973] as refit by *Dickson and Millero* [1987]. Because of the noisy character of the DIC data from the ARK-XXVI/3 cruise, DIC was additionally computed from TA and pH^{tot} using CO2SYS [*van Heuven et al.*, 2011], with the

Table 3. Water Mass Classification According to *Marnela et al.* [2008], Adapted From *Rudels et al.* [2005]

Arctic Ocean Water Masses	Density Range
Arctic Atlantic Water (AAW)	$27.70 \leq \sigma_0 < 27.97$
dense Arctic Atlantic Water (dAAW)	$27.97 \leq \sigma_0$, $\sigma_{0.5} < 30.444$, $\theta > 0$
upper Polar Deep Water (uPDW)	$\sigma_{0.5} < 30.444$, $\theta \leq 0$

Table 4. The Fitted Slopes, in μmol kg^{-1} yr^{-1}, With Its Fit (R^2) and Significance (p Value) for the Time Period of the Data of Table 5

	DIC			AOU			TA			Phosphate			Nitrate		
	Slope	R^2	p	Slope	R^2	p	Slope	R^2	p	Slope	R^2	p	Slope	R^2	p
NB	0.05	0.034	0.77	0.26	0.969	0.002	0.22	0.475	0.20	−0.0006	0.047	0.72	−0.019	0.429	0.23
AB	0.10	0.027	0.75	0.41	0.885	0.005	0.12	0.133	0.47	−0.0003	0.017	0.80	−0.004	0.008	0.87
MA	−0.32	0.467	0.31	0.35	0.808	0.038	0.38	0.346	0.30	−0.0001	0.002	0.95	−0.023	0.382	0.27

same constants as for the CARINA data set, giving a precision of the computed DIC of 2 μmol kg^{-1}. The average difference between the measured and calculated DIC is 2.3 ± 4.9 μmol kg^{-1}. This small offset is related to the choice of carbonate dissociation constants and the accuracy of the pH and TA measurements. The precision of calculated DIC (2 μmol kg^{-1}) is indeed superior to that of the direct measurements (about 4 μmol kg^{-1}) and for the remainder of this paper we therefore use the calculated DIC of ARK-XXVI/3, without considering the offset of 2.3 μmol kg^{-1}.

2.2. Deep Water Data Consistency

The quality and interconsistency of the Arctic Ocean data within the CARINA data product were evaluated by *Jutterström et al*. [2010]. To further demonstrate the interconsistency of these data sets and the more recent surveys used in the present study, the mean deep water values of the biogeochemical properties (DIC, TA, phosphate, nitrate, and AOU) were regressed against time for each of the three discerned major ocean basins.

2.3. Time Trends in Near-Surface and Intermediate Water Masses

For our assessment of time trends, we discern (from surface to intermediate depth) the Arctic Atlantic Water (AAW), the dense Arctic Atlantic Water (dAAW), and the upper Polar Deep Water (uPDW), according to Table 3.

For each station with a bottom depth of more than 3000 m and at least three measurements below 2000 m, depth-integrated mean concentrations of the properties in the AAW, dAAW, and uPDW were obtained through trapezoidal integration. The density ranges in the water mass classification (Table 3) were used to determine the depth boundaries of the water masses. The integrated inventories were divided by the local water mass height to obtain the concentrations.

Station-specific systematic errors (e.g., minor calibration inaccuracies) are removed by subtracting the mean of the deep water (DW) values from the depth-integrated mean concentrations of the intermediate waters (IW), which also will correct for any analytical biases between cruises. Thus, a difference is obtained for each station and property, expressed as ΔX ($X^{IW}_{mean} - X^{DW}_{mean}$), and for each basin and cruise the average ΔX is calculated. Linear regression analyses were done for the Nansen, Amundsen, and Makarov Basins using these cruise-specific averages. The significance of the time trends was evaluated using Analysis of Variance (ANOVA).

The effects of organic matter remineralization were deduced by assessing trends in the Δ-values of nutrients and AOU. Changes in ΔTA were investigated to see any potential effects of calcium carbonate dissolution. Effects of changes in CO_2 solubility were investigated utilizing the trends in depth-integrated mean values of salinity and potential temperature at the sampling depths.

3. Results and Discussion

3.1. Deep Water Data Consistency

The overarching assumption that there are no trends in the deep waters was tested by fitting strait lines (Table 4) to the mean concentrations of each cruise and basin for the properties below 2000 m (Table 5). The standard errors of the mean of nearly all data are within double the precision of the analytical methods. The exceptions are DIC in the 2005 Makarov Basin data and TA in the 1991 Nansen Basin data. This large error is due to a larger scatter and no significant increase of the concentration with depth. The mean data of DIC, AOU, and phosphate are also plotted versus year in Figure 2. As obvious from the fit (R^2) and significance (p value < 0.05) only the AOU data show any statistically significant trend (0.4 μmol kg^{-1} yr^{-1}). Without any corresponding trend in any of the other parameters it is not possible to ascribe the AOU trend to any biogeochemical process such as remineralization of organic matter that sediment through the water column. This is

Table 5. Mean Concentrations and Standard Errors (SE) in the Deep Waters (>2000 m) of the Nansen Basin (NB), Amundsen Basin (NB), and Makarov Basin (MB) During the Different Years[a]

		DIC		AOU		TA		Phosphate		Nitrate	
Year		Mean	SE	Mean	SE	Mean	SE	Mean	SE	Mean	SE
1991	NB	2154.0	1.2	56.7	1.0	2295.2	3.4	0.98	0.006	14.7	0.04
	AB	2153.1	1.4	52.9	0.4	2293.0	1.8	0.98	0.003	14.7	0.04
	MA	a	a	60.2	0.5	2290.5	1.0	0.99	0.001	14.9	0.04
1994	NB	2159.4	0.3	57.3	0.1	2297.5	1.3	1.03	0.009	14.5	0.02
	AB	2163.6	0.7	57.2	0.0	2301.3	0.1	1.02	0.001	14.5	0.04
	MA	2159.8	1.0	64.6	0.2	2301.5	0.9	1.04	0.004	14.5	0.01
1996	NB	2155.9	1.4	57.7	0.2	2292.6	1.6	0.97	0.004	14.5	0.05
	AB	2151.2	1.3	57.8	0.1	2294.8	1.7	0.99	0.007	13.7	0.07
	MA	nd	nd	nd	nd	nd	nd	nd	nd	nd	nd
2005	NB	nd	nd	nd	nd	nd	nd	nd	nd	nd	nd
	AB	2162.2	1.9	60.3	0.1	2295.5	0.7	1.02	0.004	14.6	0.08
	MA	2160.7	3.5	67.3	0.3	2305.9	1.0	1.04	0.005	14.8	0.07
2007	NB	2155.0	1.0	60.1	0.2	2297.5	0.9	1.00	0.002	14.6	0.06
	AB	2155.3	1.3	60.2	0.1	2297.9	0.7	1.00	0.001	14.5	0.08
	MA	2154.3	0.8	65.7	0.3	2299.9	0.5	1.02	0.004	14.6	0.06
2011	NB	2158.1	0.6	62.3	0.0	2300.1	0.6	0.97	0.003	14.0	0.07
	AB	2157.0	0.4	63.2	0.2	2299.6	0.3	0.97	0.005	14.1	0.04
	MA	2154.3	0.3	69.3	0.3	2300.6	0.3	0.99	0.007	14.1	0.03

[a]All data are in μmol kg^{-1}. nd: No samples were collected. a: too few samples for a statistical treatment.

also supported by estimates of very low export fluxes of organic matter [*Anderson et al.*, 2003; *Cai et al.*, 2010]. Furthermore, the lack of a significant trend in TA in the deep waters (as well as in the intermediate waters) leads us to conclude that temporal variability in the dissolution of calcium carbonates is insignificant and it therefore will not be considered in the assessment. The intermediate waters are supersaturated with respect to both calcite and aragonite while the deep water is slightly supersaturated for calcite but undersaturated for aragonite [*Jutterström and Anderson*, 2005]. The very low burial of carbonates in the sediment indicates little sedimentation of calcium carbonate.

Even if there is no trend in the DIC, TA, and nutrient data there is a substantial scatter in the mean data between cruises, especially for DIC up to 10 μmol kg^{-1}. As the residence times of these deep waters are long, up to hundreds of years [*Tanhua et al.*, 2009; *Rudels et al.*, 2012a], the combined data sets suggest that biogeochemical variability is a highly unlikely cause of the scatter. However, to further test the importance of organic matter decay as reason for the scatter between cruises, the DIC concentration was corrected by the variability in the AOU, phosphate, and nitrate concentrations. For this correction preformed concentrations were assumed and the RKR ratio of 1:16:106:138 for P, N, C, O_2 was used [*Redfield et al.*, 1963]. The absolute value selected as preformed concentrations are not important in investigating if the scatter in DIC will decrease by this correction, as long as the preformed concentration is constant over time. The resulting corrected DIC showed a very similar concentration range between the years (9–13 μmol kg^{-1}) but with a slightly shift to lower values during the later years when AOU was used. The latter is a natural result based on the significant temporal trend of these data. Hence, this further supports that the DIC scatter between cruises is not due to biogeochemical processes.

Data from deeper than 2500 m of the cruises in the years 1991, 1994, and 1996 have been analyzed for offsets using multilinear regression [*Jutterström et al.*, 2010]. Except for the TA of the 1994 cruise no statistical significant interconsistency in the data set could be detected that warranted an adjustment of the original data. It should be noted that during this analysis the ratios of P, N, and O_2 were allowed to vary (without any biochemical constrains) to get the least variability between the data of the different cruises. The data of the cruises in years 2005, 2007, and 2011 have not been investigated in a corresponding manner. The lack of any temporal trend in the data consistent with biogeochemical processes, together with minimal ocean mixing based on the long residence time, supports the assumption of constant concentrations in the deep water for the analysis of the intermediate water properties.

3.2. Time Trends in Near-Surface and Intermediate Water Masses

Figure 3 and Table 6 summarize the changes (relative to those of the deep water) in the Atlantic layers and the uPDW of the Arctic Ocean, for the time period between 1991 and 2011. For DIC, a significant trend is

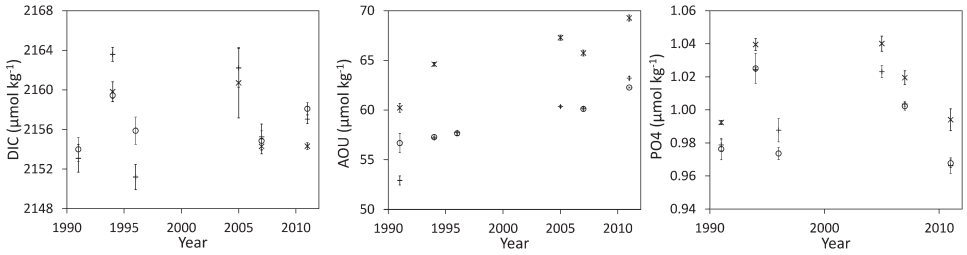

Figure 2. Deep water (≥2000 m) cruise averages (μmol kg^{-1}) including standard error bars within the Nansen (circle), Amundsen (plus), and Makarov (cross) Basins over the period of 1991–2011: (a) DIC, (b) AOU, (c) PO_4.

observed of 0.7–0.9 μmol kg^{-1} yr^{-1} ($p < 0.05$) within the Amundsen Basin (Table 6). The trend becomes less pronounced with depth. Changes within the Nansen and Makarov Basins are 0.6 μmol kg^{-1} yr^{-1} ($p < 0.05$, except for the dAAW of the Makarov Basin) in the Atlantic layers and roughly one third less in the uPDW. The changes in the dAAW and uPDW of the Makarov Basin are not significant (ANOVA, $p > 0.05$) due to the sparse data set and should be interpreted with caution.

The uncertainty in the rate of change of DIC in the different basins and water masses, expressed as the standard errors of the fits, ranges from 0.1 to 0.2 μmol kg^{-1} yr^{-1}, with the largest errors related to the Makarov Basin. The large spread of the DIC data of the IAOE 91 cruise within the Amundsen Basin (Figure 3b) contributes strongly to the uncertainty of the trends. If the IAOE 91 cruise is excluded from the regressions, the corresponding slopes are in the range of 0.6–0.9 μmol kg^{-1} yr^{-1} (ANOVA, $p < 0.05$). These trends are used in the further discussion.

Additional uncertainties may be related to the spatial representativeness of the computed averages, i.e., sample locations within the basin. However, the variation in ΔX is largely within the analytical error. For example, the standard deviation of ΔDIC for each combination of cruise, basin, and water mass is within ±4 μmol kg^{-1} for 89% of the combinations. We therefore assume that the general scarcity of data do not significantly impact the spatial representativeness of the different cruises.

The observation of increasing DIC in all three basins may be accounted for by several processes, including increasing remineralization of inorganic and organic carbon sinking through the water column, changes in water mass circulation, and the degree of CO_2 saturation and input of anthropogenic CO_2 in the inflowing water, each of which will be discussed in the following sections. However, as for the deep waters, no trend in TA was observed in the near-surface and intermediate water masses ruling out dissolution of mineral carbonates. However, as these waters are supersaturated with respect to both calcite and aragonite this is not expected and hence, this process is not considered in the following discussion.

3.3. Attribution of Trends

3.3.1. Organic Matter Mineralization

Changes in the sedimentation and subsequent mineralization of organic matter would be reflected in changes of DIC, nutrients, and oxygen that are proportional to the elemental composition of organic matter [*Redfield et al.*, 1963], and may in principle be inferred from changes in these ancillary properties. However, the oxygen and nutrient content of local waters is additionally dependent on variability of the large-scale circulation. Fortunately, the general circulation pattern within the Arctic Ocean results in a horizontally homogenous concentration field minimizing the potential influence of this effect. No interannual trend is detected in either PO_4 (Figures 3j–3l) or NO_3 (Figures 3m–3o) in the intermediate waters that could account for the significant increases in DIC. On the contrary, there is a small but significant decline in NO_3 and PO_4 in the dAAW of the Amundsen Basin (ANOVA, $p < 0.05$; Table 6). This indicates a minimal temporal trend in remineralization of organic matter over the time period of this study (provided that the residence time has not changed, as we assume here). Furthermore, there was no trend in AOU in any of the basins (Figures 3g–3i). The trend in deep water AOU does imply an equal trend in the shallower water masses. However, organic matter is typically

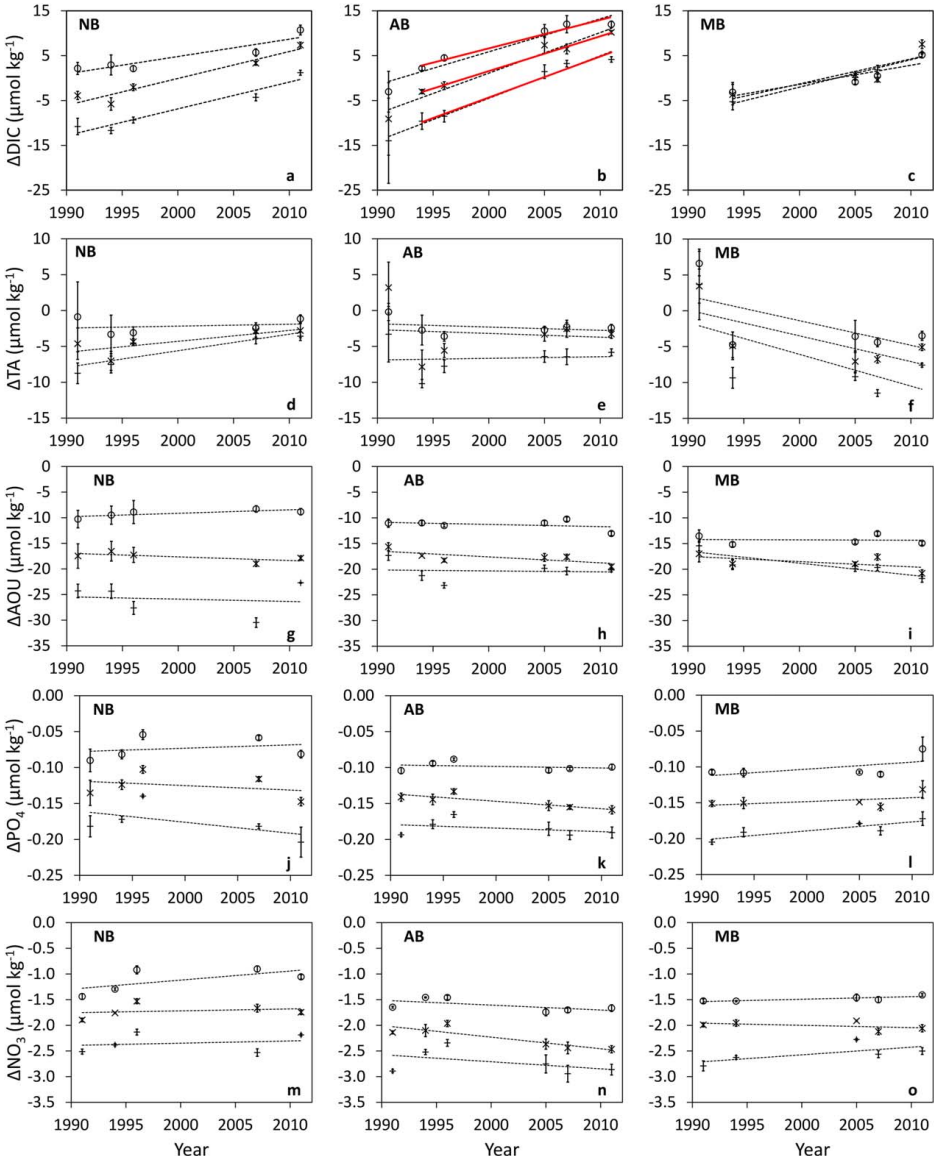

Figure 3. Average ΔDIC, ΔTA, ΔAOU, ΔPO_4, and ΔNO_3 over the period of 1991–2011 including standard error bars for the AAW (plus), dAAW (cross), and uPDW (circle) in the Nansen, Amundsen, and Makarov Basins. The red solid line in (b) is a fit without the 1991 data. Slope coefficient, standard error, *p* values, and R^2 for the different regression lines are displayed in Table 4.

remineralized all through the water column, resulting in a stronger increase of the decay products in the shallower waters compared to the deep. Because no sign of this can be seen in any property, we consider that organic matter mineralization is not a likely cause of the deep water trend in AOU.

Table 6. Slope Coefficients With Standard Error of the Fits, Significance (*p* Value) and R^2 Values[a]

	Nansen Basin				Amundsen Basin				Makarov Basin			
	Slope	SE	p	R^2	Slope	SE	p	R^2	Slope	SE	p	R^2
AAW												
ΔDIC	0.60	0.10	0.01	0.93	0.90 (0.95)	0.09 (0.07)	0.00 (0.00)	0.97 (0.98)	0.61	0.08	0.02	0.97
ΔTA	0.23	0.08	0.06	0.74	0.02	0.14	0.88	0.01	−0.44	0.31	0.25	0.41
ΔAOU	−0.05	0.21	0.84	0.02	−0.02	0.12	0.89	0.01	−0.23	0.08	0.06	0.75
ΔPO_4	−0.0015	0.0013	0.32	0.33	−0.0005	0.0006	0.48	0.13	0.0013	0.0004	0.06	0.76
ΔNO_3	0.004	0.012	0.74	0.04	−0.014	0.013	0.35	0.22	0.015	0.009	0.20	0.47
dAAW												
ΔDIC	0.60	0.10	0.01	0.93	0.79 (0.91)	0.07 (0.09)	0.00 (0.00)	0.98 (0.96)	0.56	0.24	0.14	0.74
ΔTA	0.15	0.07	0.13	0.59	−0.05	0.23	0.83	0.01	−0.36	0.20	0.17	0.52
ΔAOU	−0.07	0.04	0.20	0.47	−0.12	0.05	0.09	0.55	−0.10	0.08	0.28	0.37
ΔPO_4	−0.0006	0.0011	0.61	0.10	−0.0010	0.0003	0.03	0.75	0.0005	0.0005	0.39	0.25
ΔNO_3	0.004	0.009	0.69	0.06	−0.023	0.006	0.02	0.78	−0.004	0.005	0.43	0.22
uPDW												
ΔDIC	0.39	0.10	0.03	0.79	0.61 (0.74)	0.08 (0.10)	0.01 (0.00)	0.95 (0.93)	0.43	0.16	0.11	0.79
ΔTA	0.03	0.07	0.73	0.04	−0.04	0.07	0.54	0.10	−0.34	0.25	0.27	0.38
ΔAOU	0.07	0.03	0.11	0.62	−0.04	0.05	0.48	0.13	−0.01	0.06	0.92	0.00
ΔPO_4	0.0005	0.0010	0.68	0.07	−0.0002	0.0004	0.59	0.08	0.0010	0.0008	0.32	0.32
ΔNO_3	0.018	0.012	0.24	0.42	−0.009	0.006	0.19	0.38	0.005	0.002	0.07	0.72

[a]DIC values for the Amundsen Basin are given without the 1991 data and with the 1991 data in parentheses.

3.3.2. CO_2 Solubility Changes

The variability in depth-integrated mean values of potential temperature and salinity is displayed in Figure 4. The AAW has become warmer and saltier since 1991. This warming has been noted in several previous contributions [e.g., *Schauer et al.*, 2002; *Polyakov et al.*, 2010; *Korhonen et al.*, 2012]. Pulses of inflowing warm Atlantic water have been proposed to cause this increase [*Rudels et al.*, 2013]. A warming of 0.5°C reduces DIC by roughly 3 μmol kg^{-1} due to the decrease in CO_2 solubility (assuming that the water was in prolonged contact with the atmosphere during warming). Such an effect could come about in the source waters during their transit along the Norwegian coast and through the Barents Sea when they are in contact with the atmosphere. The limited decadal variability in temperature and salinity of all water masses but the AAW in the Nansen Basin (Figure 4) results in CO_2 solubility changes that are well below the standard error of the computed trends in inorganic carbon.

3.3.3. Anthropogenic CO_2

The magnitude and spatial distribution of the inorganic carbon changes in the central Arctic Ocean between 1991 and 2011 are thus most likely a result of the increasing C_{ant} in the source waters before leaving contact with the atmosphere. This statement is based on the absence of concomitant changes in either solubility or the mineralization rate of organic matter over the same period. The increase in the integrated column inventory over the Atlantic and intermediate layers of the Amundsen Basin is 0.9 ± 0.1 mol C m^{-2} yr^{-1}. This is nearly two thirds more than the global ocean's rate of increase of the column inventory of C_{ant} [*Sabine et al.*, 2008] and can be compared to inventory increases of 0.6 ± 0.1 mol C m^{-2} yr^{-1} in the Nansen and Makarov Basins. Estimates of the C_{ant} concentration using the transit time distribution together with the CFC distribution also showed the highest column inventory at this depth range in the Amundsen Basin [*Tanhua et al.*, 2009].

As a result of the increases in DIC, together with a constant TA, the pH is reduced by 0.02–0.05 units during the last two decades (starting at about 8.05–8.06 units). This lowers the aragonite and calcite saturation states by 0.05–0.14 and 0.08–0.22 units, respectively (starting at about 1.2–1.4 and 1.9–2.3, respectively). At such rates, it will take less than 100 years for the water to be undersaturated with respect to aragonite, a process starting in the Atlantic layers of the Amundsen Basin.

3.3.3.1. Source Waters of Anthropogenic CO_2

As the input of C_{ant} occurs at the atmosphere-ocean interface there is a need to describe the formation process of the source waters to the water masses to be assessed. The intermediate waters of the Arctic Ocean have an Atlantic origin, and enter both through Fram Strait and the relatively shallow Barents Sea. The West Spitsbergen Current (WSC) contributes to form the Fram Strait Branch of Atlantic Water (FSBW) that flows to

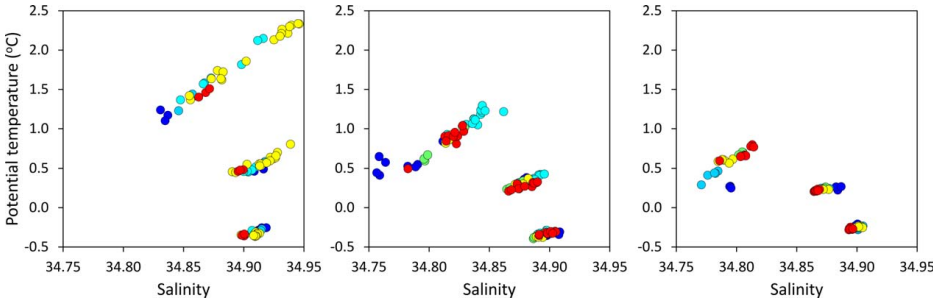

Figure 4. Depth-integrated mean values of potential temperature and salinity for each of the AAW, dAAW, and uPDW at each station in the Nansen Basin (NB), Amundsen Basin (AB), and Makarov Basin (MB), including the 1991 (dark blue), 1994 (blue), 1996 (cyan), 2005 (green), 2007 (yellow), and 2011 (red) cruises.

the east and follows the Barents Sea continental margin. The upper ~100 m melts sea ice and forms cold, low salinity upper water that separates from the warm Atlantic layer water by a strong halocline [e.g., *Rudels et al*., 1996]. At the St. Anna canyon, the FSBW meets the Barents Sea Branch Water (BSBW) and is forced into the deep Nansen Basin.

The conditions of the BSBW are set in the Barents Sea by cooling and some freshening (with sea ice melt) and by mixing with the Norwegian Coastal Current resulting in a large density range. The BSBW contributes to shelf slope convection [*Schauer et al*., 2002], which facilitates efficient surface-to-deep ocean ventilation all from the halocline to about 2000 m depth. In the deep Arctic Ocean, the BSBW flows to the east making it the main source of the intermediate waters of the Amundsen Basin, as well as the Makarov Basin [*Rudels et al*., 2013]. The flow of the BSBW forces the FSBW to turn around north of the Laptev Sea along the south side of the Gakkel Ridge and thereby mainly confines it to the Nansen Basin [e.g., *Jones et al*., 1995; *Rudels et al*., 2013].

The rate of increase of DIC in the surface waters of the Norwegian Atlantic Current (NwAC) at 66°N was 1.3 ± 0.7 μmol kg^{-1} yr^{-1} during the period 2001–2007 [*Skjelvan et al*., 2008]. Correcting for biogeochemical transformation, these authors computed the annual increase of C_{ant} to be ~1 μmol kg^{-1} at 200–400 m depth. Furthermore, *Olsen et al*. [2006] estimated C_{ant} to increase in the West Spitsbergen Current (WSC) at a rate of 0.57–0.67 μmol kg^{-1} yr^{-1} during the time period 1981–2002/2003. The surface water pCO_2 increase in the Barents Sea largely follows the atmospheric record [*Omar et al*., 2003], which means that the C_{ant} concentration increases correspondingly. The atmospheric growth rate of CO_2 at Mount Zeppelin, Ny Ålesund (1993–2012) corresponds to a time trend in DIC of 0.8 μmol kg^{-1} yr^{-1}, as computed for waters with the alkalinity, salinity, and temperature properties of the Amundsen Basin AAW at equilibrium with the atmosphere (Figure 5).

The DIC increases at rates of 0.9 and 0.8 μmol kg^{-1} yr^{-1} within the AAW and dAAW, respectively, in the Amundsen Basin. Considering the uncertainties of these rates (Table 6) they are equal to the C_{ant} growth rate of the Barents Sea (formation region of Amundsen and Makarov Basins waters) and slightly higher than the C_{ant} changes in the WSC (formation region of Nansen Basin waters) estimated by *Olsen et al*. [2006], but smaller than the C_{ant} trends in the NwAC (preformation region of all investigated waters) [*Skjelvan et al*., 2008]. In all other of our investigated water masses, the C_{ant} increase is about the same or less than that of the WSC [*Olsen et al*., 2006].

The changes within the Makarov Basin were in the same range as those in the Nansen Basin, especially within the Atlantic layers. However, the origin of these water masses is more complex than in the Nansen and Amundsen Basins. Waters of different origin with different signatures contribute in unknown proportions to the Atlantic and intermediate layers. This includes water from the Atlantic Ocean that enters over the Lomonosov Ridge and waters from the Pacific Ocean that are modified on the shelf leading to shelf plumes penetrating into different water depths.

3.3.3.2. Relation Between Anthropogenic CO_2 and the Source Water CO_2

Our trends in DIC are of the same size or lower than the increase in C_{ant} of the source waters. How realistic is this in view of the mixing regime of the water masses?

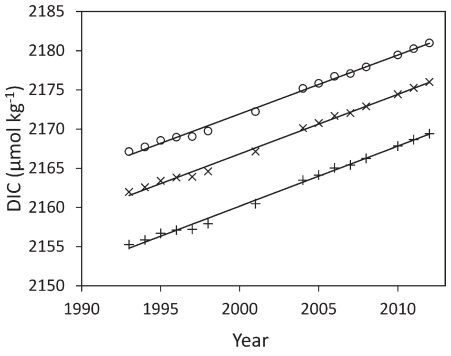

Figure 5. The estimated increase in DIC based on the annual average atmospheric CO_2 content at Mount Zeppelin, Ny Ålesund (Mount Zeppelin, Ny Ålesund, 1989–2012/1993–2012; H.-C. Hansson, personal communication 2013) and average properties of salinity, temperature, TA, phosphate, and silicate, within the AAW (+), dAAW (x), and uPDW (circle) of the Amundsen Basin, using CO2SYS [*van Heuven et al.*, 2011]. Slope coefficients, R^2, and p values for the different regression lines are for AAW 0.77 μmol kg^{-1} yr^{-1}, 0.995, and 0.00; for dAAW 0.76 μmol kg^{-1} yr^{-1}, 0.995, and 0.00; and for uPDW 0.75 μmol kg^{-1} yr^{-1}, 0.995, and 0.00.

While the boundary current around the Arctic Ocean continental margins and ridges is relatively confined and thus can be represented by a freight train model, horizontal mixing, e.g., by eddies becomes more important toward the basin interior. This means that the evolution of C_{ant} in the inflow regions likely cannot directly represent the evolution in the basins, but rather a realistic model approach has to be taken. Volume transports of the inflowing waters of 2–4 Sv [e.g., *Tsubouchi et al.*, 2012] give residence times of around 20 years for the Atlantic layers of the Nansen and Amundsen Basins, with the exact result depending on how much water enters the individual layers and basins. A simple box model illustrates the DIC evolution for a constant rate of C_{ant} increase (corresponding to the atmospheric increase at Ny Ålesund) in the inflowing water (Figure 6). As seen from the model result, the rate of DIC increase in the basin is close to our basin observations but lags by approximately 10–30 years, as seen when comparing the rates of Figures 5 and 6. However, as the rate of increase in atmospheric pCO_2 has been fairly constant for several decades this lag is not relevant for the period of observation. Hence, assuming a corresponding consistent rate of increase in surface water DIC, we conclude that our modeled rate of increase of DIC gives a good approximation of reality.

A further increase in the DIC temporal trend would occur if the ventilation rate has increased during the period of our study. This would be seen in deviations from a straight line in the slope of DIC (Figures 3a–3c). A slight deviation is observed but this is within the data precision.

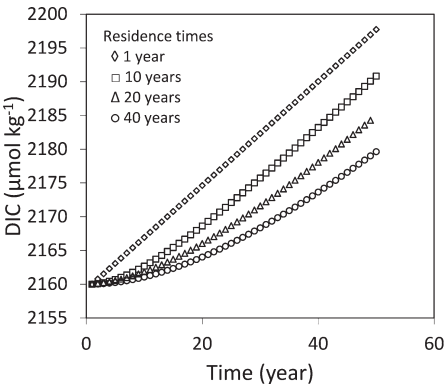

Figure 6. Time evolution of DIC in a simple box model where water of increasing DIC concentration, 0.77 μmol kg^{-1} yr^{-1}, is entering the box. Four different residence times of water in the box is presented.

4. Summary and Conclusions

Observations of DIC in the central Arctic Ocean (Nansen, Amundsen, and Makarov Basins) reveal significant temporal trends in the Atlantic and intermediate layers during the period from 1991 to 2011. The rates of change are between 0.6 and 0.9 μmol kg^{-1} yr^{-1} in the Atlantic layers and between 0.4 and 0.6 μmol kg^{-1} in the uPDW.

The increase in the column inventory of DIC of the Atlantic and intermediate layers is estimated to be between 0.6 and 0.9 mol C m^{-2} yr^{-1} in the different basins. No statistically significant trend is detected in deep water DIC over this time period. Neither is any significant trend detected in nutrients (both phosphate and nitrate) throughout the intermediate water column as well as within the deep water indicating minimal impact by biogeochemical processes. A change in AOU

is found between the cruises in the deep waters, which can, however, not be explained by information available.

If the increase in the AOU data reflects the true situation, the deep waters are not in steady state. Potential reasons for an increase in AOU are either a decrease in the ventilation of the deep waters, an increase in the organic matter sedimentation rate, or an increase in a flux of reduced chemical compounds from the Gakkel Ridge. All but the last should also result in an increase in nutrients and DIC. Changes in the summer sea ice coverage has been suggested to increase primary production and thus potentially also the sedimentation of organic matter. More open water in the fall can also potentially increase brine production leading to ventilation of subsurface waters, but the lowering of salinity by sea ice melt has the opposite effect by stabilizing the water column thus hampering ventilation. However, the change in summer sea ice coverage over the deep central basins is a relatively recent feature and it is highly unlikely that it can contribute to a change starting in the early 1990s. On the other hand, is it well known that deep water formation in the Greenland Sea more or less stopped in the 1990s [e.g., *Rudels et al.*, 2012b] and it is also known that the deep waters of the Arctic Ocean is renewed by inflow from the Norwegian Sea [e.g., *Bönisch and Schlosser*, 1995]. These inflowing waters are a mixture of outflowing Arctic Ocean deep waters and Greenland Sea deep water. A decrease in Greenland Sea deep water could result in an increase in AOU of the Arctic Ocean deep water. Further research like thorough data mining with modeling exercise including the Nordic Seas is necessary to test this potential assumption.

Because of lack of time trends in the nutrient concentrations, illustrating absence of changes in mineralization of organic matter, the DIC increase is most likely of anthropogenic origin. The time trends agree reasonably well with C_{ant} changes in the inflowing waters of the NwAC and the WSC. As a result of the increases in DIC, the pH is reduced by 0.02–0.05 units during the last two decades. If these trends continue, the Atlantic layers of the Arctic Ocean will start to become undersaturated with respect to aragonite in less than 100 years. As extensive biological life occurs in this water, especially before entering the Arctic Ocean, this will have vital consequences for their living conditions.

The observed changes in primary production and specifically in the sedimentation of ice algae will most likely result in increased AOU, nutrients as well as DIC in the future. If the mean sedimentation rate of 9 g C m^{-2} [*Boetius et al.*, 2013] is sustained annually and if most of it will decay and be added to the overlying water it can be observed within a short time. The resulting annual increase will if mixed within a 100 m thick layer be -9, 7, 1, and 0.1 μmol kg^{-1} in O_2, DIC, nitrate, and phosphate, respectively. However, it is highly unlikely that such a high spatial average sedimentation rate can be sustained by the supply of nutrients in the present Arctic Ocean.

Acknowledgments

We are grateful to K.-U. Ludwichowski and C. Burau for nutrient measurements and A. Wisotzki for oxygen probe calibration on board RV Polarstern in 2011. Measurements of DIC and TA during ARK-XXII2 were performed by S. Ober (NIOZ, Texel). The CO_2 data from Mount Zeppelin, Svalbard were provided by B. Noone and H.-C. Hansson, Department of Applied Environmental Science, Stockholm University. The atmospheric measurements are supported by the Swedish Environmental Protection Agency within its environmental monitoring program. Financial support was received from the Swedish Research Council (contract 621-2010-4084) and the European Union FP7 project CarboChange (under grant agreement 264879).

References

Anderson, L. G., E. P. Jones, and B. Rudels (1999), Ventilation of the Arctic Ocean estimated by a plume entrainment model constrained by CFCs, *J. Geophys. Res.*, *104*(C6), 13,423–13,429.

Anderson, L. G., E. P. Jones, and J. H. Swift (2003), Export production in the central Arctic Ocean evaluated from phosphate deficits, *J. Geophys. Res.*, *108*(C6), 3199, doi:10.1029/2001JC001057.

Anderson, L. G., E. Falck, E. P. Jones, S. Jutterström, and J. H. Swift (2004), Enhanced uptake of atmospheric CO_2 during freezing of seawater: A field study in Storfjorden, Svalbard, *J. Geophys. Res.*, *109*, C06004, doi:10.1029/2003JC002120.

Arrigo, K. R., and G. L. van Dijken (2011), Secular trends in Arctic Ocean net primary production, *J. Geophys. Res.*, *116*, C09011, doi:10.1029/2011JC007151.

Arrigo, K. R., P. A. Matrai, and G. L. van Dijken (2011), Primary productivity in the Arctic Ocean: Impacts of complex optical properties and subsurface chlorophyll maxima on large-scale estimates, *J. Geophys. Res.*, *116*, C11022, doi:10.1029/2011JC007273.

Årthun, M., R. B. Ingvaldsen, L. H. Smedsrud, and C. Schrum (2011), Dense water formation and circulation in the Barents Sea, *Deep Sea Res., Part I*, *58*, 801–817, doi:10.1016/j.dsr.2011.06.001.

Ballantyne, A. P., C. B. Alden, J. B. Miller, P. P. Tans, and J. W. C. White (2012), Increase in observed net carbon dioxide uptake by land and oceans during the past 50 years, *Nature*, *488*, 70–72, doi:10.1038/nature11299.

Bates, N. R., and J. T. Mathis (2009), The Arctic Ocean marine carbon cycle: Evaluation of air-sea CO_2 exchanges, ocean acidification impacts and potential feedbacks, *Biogeosciences*, *6*(11), 2433–2459.

Boetius, A., et al. (2013), Export of algal biomass from the melting Arctic sea ice, *Science*, *339*(6126), 1430–1432, doi:10.1126/science.1231346.

Bönisch, G., and P. Schlosser (1995), Deep water formation and exchange rates in the Greenland/Norwegian Sea and the Eurasian Basin of the Arctic Ocean derived from tracer data, *Prog. Oceanogr.*, *35*, 29–52.

Cai, P., M. R. van der Loeff, I. Stimac, E.-M. Nöthig, K. Lepore, and S. B. Moran (2010), Low export flux of particulate organic carbon in the central Arctic Ocean as revealed by ^{234}Th:^{238}U disequilibrium, *J. Geophys. Res.*, *115*, C10037, doi:10.1029/2009JC005595.

Clayton, T. D., and R. H. Byrne (1993), Spectrophotometric seawater pH measurements: Total hydrogen ion concentration scale calibration of *m*-cresol purple and at-sea results, *Deep Sea Res., Part I*, *40*(10), 2115–2129.

Codispoti, L. A., V. Kelly, A. Thessen, P. Matrai, S. Suttles, V. Hill, M. Steele, and B. Light (2013), Synthesis of primary production in the Arctic Ocean: III. Nitrate and phosphate based estimates of net community production, *Prog. Oceanogr., 110*, 126–150.

Dickson, A. G., and F. J. Millero (1987), A comparison of the equilibrium constants for the dissociation of carbonic acid in seawater media, *Deep Sea Res., Part A, 34*(10), 1733–1743.

Dickson, A. G., C. L. Sabine, and J. R. Christian (Eds.) (2007), *Guide to Best Practices for Ocean CO_2 Measurements, PICES Special Publication*, vol. 3, 191 pp.

Else, B. G. T., T. N. Papakyriakou, R. J. Galley, W. M. Drennan, L. A. Miller, and H. Thomas (2011), Wintertime CO_2 fluxes in an Arctic polynya using eddy covariance: Evidence for enhanced air-sea gas transfer during ice formation, *J. Geophys. Res., 116*, C00G03, doi:10.1029/2010JC006760.

Gordon, L. I., J. C. Jennings, Jr., A. A. Ross, and J. M. Krest (1994), A suggested protocol for continuous flow automated analysis of seawater nutrients (phosphate, nitrate, nitrite and silicic acid) in the WOCE Hydrographic Program and the Joint Global Ocean Fluxes Study, in *WOCE Operations Manual*, WHP Off. Rep. WHPO 91-1, WOCE Rep. 68/91, rev. 1, Woods Hole, Mass.

Haraldsson, C., L. G. Anderson, M. Hassellöv, S. Hulth, and K. Olsson (1997), Rapid, high-precision potentiometric titration of alkalinity in ocean and sediment pore waters, *Deep Sea Res., Part I, 44*(12), 2031–2044.

Harms, I. H. (1997), Water mass transformation in the Barents Sea—Application of the Hamburg Shelf Ocean Model (HamSOM), *ICES J. Mar. Sci., 54*, 351–365.

Jakobsson, M., J. Backman, A. Murray, and R. Løvlie (2003), Optically Stimulated Luminescence dating supports central Arctic Ocean cm-scale sedimentation rates, *Geochem. Geophys. Geosyst., 4*, 1016, doi:10.1029/2002GC000423.

Johansson, O., and M. Wedborg (1982), On the evaluation of potentiometric titrations of sea-water with hydrochloric-acid, *Oceanol. Acta, 5*(2), 209–218.

Johnson, K. M., J. M. Sieburth, P. J. L. Williams, and L. Brändström (1987), Coulometric total carbon dioxide analysis for marine studies: Automation and calibration, *Mar. Chem., 21*, 117–133.

Jones, E. P., B. Rudels, and L. G. Anderson (1995), Deep waters of the Arctic Ocean: Origins and circulation, *Deep Sea Res., Part I, 42*, 737–760.

Jutterström, S., and L. G. Anderson (2005), The saturation of calcite and aragonite in the Arctic Ocean, *Mar. Chem., 94*, 101–110.

Jutterström, S., and L. G. Anderson (2010), Uptake of CO_2 by the Arctic Ocean in a changing climate, *Mar. Chem., 122*, 96–104, doi:10.1016/j.marchem.2010.07.002.

Jutterström, S., L. G. Anderson, N. R. Bates, R. Bellerby, T. Johannessen, E. P. Jones, R. M. Key, X. Lin, A. Olsen, and A. M. Omar (2010), Arctic Ocean data in CARINA, *Earth Sys. Sci. Data, 2*, 71–78.

Key, R. M., T. Tanhua, A. Olsen, M. Hoppema, S. Jutterström, C. Schirnick, S. van Heuven, A. Kozyr, X. Lin, A. Velo, D. W. R. Wallace, and L. Mintrop (2010), The CARINA data synthesis project: Introduction and overview, *Earth Sys. Sci. Data, 2*, 105–121.

Korhonen, M., B. Rudels, M. Marnela, A. Wisotzki, and J. Zhao (2012), Time and space variability of freshwater content, heat content and seasonal ice melt in the Arctic Ocean from 1991 to 2011, *Ocean Sci. Discuss., 9*, 2621–2677, doi:10.5194/osd-9-2621-2012.

Laxon, S. W., et al. (2013), CryoSat-2 estimates of Arctic sea ice thickness and volume, *Geophys. Res. Lett., 40*, 732–737, doi:10.1002/grl.50193.

Lenton, A., N. Metzl, T. Takahashi, M. Kuchinke, R. J. Matear, T. Roy, S. C. Sutherland, C. Sweeney, and B. Tilbrook (2012), The observed evolution of oceanic pCO_2 and its drivers over the last two decades, *Global Biogeochem. Cycles, 26*, GB2021, doi:10.1029/2011GB004095.

Le Quéré, C., et al. (2009), Trends in the sources and sinks of carbon dioxide, *Nat. Geosci., 2*, 831–836, doi:10.1038/ngeo689.

Li, W. K. W., F. A. McLaughlin, C. Lovejoy, and E. C. Carmack (2009), Smallest algae thrive as the Arctic Ocean freshens, *Science, 326*(5952), 539, doi:10.1126/science.1179798.

Marnela, M., B. Rudels, K. A. Olsson, L. G. Anderson, E. Jeansson, D. J. Torres, M.-J. Messias, J. H. Swift, and A. J. Watson (2008), Transports of Nordic Seas water masses and excess SF_6 through Fram Strait to the Arctic Ocean, *Prog. Oceanogr., 78*, 1–11, doi:10.1016/j.pocean.2007.06.004.

Mauritzen, C. (1996), Production of dense overflow waters feeding the North Atlantic across the Greenland-Scotland Ridge. Part 1: Evidence for a revised circulation scheme, *Deep Sea Res., Part I, 43*(6), 769–806, doi:10.1016/0967-0637(96)00037-4.

Mehrbach, C., C. H. Culberson, J. E. Hawley, and R. M. Pytkowicz (1973), Measurement of the apparent dissociation constants of carbonic acid in seawater at atmospheric pressure, *Limnol. Oceanogr., 18*(6), 897–907.

Mintrop, L., F. F. Perez, M. Gonzalez-Davila, M. J. Santana-Casiano, and A. Kortzinger (2000), Alkalinity determination by potentiometry: Intercalibration using three different methods, *Cienc. Mar. 26*(1), 23–37.

Olsen, A., et al. (2006), Magnitude and origin of the anthropogenic CO_2 increase and ^{13}C Suess effect in the Nordic seas since 1981, *Global Biogeochem. Cycles, 20*, GB3027, doi:10.1029/2005GB002669.

Omar, A. M., T. Johannessen, S. Kaltin, and A. Olsen (2003), Anthropogenic increase of oceanic pCO_2 in the Barents Sea surface water, *J. Geophys. Res., 108*(C12), 3388, doi:10.1029/2002JC001628.

Omar, A. M., T. Johannessen, R. G. J. Bellerby, A. Olsen, S. Kaltin, C. Kivimae, and L. G. Anderson (2005), Sea ice and brine formation in Storfjorden: Implications for the uptake of atmospheric CO_2 in future Arctic Ocean, in *The Nordic Seas: An Integrated Perspective, AGU Monogr. Ser.*, vol. 158, edited by H. Drange et al., pp. 177–188, AGU, Washington, D. C.

Polyakov, I. V., et al. (2010), Arctic Ocean warming contributes to reduced polar ice cap, *J. Phys. Oceanogr., 40*, 2743–2756, doi:10.1175/2010JPO4339.1.

Redfield, A. C., B. H. Ketchum, and F. A. Richards (1963), The influence of organisms on the composition of sea-water, in *The Sea: Ideas and Observations on the Progress in the Study of the Seas*, vol. 2, edited by M. N. Hill, pp. 26–77, Interscience, New York.

Revelle, R. (1983), The oceans and the carbon dioxide problem, *Oceanus, 26*, 3–9.

Riebesell, U., K. G. Schulz, R. G. J. Bellerby, M. Botros, P. Fritsche, M. Meyerhöfer, C. Neill, G. Nondal, A. Oschlies, J. Wohlers, and E. Zöllner (2007), Enhanced biological carbon consumption in a high CO_2 ocean, *Nature, 450*, 545–548, doi:10.1038/nature062672007.

Rudels, B., L. G. Anderson, and E. P. Jones (1996), Formation and evolution of the surface mixed layer and halocline of the Arctic Ocean, *J. Geophys. Res., 101*(C4), 8807–8821.

Rudels, B., G. Björk, J. Nilsson, P. Winsor, I. Lake, and C. Nohr (2005), The interaction between waters from the Arctic Ocean and the Nordic Seas north of Fram Strait and along the East Greenland Current: Results from the Arctic Ocean-02 Oden expedition, *J. Mar. Syst., 55*, 1–30, doi:10.1016/j.jmarsys.2004.06.00.

Rudels, B., L. G. Anderson, P. Eriksson, E. Fahrback, M. Jakobsson, E. P. Jones, H. Melling, S. Prinsenberg, U. Schauer, and T. Yao (2012a), Observations in the ocean, in *Arctic Climate Change: The ACSYS Decade and Beyond, Atmos. Oceanogr. Sci. Libr.*, vol. 43, edited by P. Lemke and H.-W. Jacobi, pp. 117–198, doi:10.1007/978-94-007–2027-5_4. © Springer Science + Business Media B.V., pp. 117–198.

Rudels, B., M. Korhonen, G. Budéus, A. Beszczynska-Möller, U. Schauer, A. Nummelin, D. Quadfasel, and H. Valdimarsson (2012b), The East Greenland Current and its impacts on the Nordic Seas: Observed trends in the past decade, *ICES J. Mar. Sci.*, *69*, 841–851.

Rudels, B., U. Schauer, G. Björk, M. Korhonen, S. Pisarev, B. Rabe, and A. Wisotzki (2013), Observations of water masses and circulation with focus on the Eurasian Basin of the Arctic Ocean from the 1990s to the late 2000s, *Ocean Sci.*, *9*, 147–169, doi:10.5194/os-9–147-2013.

Rysgaard, S., J. Bendtsen, B. Delille, G. S. Dieckmann, R. N. Glud, H. Kennedy, J. Mortensen, S. Papadimitriou, D. N. Thomas, and J.-L. Tison (2011), Sea ice contribution to the air-sea CO_2 exchange in the Arctic and Southern Oceans, *Tellus, Ser. B*, *63B*, 823–830, doi:10.1111/j.1600-0889.2011.00571.x.

Sabine, C. L., R. A. Feely, F. J. Millero, A. G. Dickson, C. Langdon, S. Mecking, and D. Greeley (2008), Decadal changes in Pacific carbon, *J. Geophys. Res.*, *113*, C07021, doi:10.1029/2007JC004577.

Schauer, U., B. Rudels, E. P. Jones, L. G. Anderson, R. D. Muench, G. Björk, J. H. Swift, V. Ivanov, and A.-M. Larsson (2002), Confluence and redistribution of Atlantic water in the Nansen, Amundsen and Makarov basins, *Ann. Geophys.*, *20*, 257–273, doi:10.5194/angeo-20–257-2002.

Schuster, U., A. J. Watson, N. R. Bates, A. Corbiere, M. Gonzalez-Davila, N. Metzl, D. Pierrot, and M. Santana-Casiano (2009), Trends in North Atlantic sea-surface fCO_2 from 1990 to 2006, *Deep Sea Res., Part II*, *56*, 620–629, doi:10.1016/j.dsr2.2008.12.011.

Serreze, M. C., and J. A. Francis (2006), The Arctic amplification debate, *Clim. Change*, *76*, 241–264, doi:10.1007/s10584-005-9017-y.

Skjelvan, I., E. Falck, F. Rey, and S. B. Kringstad (2008), Inorganic carbon time series at Ocean Weather Station M in the Norwegian Sea, *Biogeosciences*, *5*, 549–560.

Stroeve, J., M. M. Holland, W. Meier, T. Scambos, and M. Serreze (2007), Arctic sea ice decline: Faster than forecast, *Geophys. Res. Lett.*, *34*, L09501, doi:10.1029/2007GL029703.

Stroeve, J. C., M. C. Serreze, M. M. Holland, J. E. Kay, J. Malanik, and A. P. Barrett (2012), The Arctic's rapidly shrinking sea ice cover: A research synthesis, *Clim. Change*, *110*, 1005–1027, doi:10.1007/s10584-011-0101-1.

Tanhua, T., E. P. Jones, E. Jeansson, S. Jutterström, W. M. Smethie Jr., D. W. R. Wallace, and L. G. Anderson (2009), Ventilation of the Arctic Ocean: Mean ages and inventories of anthropogenic CO_2 and CFC-11, *J. Geophys. Res.*, *114*, C01002, doi:10.1029/2008JC004868.

Tremblay, J.-É., and J. Gagnon (2009), The effects of irradiance and nutrient supply on the productivity of Arctic waters: A perspective on climate change, in *Influence of Climate Change on the Changing Arctic and Sub-Arctic Conditions*, edited by J. C. J. Nihoul and A. G. Kostianoy, pp. 73–93, Springer, New York.

Tsubouchi, T., S. Bacon, A. C. Naveira Garabato, Y. Aksenov, S. W. Laxon, E. Fahrbach, A. Beszczynska-Möller, E. Hansen, C. M. Lee, and R. B. Ingvaldsen (2012), The Arctic Ocean in summer: A quasi-synoptic inverse estimate of boundary fluxes and water mass transformation, *J. Geophys. Res.*, *117*, C01024, doi:10.1029/2011JC007174.

van Heuven, S., D. Pierrot, J. W. B. Rae, E. Lewis, and D. W. R. Wallace (2011), MATLAB program developed for CO2 system calculations, *Rep. ORNL/CDIAC-105b*, Carbon Dioxide Inf. Anal. Cent., Oak Ridge, Tenn., doi:10.3334/CDIAC/otg.CO2SYS_MATLAB_v1.1.

II

Biogeosciences, 14, 1811–1823, 2017
www.biogeosciences.net/14/1811/2017/
doi:10.5194/bg-14-1811-2017

Biogeosciences Open Access EGU

Export of calcium carbonate corrosive waters from the East Siberian Sea

Leif G. Anderson[1], Jörgen Ek[2], Ylva Ericson[3], Christoph Humborg[2,4], Igor Semiletov[5,6,7], Marcus Sundbom[2], and Adam Ulfsbo[1,8]

[1]Department of Marine Sciences, University of Gothenburg, 412 96 Gothenburg, Sweden
[2]Baltic Sea Centre, Stockholm University, 106 91 Stockholm, Sweden
[3]The University Centre in Svalbard, Pb 156, 9171 Longyearbyen, Norway
[4]Department of Environmental Science and Analytical Chemistry, Stockholm University, 106 91 Stockholm, Sweden
[5]International Arctic Research Center, University Alaska Fairbanks, Fairbanks, AK 99775, USA
[6]Pacific Oceanological Institute, Russian Academy of Sciences Far Eastern Branch, Vladivostok 690041, Russia
[7]The National Research Tomsk Polytechnic University, Tomsk, Russia
[8]Division of Earth and Ocean Sciences, Nicholas School of the Environment, Duke University, Durham, NC 27704, USA

Correspondence to: Leif G. Anderson (leif.anderson@marine.gu.se)

Received: 7 November 2016 – Discussion started: 15 November 2016
Revised: 21 February 2017 – Accepted: 13 March 2017 – Published: 5 April 2017

Abstract. The Siberian shelf seas are areas of extensive biogeochemical transformation of organic matter, both of marine and terrestrial origin. This in combination with brine production from sea ice formation results in a cold bottom water of relative high salinity and partial pressure of carbon dioxide (pCO_2). Data from the SWERUS-C3 expedition compiled on the icebreaker *Oden* in July to September 2014 show the distribution of such waters at the outer shelf, as well as their export into the deep central Arctic basins. Very high pCO_2 water, up to ~ 1000 µatm, was observed associated with high nutrients and low oxygen concentrations. Consequently, this water had low saturation state with respect to calcium carbonate down to less than 0.8 for calcite and 0.5 for aragonite. Waters undersaturated in aragonite were also observed in the surface in waters at equilibrium with atmospheric CO_2; however, at these conditions the cause of undersaturation was low salinity from river runoff and/or sea ice melt. The calcium carbonate corrosive water was observed all along the continental margin and well out into the deep Makarov and Canada basins at a depth from about 50 m depth in the west to about 150 m in the east. These waters of low aragonite saturation state are traced in historic data to the Canada Basin and in the waters flowing out of the Arctic Ocean north of Greenland and in the western Fram Strait, thus potentially impacting the marine life in the North Atlantic Ocean.

1 Introduction

The decrease in pH in the ocean as a result of uptake of anthropogenic carbon dioxide (CO_2) from the atmosphere is noted ocean acidification (e.g. Doney et al., 2009). The change in pH caused by the increase in partial pressure of CO_2 (pCO_2) from about 280 µatm in preindustrial times to about 400 µatm today is in the order of 0.1 pH unit. A continued usage of fossil fuels at the present rate has been projected to lead to an atmospheric level of close to 1000 µatm at the end of this century, resulting in a further decrease in pH by about 0.3 units in oceanic surface waters (e.g. Orr et al., 2005). Changes in pH of this range will likely impact the marine ecosystem as well as society (e.g. Gattuso et al., 2015).

Biogeochemical processes in the Arctic Ocean can have a much greater impact on ocean acidification than that of anthropogenic CO_2 (Anderson et al., 2009, 2011). Investigation of the East Siberian shelf area illustrates the substantial impact of organic matter decay on lowering pH and thus also the calcium carbonate saturation state (Semiletov et al.,

2016). The corrosive shelf water spreads far out into the deep central Arctic Ocean at a depth centred around 150 m and potentially further into the North Atlantic Ocean (Azetsu-Scott et al., 2010). Here it can have negative effects on aragonite-shelled pelagic organisms like the pteropods (e.g. Comeau et al., 2010), which are important in the Arctic Ocean and North Atlantic food web.

The Arctic Ocean is one of the oceans that experience the lowest natural pH, a result of the high gas solubility in cold waters. On the other hand, the change in pH for a given increase in pCO_2 is less in cold waters than in warm, as the buffer capacity for CO_2 is less. However, there are several other processes than air–sea exchange of CO_2 that impact pH of Arctic waters. Some Arctic shelf seas, such as the Chukchi Sea and the Barents Sea, are among the most productive of the world oceans and as such experience large natural seasonal variability in pCO_2 and pH. One consequence of the high primary productivity is low pCO_2 in the inflow shelf seas (Carmack and Wassmann, 2006; Pipko et al., 2002) is that the surface waters of the central Arctic Ocean are largely undersaturated in CO_2 (Jutterström and Anderson, 2010). This is a result of the waters being covered by sea ice that hampers air–sea flux, before the atmospheric exchange compensates for the CO_2 taken up by the phytoplankton. Decreased summer sea ice cover in the central Arctic Ocean will likely reduce this effect and adjust the surface water closer to atmospheric equilibrium.

Increased pCO_2 levels decrease carbonate ion (CO_3^{2-}) concentrations, which also reduces the solubility of calcium carbonate crystals, illustrated by the reaction

$$CaCO_3(s) \leftrightarrows Ca^{2+} + CO_3^{2-}, \quad (1)$$

where the solubility is determined by the chemical solubility product, K_{so}, which is the product of the calcium and carbonate ion concentrations at chemical equilibrium, i.e. $K_{so} = [Ca^{2+}]^{equilibrium} \times [CO_3^{2-}]^{equilibrium}$. In the ocean K_{so} is dependent on temperature, salinity and pressure. To determine whether the conditions are such that the water is supersaturated or undersaturated with respect to calcium carbonate, one often uses the saturation state, Ω.

$$\Omega = \frac{[Ca^{2+}]^{observed} \times [CO_3^{2-}]^{observed}}{K_{so}} \quad (2)$$

Hence, if Ω is less than 1 the water is undersaturated, and if greater than 1 it is supersaturated.

Calcium carbonate crystals can have different structures, each with a specific K_{so}. The most common are calcite and aragonite, but in cold environments like sea ice ikaite can also form (e.g. Dieckmann et al., 2008). Calcite and aragonite are mainly formed by biological calcification, where calcium carbonate is produced as part of an organism's structure. Even if the crystals are built up of carbonate ions it is in most cases hydrogen carbonate ions (HCO_3^-) that are extracted by the organisms from seawater and converted to CO_3^{2-} internally (e.g. Findlay et al., 2011). Thus, there might not be a direct coupling between the biological formation rate of $CaCO_3$ minerals and ocean acidification. Instead it has been suggested that it is the ratio of HCO_3^- to H^+ that controls the biotic $CaCO_3$ precipitation (Bach, 2015), or more directly the increase in H^+ (Cyronak et al., 2016). However, the opposite reaction, i.e. dissolution of $CaCO_3$ minerals, is influenced by ocean acidification through the chemical solubility product, at least as long as the crystals are directly exposed to seawater.

Among the biologically produced calcium carbonates, aragonite is more soluble than calcite, making the former more sensitive to ocean acidification. During biological formation of calcite, magnesium can be incorporated instead of calcium, which increases the solubility; the higher the content of magnesium, the higher the solubility (e.g. Haese et al., 2014). High-magnesium calcite has a higher solubility than aragonite, making this the most sensitive form. A range of these mineral forms are produced by organisms living in the Arctic Ocean. Among those producing aragonite skeletons are cold-water corals and pteropods, while most benthic organisms tend to produce a larger fraction of calcite. Consequently, there is a substantial diversity in the biological produced $CaCO_3$ minerals and thus also different sensitivities to ocean acidification.

The very large shelf areas north of Siberia are heavily impacted by river input, adding fresh water and chemical constituents. The direct addition of high pCO_2 runoff together with biochemical processes such as primary production and decay of organic matter, of both marine and terrestrial origin, strongly impact the calcium carbonate saturation state. The distribution of this specific water characteristic on the shelf as well as its export into, and circulation within, the deep basins is determined by the atmospheric pressure field that drives the oceanic currents (e.g. Jahn et al., 2010; Pipko et al., 2011).

In this contribution we show the importance of the Siberian shelves in producing calcium carbonate undersaturated waters that spread out into the deep Arctic Ocean and further towards the Atlantic Ocean. The processes behind the under-saturation are elucidated as well as the flow path of this signature in the Arctic Ocean.

2 Methods

This contribution is based on data that were collected during the SWERUS-C3 (Swedish–Russian–US Arctic Ocean Investigation of Climate-Cryosphere-Carbon Interactions) expedition with the Swedish icebreaker *Oden* along the outer Siberian shelf and covers a longitudinal range between about 125° E and 175° W (see Fig. 1 for station positions). Sampling was intensified across the shelf break along sections (A–F). Furthermore, historic data are used to evaluate how the waters from the Siberian shelf are spread out in the cen-

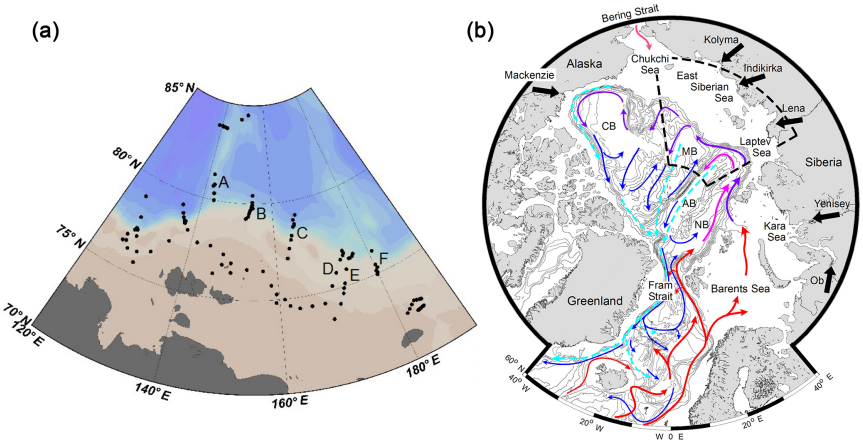

Figure 1. Map illustrating the station locations, with **(a)** sections noted and **(b)** general water mass circulation in the deep Arctic Ocean and its connection to surrounding oceans. The location of map in **(a)** is shown by the dotted insert in map **(b)**.

tral Arctic Ocean and further towards Fram Strait on their way to the North Atlantic Ocean. These include data from north of Greenland collected during the *Oden* 1991 cruise (Anderson et al., 1994), data from the northern Fram strait collected in 2002 (Jutterström et al., 2008), and data from the Canada Basin collected in 2005 (Jones et al., 2008a).

The SWERUS-C3 data were gathered at about 100 stations, occupied between 15 July and 25 September 2014. Water samples were collected using a rosette system equipped with 24 bottles of Niskin type, each having a volume of 7 L. The bottles were closed during the return of the CTD-rosette package from the bottom to the surface and water samples for all constituents were drawn soon after the rosette was secured in the CTD container.

The following constituents are used: dissolved inorganic carbon (DIC) (only stations visited after 24 August), total alkalinity (TA), pH, oxygen, nutrients, and bottle salinity. The order of sampling was determined by the risk of contamination, meaning that oxygen samples were collected first followed by the carbonate system parameters, the nutrients, and salinity. Water samples for salinity were analysed for more than 90 % of the depths and when no data were available the CTD salinity was used. Temperature data were taken from the CTD.

Salinity and temperature data were collected using a Sea-Bird 911+ CTD with dual Sea-Bird temperature (SBE 3), conductivity (SBE 04C) and oxygen sensors (SBE 43) attached to the rosette system. Salinity was calibrated against deep water samples analysed on board using an AUTOSAL 8400B lab salinometer. The salinometer was calibrated using one standard sea water ampoule (IAPSO standard sea water, OSIL Environmental Instruments and Systems) before each batch of 24 samples. The accuracies of the Autosal salinities and CTD salinities were both within ± 0.003 psu and the accuracy for temperature was ± 0.002 °C.

DIC was determined by a coulometric titration method based on Johnson et al. (1987), having a precision of $2\,\mu mol\,kg^{-1}$, estimated from duplicates, with the accuracy set by calibration against certified reference materials (CRM), supplied by A. Dickson, Scripps Institution of Oceanography (USA). TA was determined by automated open-cell potentiometric titration (Haraldsson et al., 1997), precision better than $2\,\mu mol\,kg^{-1}$, with the accuracy set the same way as for DIC. Seawater pH was determined by a spectrophotometric method, based on the absorption ratio of the sulfonephtalein dye, *m*-cresol purple (mCP) (Clayton and Byrne, 1993). Purified mCP (Liu et al., 2011) was purchased from the laboratory of Robert H. Byrne, University of South Florida, USA. The accuracy was estimated to 0.006 from internal consistency calculations of analysed CRM samples and the precision, defined as the absolute mean difference of duplicate samples, was ~ 0.001 pH units.

Oxygen was measured by an automated Winkler titration system giving a precision of $\sim 1\,\mu mol\,kg^{-1}$. The accuracy was set by titrating known amounts of KIO_3 salts that were dissolved in sulfuric acid. As the amount was known to better than 0.1 % the accuracy should be significantly better than the precision. The deviation from saturation concentration was computed as apparent oxygen utilization (AOU) as $[O_2]^{sat} - [O_2]^{measured}$.

Dissolved inorganic nitrogen species (NH_4, $NO_2 + NO_3$), orthophosphate (PO_4) and dissolved silicate were measured on board using a four-channel continuous flow analyser (QuAAtro system, SEAL Analytical). Within each analysis run a calibration was done using standard solutions of NH_4Cl, KNO_3, K_2HPO_4 and a commercial stable silica-

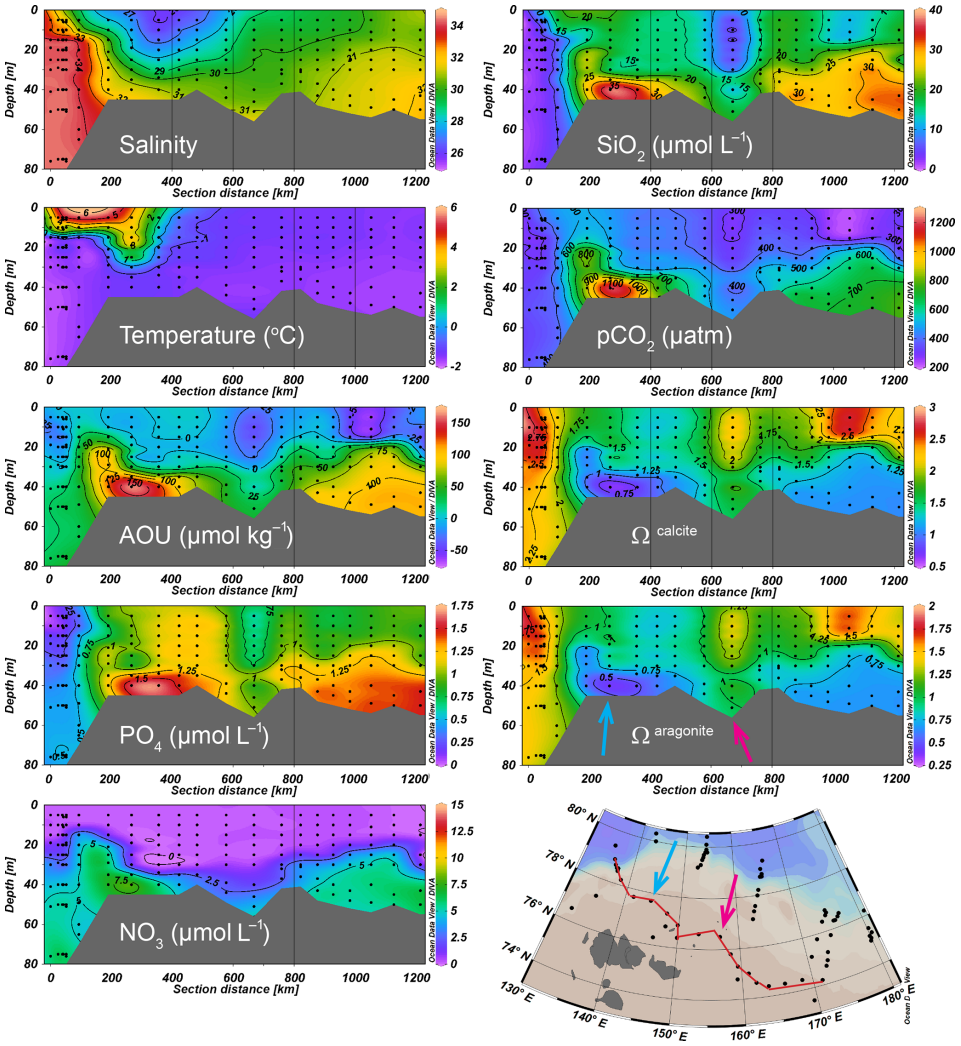

Figure 2. Sections along the outer East Siberian continental shelf as shown by the red line of the map. The location of the minimum in saturation state of calcium carbonate is noted by the blue arrow and the local maximum by the purple arrow.

compound solution. Analysis quality was further assured by automatic drift control using standard solutions and including CRM solutions prepared from commercial ampoules (QC RW1, batch VKI-9-3-0702) in the analysis run. Accuracy expressed as the median deviation of the measurements from the CRM solution for NH_4, $NO_2 + NO_3$ and PO_4 was -0.15, -0.11, and $-0.018\,\mu mol\,L^{-1}$, respectively. The CRM is not certified for silicate. The precision was, based on 28 determinations of standards, 3.7, 1.2, 2.7 and 1.3 % for NH_4, NO_2+NO_3, PO_4 and SiO_4, respectively.

The saturation states of the two major forms of calcium carbonate ($\Omega^{aragonite}$ and $\Omega^{calcite}$) and pCO_2 were calculated from the combination of pH and TA, as well as pH and DIC when the latter was available, using CO2SYS (van Heuven et al., 2011) with the carbonate dissociation constants (K_1 and K_2) of Lueker et al. (2000), the solubility product, K_{so} according to Mucci (1983) and the salinity–calcium ion concentration ratio of Riley and Tongudai (1967). When two computations were performed the reported values are the average of the two calculated for each sample. Input data in-

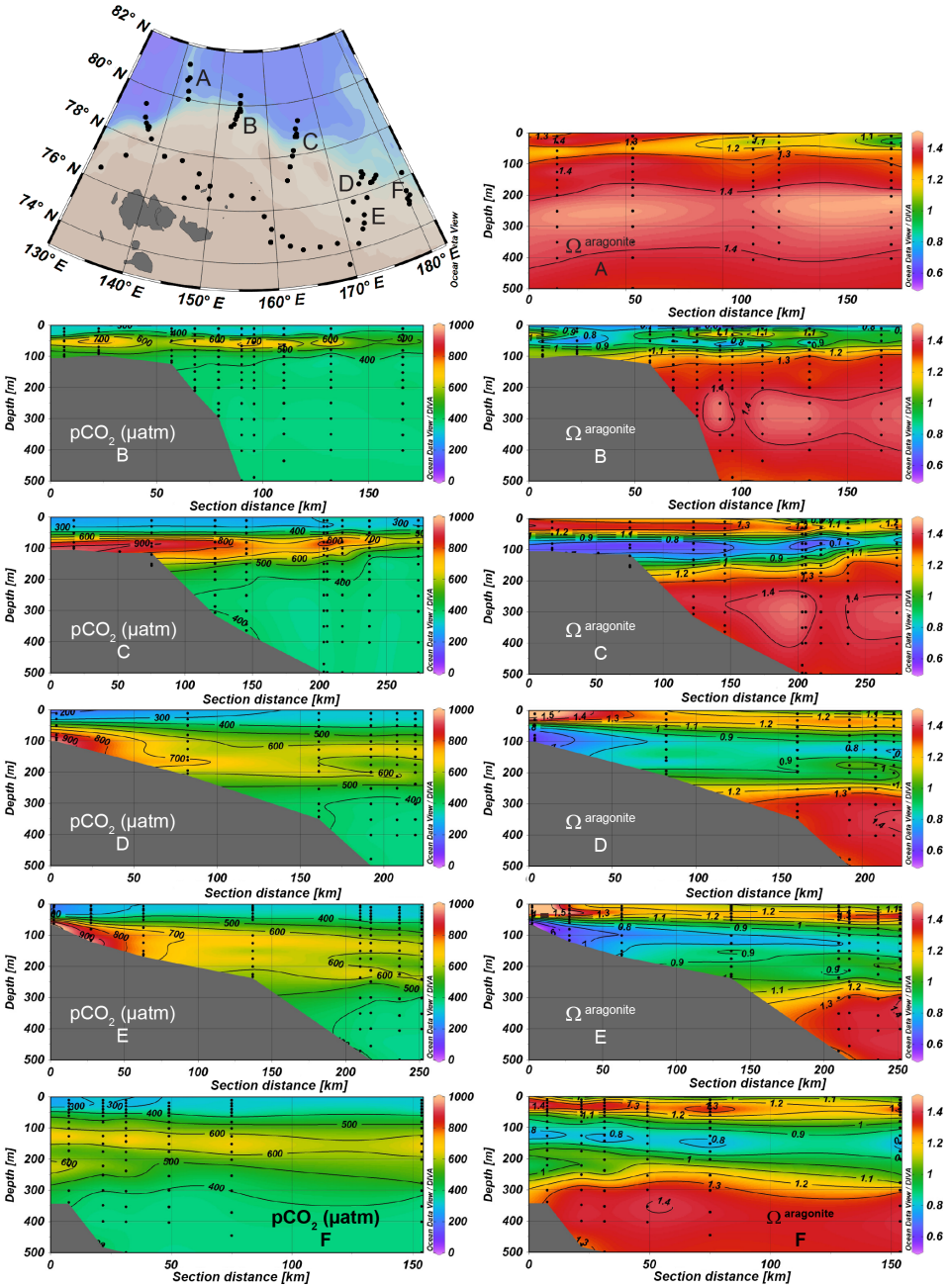

Figure 3. Sections A to F across the East Siberian shelf break, partial pressure of carbon dioxide (pCO_2) to the left and saturation state of aragonite ($\Omega^{aragonite}$) to the right. On all sections the colour scale is from 0 to 1000 µatm for pCO_2 and 0.5 to 1.5 for $\Omega^{aragonite}$. Note the variable horizontal extent of the different sections. The locations of the sections are noted on the inserted map.

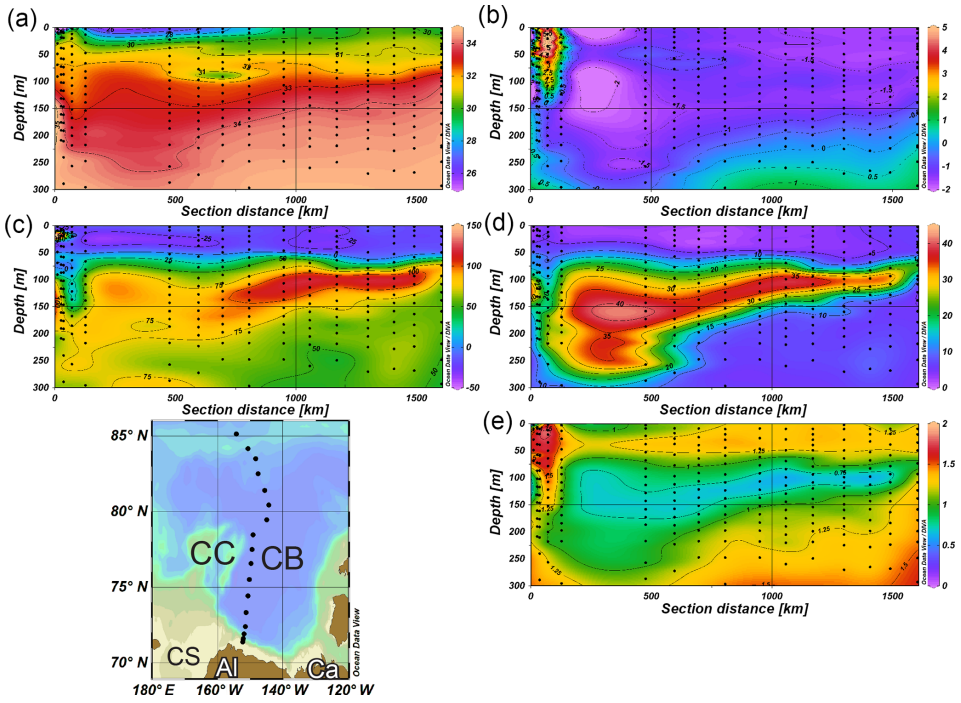

Figure 4. Sections of **(a)** salinity, **(b)** temperature, **(c)** AOU, **(d)** silicate, and **(e)** $\Omega^{\text{aragonite}}$ in the top 300 m across the Canada Basin as observed during the Beringia 2005 expedition. Station positions are noted on the map, with the abbreviations being CB, Canadian Basin; CC, Chukchi Cape; CS, Chukchi Sea; Al, Alaska; and Ca, Canada.

cluded salinity, temperature, PO_4 and SiO_4 data. The uncertainty was computed using a Monte Carlo approach (Legge et al., 2015) and expressed as double standard deviation, and it was about 2.5 % for pCO_2 and less than 1 % for Ω.

Furthermore, as the carbonate system was overdetermined the internal consistency (or thermodynamic consistency) was assessed by comparing measured values to calculated values (from any two of the three determined parameters DIC, TA and pH) using the same CO2SYS MATLAB program (Van Heuven et al., 2011). The average mean differences between measured and calculated values were evaluated for pH to about 0.02 and for TA and DIC to about 7 µmol kg^{-1} for each.

3 Results

Water undersaturated with respect to calcium carbonate was observed along the bottom of the shelf at most stations (Fig. 2), associated with high nutrient and low oxygen concentrations. The strongest signal was north of the New Siberian Islands, a local minimum in saturation state at about 157° E followed by a less strong signal further to the east. Low saturation state with under-saturation in aragonite was also observed in the surface water north of the New Siberian Islands. This water had low salinity, high phosphate, and high silicate concentrations and relatively high pCO_2 despite having nitrate concentrations as low as about 0.2 µmol L^{-1}.

The extension of this high pCO_2 and low $\Omega^{\text{aragonite}}$ water out into the deep basin was seen in a layer centred at about 100 m depth all along the shelf break from the east of the Lomonosov Ridge to 180° E (Fig. 3). Over the Lomonosov Ridge (section A) there was a faint minimum in $\Omega^{\text{aragonite}}$ even if the waters were never undersaturated. Moving east to section B undersaturated waters were observed both in the surface and at approximately 50 m depth. Further to the east, sections C, D and E have strong $\Omega^{\text{aragonite}}$ minima centred at ∼ 100 m depth. In the most eastern section of this study, section F, the minimum was less intense and was also found at somewhat greater depth, ∼ 150 m. In all sections the minimum in $\Omega^{\text{aragonite}}$ was closely followed by a maximum in pCO_2 (Fig. 3). In section C and even more so in D and E the $\Omega^{\text{aragonite}}$ minima were observed in close vicinity to the sediment.

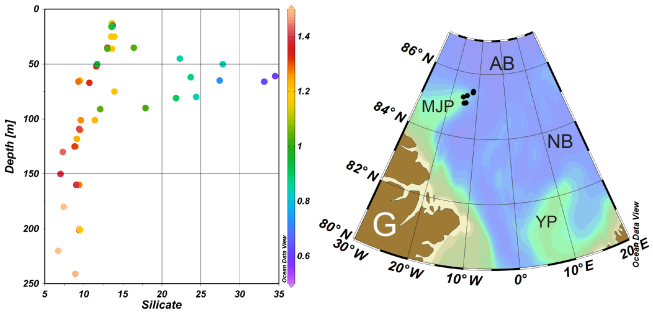

Figure 5. Silicate profiles of six stations over the Morris Jesup Plateau (MJP), colour-coded by $\Omega^{\text{aragonite}}$, as observed during the *Oden* 91 cruise. Station positions are noted on the map, with the abbreviations being AB, Amundsen Basin; NB, Nansen Basin; YP, Yermak Plateau; and G, Greenland.

This low saturated water has been observed in the Canada Basin on several occasions (e.g. Yamamoto-Kawai et al., 2009; Anderson et al., 2010). During the Beringia 2005 expedition, where $\Omega^{\text{aragonite}}$ levels as low as 0.6 were observed at 100 m depth (Fig. 4), the layer of under-saturation was between 50 and 100 m thick and had the upper limit at about 75 m depth. It also had the typical signature of low oxygen and high nutrient concentrations from decay of organic matter. Water with high silicate and undersaturated in aragonite was observed at the tip of the Morris Jesup Plateau in 1991 (Fig. 5), where the subsurface waters from the Canadian Basin follow the continental margin towards the Fram Strait (Rudels et al., 1994). Water of similar signature, but less pronounced, was also seen at a depth of 50–75 m in the northwestern Fram Strait in May 2002, while the overlying low-salinity surface water was well above saturation with respect to calcium carbonate (Fig. 6). A distinct maximum in silicate was present at the Greenland continental margin and centred around a salinity of 33. It was associated with a minimum in pH and thus also in $\Omega^{\text{aragonite}}$, but with a less pronounced oxygen minimum (AOU maximum).

4 Discussion

The two major factors that impact calcium carbonate solubility in the surface ocean are salinity and pH, where the former affects the calcium ion and DIC concentrations and the latter controls the relative distribution of the inorganic carbon speciation. In the open ocean the latter is mainly determined by CO_2, either controlled by exchange with the atmosphere or through primary production/decay of organic matter. The concentrations of nutrients and AOU are high close to the bottom at most stations occupied on the shelf (Fig. 2), showing the importance of organic matter decay in controlling the chemical signature of the Siberian shelf bottom waters. Low $\Omega^{\text{aragonite}}$ and Ω^{calcite} values are associated with high pCO_2 (low pH) and high nutrient concentrations as well as low oxygen (high AOU). The corrosive water extending out into the deep basin is strongly associated with high pCO_2 (Fig. 3) and high nutrients, further illustrating that decay of organic matter also here is the cause of this signature.

However, mixing with low-salinity water also has an impact, especially on the shelf where the influence from river discharge is stronger and melting sea ice occurs that add to lowering salinity. As illustrated in Fig. 7a aragonite undersaturation is found in most surface waters of salinity < 28, waters that are found north of the New Siberian Islands (Fig. 2). In this region the surface water (top 10 m) nitrate concentration is very low, averaging $0.25 \pm 0.05\,\mu\text{mol}\,\text{L}^{-1}$, illustrating that phytoplankton blooms are well advanced and that nitrate is the limiting nutrient as the phosphate concentration is high, averaging $1.1 \pm 0.1\,\mu\text{mol}\,\text{L}^{-1}$ (Fig. 2). Despite these signatures of primary production, CO_2 is slightly supersaturated, averaging $420 \pm 30\,\mu\text{atm}$ and oxygen is close to equilibrium, averaging $100 \pm 1\,\%$, i.e. AOU is around zero. Hence the rate of CO_2 consumption by primary production is exceeded by respiration of organic matter low in nutrient content, and this is likely of terrestrial origin (Anderson et al., 2009). CO_2 can also be produced by photo degradation of dissolved organic matter (e.g. Cory et al., 2015), at least if the water is not too turbid. However, our data cannot assess the relative roles of these two processes.

The very high silicate concentrations indicate that mainly river runoff and not sea-ice melt is the source of freshwater to low-salinity waters. Consequently, this region is most likely heavily impacted by the plume of the large Siberian rivers, here dominated by the Lena River. The fact that CO_2 is supersaturated strongly indicates that the river runoff not only lowers the calcium and carbonate concentrations by dilution but also decreases pH by addition of CO_2. This could be either from high pCO_2 in the river water itself or from decay of organic carbon that is added by the river runoff. Considering a freshwater residence time on the Laptev shelf of several years (Schlosser et al., 1994), the latter is the most plausi-

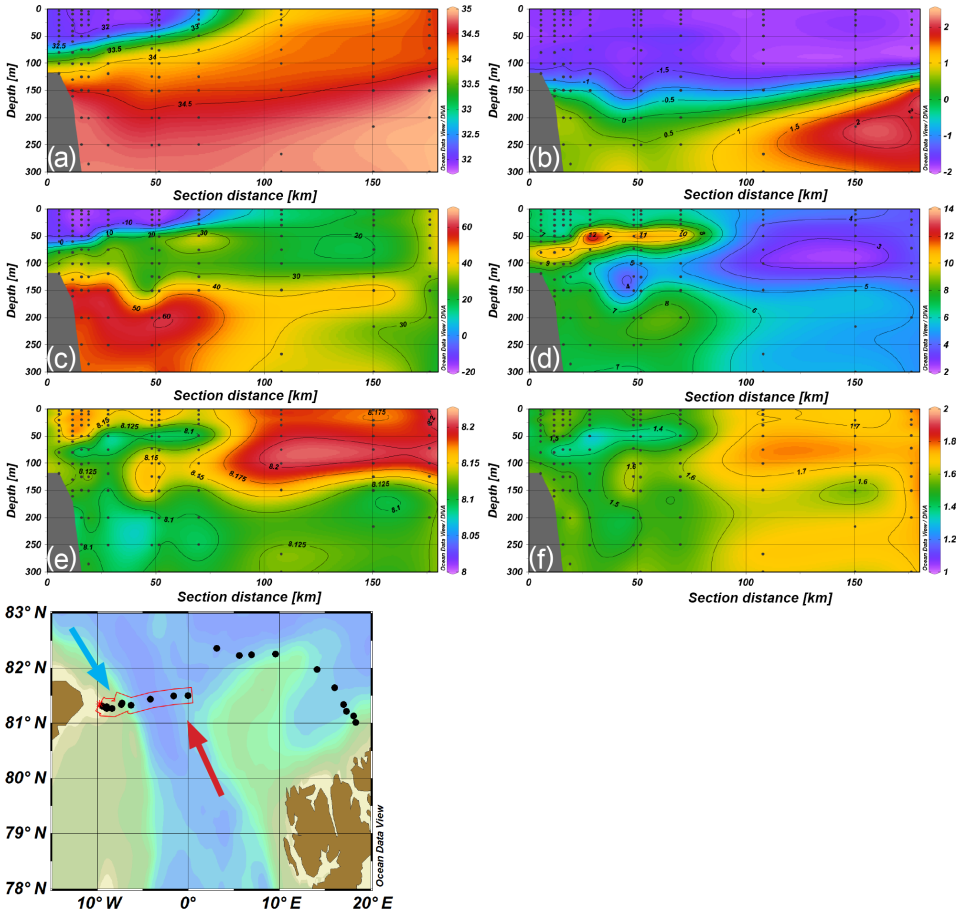

Figure 6. Sections of **(a)** salinity, **(b)** temperature, **(c)** AOU, **(d)** SiO_2, **(e)** $pH^{tot}_{in\ situ}$, and **(f)** $\Omega^{aragonite}$, across the northern Fram Strait at about 81.5° N from the Yermak Plateau to Greenland as noted on the map, collected in May 2002. The arrows illustrate the north-flowing warm Atlantic and the south-flowing cold Arctic surface waters.

ble explanation as CO_2 from the runoff would have time to largely equilibrate during the transit to the area of observation. This is supported by reconstructed velocity fields (using a 4-D variational approach) and trajectories of passive tracers launched in the East Siberian Arctic Shelf, which show that during 2 years the surface water mass approaches the area near the North Pole (Shakhova et al., 2015).

Summer water pCO_2 values of the central Arctic Ocean has normally been observed to be well below atmospheric levels (e.g. Jutterström and Anderson, 2010; Ulfsbo et al., 2014), but during the Russian North Pole-33 drifting station CO_2 supersaturation of up to 100 µatm was observed over the Amundsen Basin at about 86° N (Semiletov et al., 2007). This is the region where the Lena River plume typically passes (e.g. Anderson et al., 2004) and these high pCO_2 values can thus be an indication of a direct contribution from the Lena River plume, mineralization of terrestrial DOC following the river plume, rapid turnover of sub-ice dissolved organic matter which is closely connected with high sea-ice production, or any combination of these sources (Semiletov et al., 2007). A time lag of 4–6 years between the Lena River discharge anomalies, ice conditions in the Siberian seas, and ice export through Fram Strait was found with a correlation of ∼0.7 (Semiletov et al., 2000). During this passage over the central Arctic Ocean the pCO_2 levels decreases by outgassing, mixing of water masses as well as by primary production, resulting in that the surface water that flow out

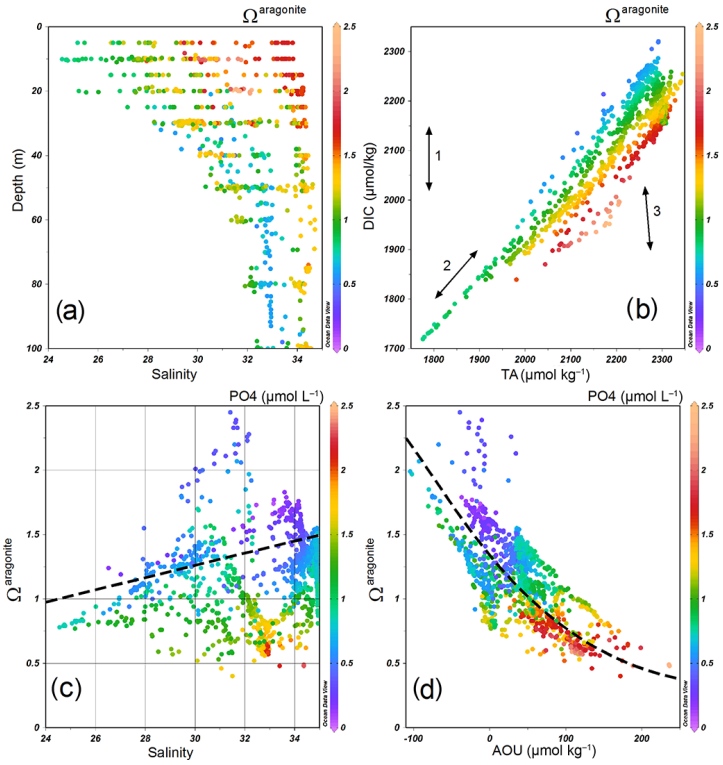

Figure 7. Plot of **(a)** salinity versus depth **(b)** DIC versus TA, both colour-coded by $\Omega^{\text{aragonite}}$, and **(c)** $\Omega^{\text{aragonite}}$ versus salinity and **(d)** $\Omega^{\text{aragonite}}$ versus AOU, both colour-coded by PO_4. In **(b)** arrows are drawn where the slope are to illustrate the impact by air–sea CO_2 gas exchange (1), dilution of water with zero DIC and TA (2) and primary production (down) and decay of organic matter (up) (3). The location and length of the arrows are arbitrary. In **(c)** a line is drawn that represents the dilution of Atlantic layer water with water of zero S, DIC and TA, and in **(d)** a line is drawn that represents a typical surface water that is impacted by primary production and decay of organic matter. Details of these lines are given in the text.

through Fram Strait in the East Greenland Current is supersaturated with respect to calcium carbonate (Fig. 6).

The dilution is not a dominating process of low $\Omega^{\text{aragonite}}$ throughout the water column in the study region as seen in a DIC–TA plot (Fig. 7b). The degree of saturation varies more with shifts in DIC by air–sea exchange (direction of arrow 1) and primary production/organic matter decay (direction of arrow 3) than dilution (direction of arrow 2), where the latter has an effect on both TA and DIC. No clear trend can be seen when $\Omega^{\text{aragonite}}$ is plotted as a function of salinity (Fig. 7c) and the data certainly do not follow the dilution line (representing dilution of Atlantic layer water having $S = 34.85$, $T = -1\,^{\circ}\text{C}$, $\text{DIC} = 2170\,\mu\text{mol kg}^{-1}$, $\text{TA} = 2300\,\mu\text{mol kg}^{-1}$ with water of zero S, DIC and TA), even if there is less water supersaturated at the lower salinities. Rather, the low $\Omega^{\text{aragonite}}$ is associated with high PO_4, implying organic matter decay as the main cause. This conclusion is strengthened

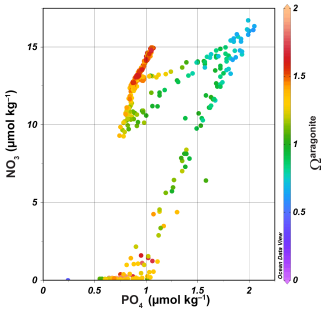

Figure 8. Nitrate versus phosphate as observed in the Canada Basin during the Beringia 2005 expedition (station locations same as in Fig. 4), colour-coded by $\Omega^{\text{aragonite}}$.

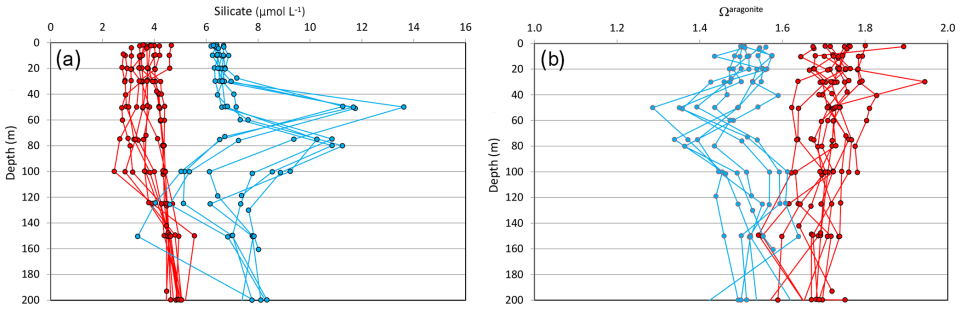

Figure 9. Depth profiles of silicate **(a)** and $\Omega^{\text{aragonite}}$ **(b)** in the Fram Strait around 82° N in 2002. The 2002 $\Omega^{\text{aragonite}}$ values are all computed from pH and TA and cover the whole strait. There is a distinct difference in both the silicate and $\Omega^{\text{aragonite}}$ properties in the north-flowing Atlantic water (red with a surface salinity around 34.5) and the south-flowing Arctic waters (blue with a surface salinity around 32). Both in- and outflowing water has a surface temperature below −1 °C, making the effects of salinity and temperature on $\Omega^{\text{aragonite}}$ in the order of maximum 0.05.

by the association between $\Omega^{\text{aragonite}}$ and AOU (Fig. 7d). A line is drawn that represents a typical surface water ($S = 33$, $T = -1\,^{\circ}\text{C}$, $PO_4 = 1\,\mu\text{mol L}^{-1}$, $NO_3 = 16\,\mu\text{mol L}^{-1}$, $\text{AOU} = 0$, $\text{DIC} = 2046\,\mu\text{mol kg}^{-1}$, $\text{TA} = 2169\,\mu\text{mol kg}^{-1}$) that is impacted by primary production and decay of organic matter having the classical Redfield–Ketchum–Richards ratio of the elements $\text{C:N:P:O}_2 = 106:1:16:-138$ (Redfield et al., 1963). This computation is done assuming classical marine organic matter having this elemental composition. However, the correlation between $\Omega^{\text{aragonite}}$ and AOU will not be much impacted if instead terrestrial organic matter of lower nutrient content decays. Most of the data, in general, follow the shape of this line even if the spread is substantial. It should be noted that all data collected during the expedition are included, i.e. including water originating from both the Atlantic and the Pacific oceans with large variability in time since contact with the atmosphere. One example is the blue data that deviate from the line in the upper left of the graph, which likely is a result of photosynthesis in the surface water, where outgassing of oxygen to the atmosphere is faster than the uptake of CO_2. These are surface waters of salinities around 32 (Fig. 7a and c).

The low $\Omega^{\text{aragonite}}$ water observed along the continental margin (Fig. 3) likely flows to the east and spreads out into the deep basin. In 2005 it was seen in the Canada Basin (Fig. 4) and likely confined to the Beaufort Gyre and hence its extension depends on the atmospheric pressure field (e.g. Proshutinsky et al., 2009; Carmack et al., 2016). Decadal variability in the fresh water content of the Beaufort Gyre experienced a significant change in the 1990s, forced by a change in the atmospheric circulation regime. For instance, in 1979 silicate concentrations as high as $40\,\mu\text{mol L}^{-1}$ were observed over the Lomonosov ridge close to the North Pole during the LOREX ice camp (Moore et al., 1983), but in 1991 the silicate maximum was completely absent even in the Makarov Basin close to the North Pole (Anderson et al., 1994). One consequence of this variable extent of the Beaufort Gyre is that the export of the high-nutrient, low-$\Omega^{\text{aragonite}}$ water out into the North Atlantic Ocean is fluctuating with time.

Jones et al. (2003) identified Pacific-originating water by its excess phosphate concentration relative to nitrate and used the nitrate to phosphate relationship to trace it in the North Atlantic Ocean and found significant fractions in the Fram Strait, the Denmark Strait, and the Labrador Sea, but these were variable between different years. For many of the cruises discussed by Jones et al. (2003) there were no carbonate system data measured and hence $\Omega^{\text{aragonite}}$ could not be computed. However, it is evident that the aragonite undersaturated water is well confined to the water high in nutrients and with an excess of phosphate (Fig. 8), i.e. a property that was observed in parts of the North Atlantic by Jones et al. (2003). Hence, this undersaturated water is also likely exported well into the North Atlantic Ocean.

The 2002 observations show a minimum of less than 1.4 in aragonite saturation, but not undersaturated, in the northwestern Fram Strait (Fig. 6). This minimum is centred around a salinity of 33, but the computed fraction of Pacific water was about 2 % with the major fraction of freshwater being river runoff (Jones et al., 2008b). Hence, the signature of calcium carbonate undersaturation was lessened from the source to the observation of this investigation, i.e. the East Siberian Arctic shelves, by water mass mixing.

However, when one compares the conditions of the waters flowing into the Arctic Ocean in the West Spitsbergen Current and the one flowing out in the East Greenland Current there are distinct differences (Fig. 9). The silicate concentration is at least $2\,\mu\text{mol L}^{-1}$ higher in the top 200 m, while the $\Omega^{\text{aragonite}}$ values are in the order 0.2 lower in the top 100 m. This is most likely a result of addition of freshwater by both river runoff and sea ice melt, but even more important is the

decay of organic matter. The effect by freshening can decrease $\Omega^{aragonite}$ by no more than 0.05 under the conditions observed, pointing to the importance of organic matter decay during the circulation of these waters in the Arctic Ocean.

5 Conclusions

Corrosive surface water is exported to the central Arctic Ocean by the plumes of the large Siberian rivers, dominated by the Lena River in the Laptev–East Siberian seas region. This signature is maintained in the shelf by photo degradation (e.g. Cory et al., 2015) and/or microbial degradation of organic matter that to a large degree is of terrestrial origin (e.g. Alling et al., 2012; Tesi et al., 2014; Vonk et al., 2014). However, the signature of surface water undersaturated with respect to calcium carbonate does not spread far out into the deep central basins as mixing with surrounding water masses and outgassing of CO_2 to the atmosphere increase the saturation state with time. Furthermore, the saturation state is also lowered by primary production in the surface waters when light and nutrients are available.

Highly calcium carbonate corrosive waters are produced along the bottoms of the East Siberian seas through degradation of organic matter. This water is exported into the deep Makarov and Canada basins at a depth range of about 50–150 m. The signature of this subsurface water is maintained within the Beaufort Gyre and is exported out to the North Atlantic through eastern Fram Strait, and likely also through the Canadian Arctic Archipelago.

The salinity range of this water is 32–34 and there is a potential for this water to be mixed up to layers inhabited by aragonite-forming organisms such as pteropods. Such mixing can be either a result of wind or through sea ice formation when the surface layer gets homogenized by brine release.

Data availability. Data are available upon request to the corresponding author.

Competing interests. The authors declare that they have no conflict of interest.

Acknowledgements. This research was supported by the Swedish Knut and Alice Wallenberg Foundation (KAW); the Swedish Research Council, VR (L.G.A. 621-2013-5105); the Swedish Research Council Formas (A.U. #2014-1165); and the Russian Government (I.S. grant no. 14,Z50.31.0012/03.19.2014). We thank the supporting crew and captain of I/B *Oden* and are grateful for the support of the Swedish Polar Secretariat, as well as for the constructive comments by Johan Ingri and two anonymous reviewers on an earlier version of this paper.

Edited by: Ö. Gustafsson
Reviewed by: J. Ingri and two anonymous referees

References

Alling, V., Porcelli, D., Mörth, C.-M., Anderson, L. G., Sanchez-Garcia, L., Gustafsson, Ö., Andersson, P. S., and Humborg, C.: Degradation of terrestrial organic carbon, primary production and out-gassing of CO_2 along the Laptev and East Siberian Seas as inferred from $\delta^{13}C$ values of DIC, Geochim. Cosmochim. Ac., 95, 143–159, 2012.

Anderson, L. G., Björk, G., Holby, O., Kattner, G., Koltermann, P. K., Jones, E. P., Liljeblad, B., Lindegren, R., Rudels, B., and Swift, J.: Water Masses and Circulation in the Eurasian Basin: Results from the Oden 91 North Pole Expedition, J. Geophys. Res., 99, 3273–3283, 1994.

Anderson, L. G., Jutterström, S., Kaltin, S., Jones, E. P., and Björk, G.: Variability in river runoff distribution in the Eurasian Basin of the Arctic Ocean, J. Geophys. Res., 109, C01016, doi:10.1029/2003JC001773, 2004.

Anderson, L. G., Jutterström, S., Hjalmarsson, S., Wåhlström, I., and Semiletov, I. P.: Out-gassing of CO_2 from Siberian Shelf Seas by terrestrial organic matter decomposition, Geophys. Res. Lett., 36, L20601, doi:10.1029/2009GL040046, 2009.

Anderson, L. G., Tanhua, T., Björk, G., Hjalmarsson, S., Jones, E. P., Jutterström, S., Rudels, B., Swift, J. H., and Wåhlström, I.: Arctic Ocean shelf – basin interaction, an active continental shelf CO_2 pump and its impact on the degree of calcium carbonate dissolution, Deep-Sea Res. Pt. I, 57, 869–879 doi:10.1016/j.dsr.2010.03.012, 2010.

Anderson, L. G., Björk, G., Jutterström, S., Pipko, I., Shakhova, N., Semiletov, I., and Wåhlström, I.: East Siberian Sea, an Arctic region of very high biogeochemical activity, Biogeosciences, 8, 1745–1754, doi:10.5194/bg-8-1745-2011, 2011.

Azetsu-Scott, K., Clarke, A., Falkner, K., Hamilton, J., Jones, E. P., Lee, C., Petrie, B., Prinsenberg, S., Starr, M., and Yeats, P.: Calcium carbonate saturation states in the waters of the Canadian Arctic Archipelago and the Labrador Sea, J. Geophys. Res., 115, C11021, doi:10.1029/2009JC005917, 2010.

Bach, L. T.: Reconsidering the role of carbonate ion concentration in calcification by marine organisms, Biogeosciences, 12, 4939–4951, doi:10.5194/bg-12-4939-2015, 2015.

Carmack, E. and Wassmann, P.: Food webs and physical–biological coupling on pan-Arctic shelves: Unifying concepts and comprehensive perspectives, Prog. Oceanogr., 71, 446–477, doi:10.1016/j.pocean.2006.10.004, 2006.

Carmack, E. C., Yamamoto-Kawai, M., Haine, T. W. N., Bacon, S., Bluhm, B. A., Lique, C., Melling, H., Polyakov, I. V., Straneo, F., Timmermans, M.-L., and Williams, W. J.: Freshwater and its role in the Arctic Marine System: Sources, disposition, storage, export, and physical and biogeochemical consequences in the Arctic and global oceans, J. Geophys. Res.-Biogeo., 121, 675–717, doi:10.1002/2015JG003140, 2016.

Clayton, T. D. and Byrne, R. H.: Spectrophotometric seawater pH measurements: total hydrogen ion concentration scale calibration of m-cresol purple at-sea results, Deep-Sea Res. Pt. I, 40, 2115–2129, 1993.

Comeau, S., Jeffree, R., Teyssié, J.-L., and Gattuso, J.-P.: Response of the Arctic pteropod Limacina helicina to projected future environmental conditions, PloS one, 5, e11362, doi:10.1371/journal.pone.0011362, 2010.

Cory, R. M., Harrold, K. H., Neilson, B. T., and Kling, G. W.: Controls on dissolved organic matter (DOM) degradation in a headwater stream: the influence of photochemical and hydrological conditions in determining light-limitation or substrate-limitation of photo-degradation, Biogeosciences, 12, 6669–6685, doi:10.5194/bg-12-6669-2015, 2015.

Cyronak, T., Schultz, K. G., and Lokiel, P. L.: The Omega myth: what really drives lower calcification rates in an acidifying ocean, ICES J. Mar. Sci., 73, 558–562, 2016.

Dieckmann, G. S., Nehrke, G., Papadimitriou, S., Göttlicher, J., Steininger, R., Kennedy, H., Wolf-Gladrow, D., and Thomas, D. N.: Calcium carbonate as ikaite crystals in Antarctic sea ice, Geophys. Res. Lett., 35, L08501, doi:10.1029/2008GL033540, 2008.

Doney, S. C., Fabry, V. J., Feely, R. A., and Kleypas, J. A.: Ocean acidification: the other CO_2 problem, Annu. Rev. Mar. Sci., 1, 169–192, doi:10.1146/annurev.marine.010908.163834, 2009.

Findlay, H. S., Wood, H. L., Kendall, M. A., Spicer, J. I., Twitchett, R. J., and Widdicombe, S.: Comparing the impact of high CO_2 on calcium carbonate structures in different marine organisms, Mar. Biol. Res., 7, 565–575, 2011.

Gattuso, J.-P., Magnan, A., Billé, R., Cheung, W. W. L., Howes, E. L., Joos, F., Allemand, D., Bopp, L., Cooley, S. R., Eakin, C. M., Hoegh-Guldberg, O., Kelly, R. P., Pörtner, H.-O., Rogers, A. D., Baxter, J. M., Laffoley, D., Osborn, D., Rankovic, A., Rochette, J., Sumaila, U. R., Treye, S., and Turley C.: Contrasting futures for ocean and society from different anthropogenic CO_2 emissions scenarios, Science, 349, 6243, doi:10.1126/science.aac4722, 2015.

Haese, R. R., Smith, J., Weber, R., and Trafford, J.: High-magnesium calcite dissolution in tropical continental shelf sediments controlled by ocean acidification, Environ. Sci. Technol., 48, 8522–8528, 2014.

Haraldsson, C., Anderson, L. G., Hassellöv, M., and Hulth, S.: Rapid, high-precision potentiometric titration of alkalinity in ocean and sediment pore waters, Deep-Sea Res., 44, 2031–2044, 1997.

Jahn, A., Tremblay, B., Mysak, L. A., and Newton, R.: Effect of the large-scale atmospheric circulation on the variability of the Arctic Ocean freshwater export, Clim. Dynam. 34, 201–222, doi:10.1007/s00382-009-0558-z, 2010.

Johnson, K. M., Sieburth, J. M., Williams, P. J., and Brandström, L.: Coulometric total carbon dioxide analysis for marine studies: automation and calibration, Mar. Chem., 21, 117–133, 1987.

Jones, E. P., Swift, J. H., Anderson, L. G., Lipizer, M., Civitarese, G., Falkner, K., Kattner, G., and McLaughlin, F.: Tracing Pacific Water in the North Atlantic Ocean, J. Geophys. Res., 108, 3114, doi:10.1029/2001JC001141, 2003.

Jones, E. P., Anderson, L. G., Jutterström, S., Mintrop, L., and Swift, J. H.: Pacific freshwater, river water and sea ice meltwater across Arctic Ocean basins: Results from the 2005 Beringia Expedition, J. Geophys. Res., 113, C08012, doi:10.1029/2007JC004124, 2008a.

Jones, E. P., Anderson, L. G., Jutterström, S., and Swift, J. H.: Sources and Distribution of Fresh water in the East Greenland Current, Prog. Oceanogr., 78, 37–44, doi:10.1016/j.pocean.2007.06.003, 2008b.

Jutterström, S. and Anderson, L. G.: Uptake of CO_2 by the Arctic Ocean in a changing climate, Mar. Chem., 122, 96–104, doi:10.1016/j.marchem.2010.07.002, 2010.

Jutterström, S., Jeansson, E., Anderson, L. G., Bellerby, R., Jones, E. P., Smethie Jr., W. M., and Swift, J. H.: Evaluation of anthropogenic carbon in the Nordic Seas using observed relationships of N, P and C versus CFCs, Prog. Oceanogr., 78, 78–84, doi:10.1016/j.pocean.2007.06.001, 2008.

Legge, O. J., Bakker, D. C. E., Johnson, M. T., Meredith, M. P., Venables, H. J., Brown, P. J., and Lee, G. A.: The seasonal cycle of ocean-atmosphere CO_2 flux in Ryder Bay, west Antarctic Peninsula, Geophys. Res. Lett., 42, 2934–2942, doi:10.1002/2015GL063796, 2015.

Liu, X., Patsavas, M. C., and Byrne, R. H.: Purification and Characterization of meta-Cresol Purple for Spectrophotometric Seawater pH Measurements, Environ. Sci. Technol., 45, 4862–4868, doi:10.1021/es200665d, 2011.

Lueker, T. J., Dickson, A. G., and Keeling, C. D.: Ocean pCO_2 calculated from dissolved inorganic carbon, alkalinity, and equations for K1 and K2: validation based on laboratory measurements of CO_2 in gas and seawater at equilibrium, Mar. Chem., 70, 105–119, 2000.

Moore, R. M., Lowings, M. G., and Tan, F. C.: Geochemical profiles in the Central Arctic Ocean: Their relation to freezing and shallow circulation, J. Geophys. Res., 88, 2667–2674, 1983.

Mucci, A.: The solubility of calcite and aragonite in seawater at various salinities, temperatures, and one atmospheric pressure, Am. J. Sci., 283, 781–799, 1983.

Orr, J. C., Fabry, V. J., Aumont, O., Bopp, L., Doney, S. C., Feely, R. A., Gnanadesikan, A., Gruber, N., Ishida, A., Joos, F., Key, R. M., Lindsay, K., Maier-Reimer, E., Matear, R., Monfray, P., Mouchet, A., Najjar, R. G., Plattner, G.-K., Rodgers, K. B., Sabine, C. L., Sarmiento, J. L., Schlitzer, R., Slater, R. D., Totterdell, I. J., Weirig, M.-F., Yamanaka, Y., and Yoo, A.: Anthropogenic ocean acidification over the twenty-first century and its impact on calcifying organisms, Nature, 437, 681–686, doi:10.1038/nature04095, 2005.

Pipko, I. I., Semiletov, I. P., Tishchenko, P. Ya., Pugach, S. P., and Christensen, J. P.: Carbonate chemistry dynamics in Bering Strait and the Chukchi Sea, Prog. Oceanogr., 55, 77–94, 2002.

Pipko, I. I., Semiletov, I. P., Pugach, S. P., Wåhlström, I., and Anderson, L. G.: Interannual variability of air-sea CO_2 fluxes and carbon system in the East Siberian Sea, Biogeosciences, 8, 1987–2007, doi:10.5194/bg-8-1987-2011, 2011.

Proshutinsky, A., Krishfield, R., Timmermans, M.-L., Toole, J., Carmack, E., McLaughlin, F., Williams, W. J., Zimmermann, S., Itoh, M., and Shimada, K.: Beaufort Gyre freshwater reservoir: State and variability from observations, J. Geophys. Res., 114, C00A10, doi:10.1029/2008JC005104, 2009.

Redfield, A. C., Ketchum, B. G. H., and Richards, F. A.: The influence of organisms on the composition of sea-water, in: The Sea: Ideas and Observations on the Progress in the Study of the Seas, Vol. 2, edited by: Hill, M. N., 26–77, Interscience, New York, 1963.

Riley, J. P. and Tongudai, M.: The major cation/chlorinity ratios in sea water, Chem. Geol., 2, 263–269, 1967.

Rudels, B., Jones, E. P., Anderson L. G., and Kattner, G.: On the intermediate depth waters of the Arctic Ocean, in: The Polar Oceans and Their Role in Shaping the Global Environment, edited by: Johannessen, O. M., Muench, R. D., and Overland, J. E., 33–46, American Geophysical Union, Washington, D.C., 1994.

Schlosser, P., Bauch, D., Fairbanks, R., and Bonisch, G.: Arctic river runoff: Mean residence time on the shelves and in the halocline, Deep-Sea Res. Pt. I, 41, 1053–1068, doi:10.1016/0967-0637(94)90018-3, 1994.

Semiletov, I., Pipko, I. I., Repina, I. A., and Shakhova, N.: Carbonate dynamics and carbon dioxide fluxes across the atmosphere-ice-water interfaces in the Arctic Ocean Pacific sector of the Arctic, J. Mar. Syst., 66, 204–226, 2007.

Semiletov, I., Pipko, I., Gustafsson, Ö., Anderson, L. G., Sergienko, V., Pugach, S., Dudarev, O., Charkin, A., Gukov, A., Bröder, L., Andersson, A., Spivak, E., and Shakhova, N.: Acidification of East Siberian Arctic Shelf waters through addition of freshwater and terrestrial carbon, Nat. Geosci., 9, 361–365, doi:10.1038/ngeo2695, 2016.

Semiletov, I. P., Savelieva, N. I., Weller, G. E., Pipko, I. I., Pugach, S. P., Gukov, A. Yu., and Vasilevskaya, L. N.: The dispersion of Siberian river flows into coastal waters: meteorological, hydrological and hydrochemical aspects, in: The Freshwater Budget of the Arctic Ocean, edited by: Lewis, E. L., 323–366, Kluwer Academic Publishers, Dordrecht, NATO Meeting/NATO ASI Series, 2000.

Shakhova, N., Semiletov, I., Sergienko, V., Lobkovsky, L., Yusupov, V., Salyuk, A., Salomatin, A., Chernykh, D., Kosmach, D., Panteleev, G., Nicolsky, D., Samarkin, V., Joye, S., Charkin, A., Dudarev, O., Meluzov, A., and Gustafsson, Ö.: The East Siberian Arctic Shelf: Towards further assessment of permafrost-related methane fluxes and role of sea ice, Philos. T. R. Soc. A, 373, 20140451, doi:10.1098/rsta.2014.0451, 2015.

Tesi, T., Semiletov, I., Hugelius, G., Dudarev, O., Kuhry, P., and Gustafsson, O.: Composition and fate of terrigenous organic matter along the Arctic land-ocean continuum in East Siberia: Insights from biomarkers and carbon isotopes, Geochim. Cosmochim. Ac., 133, 235–256, 2014.

Ulfsbo, A., Cassar, N., Korhonen, M., van Heuven, S., Hoppema, M., and Anderson, L. G.: Late summer net community production in the central Arctic Ocean using multiple approaches, Global Biogeochem. Cy., 28, 1129–1148, doi:10.1002/2014GB004833, 2014.

van Heuven, S., Pierrot, D., Rae, J. W. B., Lewis, E., and Wallace, D. W. R.: MATLAB Program Developed for CO_2 System Calculations, ORNL/CDIAC-105b, Carbon Dioxide Information Analysis Center, Oak Ridge National Laboratory, US Department of Energy, Oak Ridge, Tennessee, doi:10.3334/CDIAC/otg.CO2SYS_MATLAB_v1.1, 2011.

Vonk, J. E., Semiletov, I. P., Dudarev, O. V., Eglington, T. I., Andersson, A., Shakhova, N., Charkin, A., Heim, B., and Gustafsson, O.: Preferential burial of permafrost-derived organic carbon in Siberian–Arctic shelf waters, J. Geophys. Res., 119, 8410–8421, doi:10.1002/2014JC010261, 2014.

Yamamoto-Kawai, M., Mclaughlin, F. A., Carmack, E. C., Nishino, S., and Shimada, K.: Aragonite undersaturation in the Arctic Ocean: effects of ocean acidification and sea ice melt, Science, 326, 1098–1100, doi:10.1126/science.1174190, 2009.

III

Journal of Geophysical Research: Oceans

RESEARCH ARTICLE
10.1029/2018JC014073

Key Points:
- Large undersaturation of surface water pCO_2 with respect to atmospheric pCO_2 was observed in an Arctic fjord following two annual cycles
- Biological activity and temperature are key drivers for the observed monthly variability in surface water pCO_2
- The uptake of CO_2 is enhanced when Arctic origin waters are present in the fjord as compared to Atlantic origin waters

Correspondence to:
Y. Ericson,
ylva.ericson@unis.no

Citation:
Ericson, Y., Falck, E., Chierici, M., Fransson, A., Kristiansen, S., Platt, S. M., et al. (2018). Temporal variability in surface water pCO_2 in Adventfjorden (West Spitsbergen) with emphasis on physical and biogeochemical drivers. *Journal of Geophysical Research: Oceans*, *123*. https://doi.org/10.1029/2018JC014073

Received 11 APR 2018
Accepted 14 JUN 2018
Accepted article online 26 JUN 2018

Temporal Variability in Surface Water pCO_2 in Adventfjorden (West Spitsbergen) With Emphasis on Physical and Biogeochemical Drivers

Y. Ericson[1,2], E. Falck[1,2], M. Chierici[1,3], A. Fransson[4], S. Kristiansen[5], S. M. Platt[6], O. Hermansen[6], and C. L. Myhre[6]

[1]Department of Arctic Geophysics, University Centre in Svalbard, Longyearbyen, Norway, [2]Geophysical Institute, University of Bergen, Bergen, Norway, [3]Institute of Marine Research, Fram Centre, Tromsø, Norway, [4]Norwegian Polar Institute, Fram Centre, Tromsø, Norway, [5]Department of Arctic and Marine Biology, UiT-The Arctic University of Norway, Tromsø, Norway, [6]NILU-Norwegian Institute for Air Research, Kjeller, Norway

Abstract Seasonal and interannual variability in surface water partial pressure of CO_2 (pCO_2) and air-sea CO_2 fluxes from a West Spitsbergen fjord (IsA Station, Adventfjorden) are presented, and the associated driving forces are evaluated. Marine CO_2 system data together with temperature, salinity, and nutrients, were collected at the IsA Station between March 2015 and June 2017. The surface waters were undersaturated in pCO_2 with respect to atmospheric pCO_2 all year round. The effects of biological activity (primary production/respiration) followed by thermal forcing on pCO_2 were the most important drivers on a seasonal scale. The ocean was a sink for atmospheric CO_2 with annual air-sea CO_2 fluxes of -36 ± 2 and -31 ± 2 g C·m^{-2}·year^{-1} for 2015–2016 and 2016–2017, respectively, as estimated from the month of April. Waters of an Arctic origin dominated in 2015 and were replaced in 2016 by waters of a transformed Atlantic source. The CO_2 uptake rates over the period of Arctic origin waters were significantly higher (2 mmol C·m^{-2}·day^{-1}) than the rates of the Atlantic origin waters of the following year.

1. Introduction

The West Spitsbergen fjords provide a unique and dynamic coastal environment, influenced by seasonal contributions of snow, glacial, and sea ice meltwaters (e.g., Cottier et al., 2005; Nilsen et al., 2008; Svendsen et al., 2002). These fjords are affected by the Atlantic Water (AW, $S > 34.9$) of the West Spitsbergen Current that flows north along the continental slope (Figure 1), as well as of the cold and fresh Arctic Water (ArW, $S < 34.7$) that flows northward on the shelf with the Coastal Current (e.g., Cottier et al., 2005; Nilsen et al., 2008). The former is typically mixed with the latter on the shelf and modified to Transformed Atlantic Water (TAW, $34.7 < S < 34.9$). The distribution and presence of these water masses inside the fjords vary with time (e.g., Cottier et al., 2005; Nilsen et al., 2008, 2016).

A few observations of the CO_2 system from West Spitsbergen fjords exist that show that the surface waters were undersaturated in the partial pressure of CO_2 (pCO_2) with respect to the atmospheric pCO_2 during the observed periods (Adventfjorden, Andersson et al., 2017; Kongsfjorden, Fransson et al., 2016; Tempelfjorden, Fransson et al., 2015), like most surface waters in the Arctic Ocean (e.g., Bates & Mathis, 2009; Jutterström & Anderson, 2010; Yasunaka et al., 2016). These areas have thereby the potential to act as net CO_2 sinks. A feature partly related to the temperature- and salinity-dependent solubility of CO_2, which reflects the cold and rather fresh surface layer of the Arctic. Still, Arctic coastal regions show great variability in surface water pCO_2 as well as in air-sea CO_2 fluxes, both in space and time (e.g., Else et al., 2013; Evans et al., 2015; Fransson et al., 2017; Pipko et al., 2011; Semiletov et al., 2007). This is intricately linked to local conditions of primary production/respiration, sea ice processes, terrestrial runoff, and vertical mixing, as observed in different regions of the Arctic Ocean (e.g., Chierici et al., 2011; Else et al., 2012; Fransson et al., 2013, 2017; Pipko et al., 2011; Sejr et al., 2011).

In waters north of Svalbard, the effect of sea ice processes on surface water pCO_2, mainly through the dissolution of calcium carbonate ($CaCO_3$) in the surface waters, dominates changes (i.e., undersaturation) in surface water pCO_2 on a 6 months' time scale (January to June, Fransson et al., 2017). Further south, in Isfjorden, the largest fjord along the West Spitsbergen coast, the amount of sea ice has decreased substantially over the last decade, both in terms of maximum sea ice cover and days of fast ice (Isaksen et al., 2016;

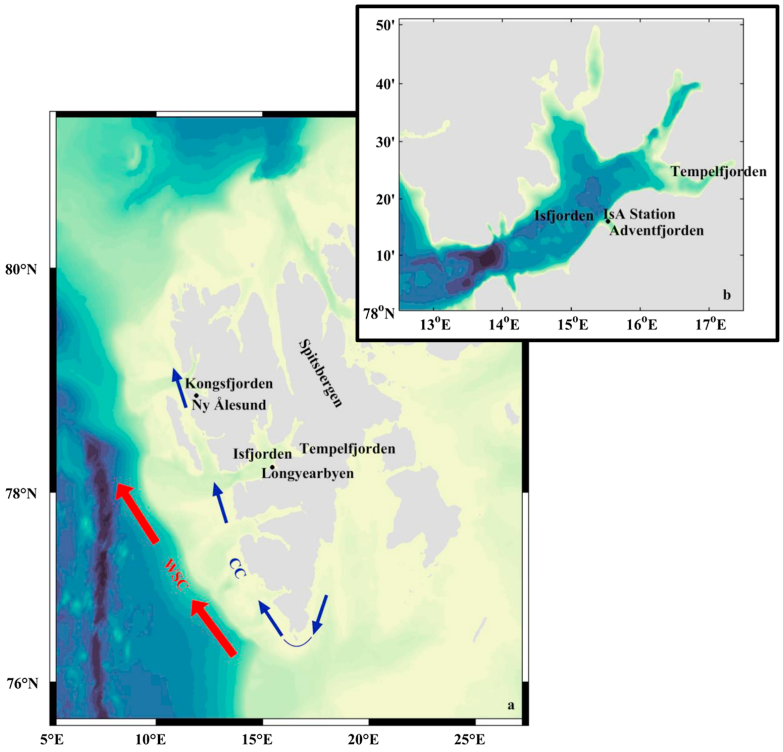

Figure 1. (a) Map of Spitsbergen showing Isfjorden, the locations of Ny Ålesund and Longyearbyen (black dots), and the surrounding shelf with the Coastal Current (CC) shown with blue arrows and the West Spitsbergen Current (WSC) depicted with red arrows, and, (b) map of Isfjorden showing the location of the IsA Station (N78°16.0, E15°32.0, with a depth of 94 m, black dot) in Adventfjorden.

Muckenhuber et al., 2016). This fjord is surrounded by glaciers and nearly 3000×10^6 m^3 of glacial meltwater feeds the system every year (Nilsen et al., 2008, and references therein). Studies from other glacier-influenced fjords in Svalbard (Fransson et al., 2015, 2016) and on the Greenland coast (Meire et al., 2015; Rysgaard et al., 2012) show that glacial meltwater may promote an uptake of CO_2 from the atmosphere.

The annual magnitude and the interannual variability of the CO_2 sink in the Isfjorden system are so far not well known. In the present study marine CO_2 system data from March 2015 to June 2017 from Adventfjorden (IsA Station, N78°16.0, E15°32.0, Figure 1), a small branch of the Isfjorden system, are presented and investigated. More specifically, the seasonal to interannual variability in surface water pCO_2 and the corresponding air-sea CO_2 fluxes are studied and the effects of key physical and biological drivers on the surface water pCO_2 are evaluated. In addition, the impact on the air-sea CO_2 fluxes between surface water of Arctic and Atlantic origins are compared.

2. Materials and Methods

2.1. Data Collection

Hydrographic work was carried out at the IsA Station between March 2015 and June 2017, in total 38 times during all seasons (see Table A1). Freshwater runoff was also collected from the Advent Valley riverbed in June 2015 (for total alkalinity [TA] and pH measurements). Temperature (*T*) and salinity (*S*) were measured using different types of conductivity-temperature-depth (CTD) devices (SAIV A/S SD204, Sea-Bird

SBE9/SBE37/SBE19+). From February 2016 and onward, the sampling was performed with a SBE19+ with a few exceptions. The SBE19+ was calibrated each year and cross-checked with the SD204 and SBE37. The SBE19+ has a better resolution and accuracy than the SD204 (see Table A2), and the two instruments were deployed together on four occasions. This resulted in corrections of −0.10, −0.13, and −0.14 of the salinity data obtained from the SD204 in spring 2016 (28 April), autumn 2016 (20 September), and spring 2017 (24 February, 21 March, and 3 April), respectively. The SD204 failed to log temperature on one occasion (22 April 2015). To be able to use the corresponding water samples that were collected on that occasion, CTD data collected 5 days earlier (17 April 2015) at the station were used instead, assuming little variability during the period.

Discrete samples of pH, TA, and nutrients (nitrate, phosphate) were collected typically using handheld Niskin bottles (1.7, 5 or 10 L). The surface sample was in general collected from 2 m. The pH/TA samples were transferred into rinsed 250-ml borosilicate bottles that were filled from the bottom. The water was allowed to overflow to flush out the water that had been in contact with air. Generally, these samples, with few exceptions, were analyzed the day after at the University Centre of Svalbard (UNIS), Longyearbyen, Norway. The nutrient samples were collected in 125-ml Nalgene® bottles and stored frozen.

pH was determined spectrophotometrically on the total hydrogen scale (pH_T) using the indicator *m*-cresol purple (*m*Cp, Clayton & Byrne, 1993). The perturbation of the sample pH as a result of the addition of the indicator was corrected for as suggested by Chierici et al. (1999). The precision, as estimated from the average of all absolute valued differences between duplicate sample runs, was ±0.001. The UNIS laboratory participated in a CO_2 interlaboratory comparison in May 2017, and both batches of unpurified *m*Cp used in this study were tested. In average the measured pH was 0.005 ± 0.001 higher than the certified value for ambient pCO_2 conditions.

TA was analyzed using a nonpurged open cell potentiometric method (Metrohm ©Titrando system, Switzerland). A nonlinear least squares optimization was used in the TA determination (Department of Energy, 1994). This method assumes no air-sample gas exchange. The impact of CO_2 loss on the TA calculation is minimal for titrations of ~3 min. For longer titrations, for example, 10 min, the calculated TA for a closed system is ~0.2% higher than the calculated TA for a system that includes gas exchange in the nonlinear least squares optimization. The method has a precision of around ±2 μmol/kg. For eight of the samples over the entire period the nonlinear least squares method failed due to noisy electrode response and an optimized endpoint determination was used (Metrohm ©tiamo™: titration software, Switzerland) with a precision of roughly ±4 μmol/kg. The average difference between the two methods was 2.0 ± 3.6 μmol/kg. The accuracy of the TA measurements was set by the use of Certified Reference Materials purchased from A. Dickson, Scripps Institution of Oceanography (United States). This one-point calibration largely removes the uncertainty in the calculated TA due to gaseous exchange. In the CO_2 interlaboratory comparison in 2017 the measured TA, using the nonlinear least square method and the endpoint determination, differed from the certified values with −0.1 ± 0.9 and 0.7 ± 0.8 μmol/kg, respectively.

The nutrient samples that were collected between April 2015 and May 2016, except for 2 May 2015, were measured at the Institute of Marine Research, Bergen, Norway. The detection limits for nitrate (NO_3^-) and phosphate (PO_4^{3-}) were 0.4 and 0.06 μmol/L, respectively. The samples from 2 May 2015 were analyzed at UiT The Arctic University of Norway. The detection limits for NO_3^- and PO_4^{3-} were 0.04 and 0.01 μmol/L, respectively. The remaining samples were analyzed at the UNIS, Longyearbyen, Norway. Here the detection limit was determined from blank measurements using a *t* test to 0.05 and 0.005 μmol/L for NO_3^- and PO_4^{3-}, respectively (n = 10, significance level: 0.01). Precision as estimated from duplicate sample runs was ±0.03 and ± 0.006 μmol/L for NO_3^- and PO_4^{3-}, respectively (n = 29). The nutrient data were converted to micromoles per kilogram using the sample density at 1 atm, in situ salinity, and a laboratory temperature measured at UNIS of 21°C, which was assumed to be comparable between laboratories.

2.2. Calculations of Surface Water pCO_2 and Air-Sea CO_2 Fluxes

The surface water pCO_2 and total dissolved inorganic carbon (DIC) were calculated from the combination of TA and pH together with the sea surface temperature (SST), sea surface salinity (SSS), and pressure data using CO2SYS MATLAB-version 1.1 (van Heuven et al., 2011). The DIC of the freshwater samples from the Advent Valley riverbed was also calculated using CO2SYS with K_1 and K_2 of Millero (1979). In terms of the seawater

samples, Chen et al. (2015) found that for Arctic surface waters the stoichiometric dissociation constants of carbonic acid (K_1 and K_2) of Mehrbach et al. (1973) as refit by Dickson and Millero (1987) and of Lueker et al. (2000) had the best agreement between calculated and measured pCO_2. This finding was also supported by the study of Woosley et al. (2017), although as pointed out by the authors, a better internal consistency does not necessarily guarantee a better accuracy. The K_1 and K_2 of Mehrbach et al. (1973) as refit by Dickson and Millero (1987), together with the dissociation constant of bisulphate (K_{SO4}) of Dickson (1990) and total borate according to Uppström (1974), were used in all further calculations of the inorganic carbon system using the CO2SYS script.

The uncertainties of the calculated pCO_2 and DIC at output condition with variations in input parameters (TA, pH, S, T, K_1, and K_2) were estimated in terms of $\left(\frac{\partial y}{\partial x_i}\right)$ referred to as the partial in the original CO2SYS software (Lewis & Wallace, 1998). Here the calculated property y represents either pCO_2 or DIC. The input parameters were treated as independent with the uncertainty calculated as follows:

$$(\delta y)^2 = \sum_i \left(\frac{\partial y}{\partial x_i}\delta x_i\right)^2 \tag{1}$$

where δx_i refers to the uncertainty/standard deviation of the measured property and δy refers to the uncertainty in the calculated variable. The uncertainties in the input parameters are presented in Table A2.

The bulk formula for air-sea CO_2 fluxes (F_{asf}) is commonly written as the product between the gas coefficient (kK_0) and the partial pressure difference between air (pCO_{2a}) and water (pCO_{2w}):

$$F_{asf} = kK_0(pCO_{2w} - pCO_{2a}) \tag{2}$$

where k is the gas transfer velocity (cm/hr) and K_0 is the solubility coefficient of CO_2 (mol·m^{-3}·atm^{-1}). K_0 was determined from in situ salinity and temperature according to Weiss (1974) who also suggested an uncertainty in the estimated K_0 in the order of 0.2%. The gas transfer velocity is a key uncertainty in bulk flux calculations. Unfortunately, there are no robust wind speed parameterizations of k that applies to the Arctic environment where wintertime convection is important (Andersson et al., 2017). For this work the formula of Wanninkhof (2014), which has an estimated uncertainty of 20% on a basin scale, was used:

$$k = 0.251 < U_{10}^2 > \left(\frac{Sc}{660}\right)^{-0.5} \tag{3}$$

where U_{10} is the wind speed at 10 m and Sc is the Schmidt number. The coefficient of 0.251 was estimated for the Cross-Calibrated Multi-Platform wind speed product, which does not cover the Arctic region. Still, the wind speed relationship of Wanninkhof (2014) agrees well with, among several others, the gas exchange study of Nightingale et al. (2000) from the North Sea, and the hybrid model of Wanninkhof et al. (2009) that includes nonwind effects on the gas transfer velocity such as chemical enhancement and buoyancy fluxes. Hourly measured wind speed data at 10 m from Svalbard Airport (Longyearbyen) were obtained from the Norwegian Meteorological Institute (eklima.met.no/). Monthly averages of the squared wind speed were calculated and used in equation (3). The seawater Schmidt number polynomial of Wanninkhof (2014) was used in the calculations.

Atmospheric pCO_2 data for use in equation (2) were obtained from the Zeppelin Mountain at 474 m in Ny Ålesund (Zeppelin Observatory, Spitsbergen, NILU-Norwegian Institute for Air Research, http://ebas.nilu.no/). The data are given as hourly averaged xCO_2 in dry air and hence must be converted to pCO_2 in wet air. To do this the following equation has been used:

$$pCO_2 = (P - p_{H_2O})xCO_2 \tag{4}$$

where P is air pressure at sea level taken from Svalbard Airport and p_{H2O} is the vapor pressure calculated according to the World Meteorological Organization (2014, WMO-No. 8) using P, temperature, and relative humidity from Longyearbyen airport (data from the Norwegian Meteorological Institute, eklima.met.no/). Low-quality xCO_2 data (e.g., flagged with 682, standard deviation$>$1 μmol mol^{-1}, or outliers) were removed.

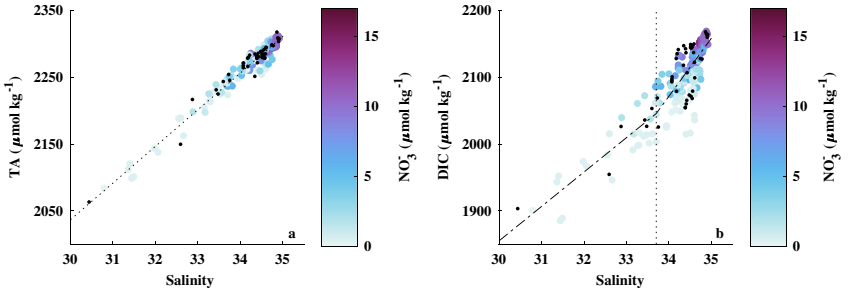

Figure 2. Plot of (a) TA versus salinity (linear equation: $y = 55.0 \cdot S + 387$, $R^2 = 0.96$) and (b) DIC versus salinity (break points: $DIC_{S=30} = 1{,}855.0$, $DIC_{S=33.7} = 2{,}045.7$, and $DIC_{S=35} = 2{,}158.8$, $R^2 = 0.78$). Coloring shows the NO_3^- concentration; black dots indicate no NO_3^- data. TA = total alkalinity; DIC = dissolved inorganic carbon.

The air-sea pCO_2 gradient was then calculated from the difference between the observed surface water pCO_2 and the atmospheric pCO_2 at the Zeppelin Station. At two occasions the atmospheric pCO_2 was linearly interpolated since there were some gaps in the data set. The uncertainty in these interpolated values should be reflected in the standard deviation of the atmospheric pCO_2 over a longer period, for example, a month, which typically varies around 4 μatm. This gives an uncertainty in the interpolated pCO_2 of ±1%.

The uncertainty in the estimated fluxes ranged between 20% and 33% as estimated from uncertainties in k, K_0, and the air-sea pCO_2 gradient of 20%, 0.2%, and 4–26%, respectively. The fluxes were integrated over the annual cycle using trapezoidal integration. The uncertainty in the annual flux was obtained by taking care of the error propagation at each area calculation and summation step of the trapezoidal integration.

2.3. Drivers of pCO_2 Variability

Variability in surface water pCO_2 can be explained by several processes of which thermal forcing, changes in salinity, mixing/advection, air-sea CO_2 fluxes, and biological forcing will be considered here. Since there was no sea ice in Adventfjorden apart from a brief period in mid-March 2015, changes in pCO_2 due to $CaCO_3$ dissolution/formation are omitted. Riverine input of TA and DIC are included in the assessment of mixing and advection, whereas riverine nutrients and organic matter will mainly be covered in the discussion section. The monthly effects of the individual processes on surface water pCO_2 were estimated as done previously by a number of authors (e.g., Chierici et al., 2006; Fransson et al., 2017; Lüger et al., 2004).

The change in pCO_2 as a result of a change in temperature is commonly estimated according to Takahashi et al. (1993):

$$\partial \ln pCO_2 / \partial T = 0.0423/^{\circ}\mathrm{C} \tag{5}$$

for salinities and temperatures of 34–36 and 2–28°C, respectively. To take into account the cold climate and seasonal discharges of freshwater at the study site, the temperature coefficient above (0.0423/°C) may not be valid. A model was therefore set up to estimate a value for colder (−1.8 and 10°C) and less saline waters ($30 < S < 35$) using CO2SYS with a resolution of 0.1 in salinity. For each step in salinity, TA and DIC were used to estimate pCO_2 for the temperature range −1.8 and 10°C. To see which TA and DIC values to use for the different salinity steps, all TA and DIC values are plotted against salinity in Figure 2. Typical TA and DIC values for the salinity range and resolution in question were obtained from linear regression. For the DIC data the regression was segmented with a break point at $S = 33.7$. The variability in DIC for $S > 33.7$ is affected by primary production to a larger degree then for $S < 33.7$ as indicated by the sharp decline in NO_3^- in the salinity range of 33.7 to 35 (Figure 2). A segmented regression for the DIC values therefor captures the natural variability better.

The relationship between the natural logarithm of pCO_2 for each salinity level and temperature was evaluated with a linear least square fit. The obtained temperature coefficients (β), that is, $\partial \ln pCO_2/\partial T$, were

Table 1
Mean Temperature Coefficients (β) for Specific Salinity Intervals

Salinity	β (°C^{-1})
30–32	0.0459
32–33	0.0458
33–34	0.0457
34–34.5	0.0456
34.5–35	0.0454

binned to salinity intervals according to Table 1. The change in pCO_2 between two sampling occasions as a result of temperature changes ($\Delta pCO_{2,T}$) was then estimated for each salinity bin:

$$\Delta pCO_{2,T} = pCO_{2,pm} e^{\beta \Delta T} - pCO_{2,pm} \quad (6)$$

where β is taken from Table 1 according to the salinity, ΔT is the observed change in temperature between two sampling occasions, and pm denotes the previous measurement.

Changes in salinity also affect the solubility of CO_2, and this effect on pCO_2 was estimated according to equation (7) (Sarmiento & Gruber, 2006):

$$\Delta pCO_{2,S} = \Delta S \frac{pCO_{2,pm}}{S_{pm}} (\partial \ln pCO_2 / \partial \ln S)_{pm} \quad (7)$$

where S is salinity and ΔS is the observed change in salinity. Again, pm denotes the previous measurement.

When sea ice is absent, salinity varies mainly due to evaporation, precipitation, mixing between different water masses including freshwater runoff, and advection. These processes will also result in changes in TA and DIC, which consequently will affect the surface water pCO_2. This change in pCO_2 ($\Delta pCO_{2,mix,adv}$) was estimated from TA-S and DIC-S relationships:

$$TA = 57.5S + 294 \quad (8a)$$

$$DIC = 52.0S + 339 \quad (8b)$$

Changes in salinity (ΔS) between sampling occasions were used to calculate the corresponding changes in TA (ΔTA_s) and DIC (ΔDIC_s). ΔTA_s and ΔDIC_s were added to the TA and DIC of the previous occasion and the perturbed pCO_2 was calculated using CO2SYS for the salinity and temperature conditions of the previous sampling. The change in pCO_2 was determined from the difference between the perturbed pCO_2 and the pCO_2 of the previous sampling occasion. Equations (8a) and (8b) were derived for mixing between TAW (prebloom mean values from 2016: S = 34.8, TA = 2,295 μmol/kg, DIC = 2,150 μmol/kg) and land runoff (TA = 294 ± 3 μmol/kg, DIC = 339 ± 7 μmol/kg). The corresponding equations for mixing between ArW (i.e., prebloom values from 2015: S = 34.5, TA = 2276 μmol/kg, DIC = 2,140 μmol/kg) and land runoff differ by less than 1%, and no distinction is therefor made to discriminate between ArW and TAW. Furthermore, the $\Delta TA/\Delta S$ and $\Delta DIC/\Delta S$ ratios of equations (8a) and (8b) are 4% and 1% higher than the ratios of the linear relationship in Figure 2a and the segmented regression ($S < 33.7$) in Figure 2b, respectively. In comparison, the $\Delta TA/\Delta S$ and $\Delta DIC/\Delta S$ ratios of equations (8a) and (8b) are 15% and 19% lower, respectively, than the corresponding ratios for a purely precipitation/evaporation driven TA and DIC variability. This confirms that the effect of land runoff on the TA and DIC variability dominates over the effects of evaporation and precipitation.

The change in pCO_2 between observations due to air-sea exchange was estimated from the expression below:

$$\Delta pCO_{2,asf} = \int_{t_{pm}}^{t_m} F_{asf} dt \frac{(\partial \ln pCO_2 / \partial \ln DIC)_{pm}}{h_{BD}} \frac{pCO_{2,pm}}{DIC_{pm}} \quad (9)$$

using trapezoidal integration of the flux (F_{asf}, equation (2)) between sampling occasions, that is, between the previous measurement at time, t_{pm}, and the current measurement at time, t_m. Equation (9) is based on the assumption that the absorbed CO_2 is distributed over the equivalent to the mixed layer depth, h_{BD}, at time t_m. This property was developed by Randelhoff et al. (2017) for the marginal ice zone where the impact of sea ice melt results in a similar shift from a nonstratified to a stratified water column as observed in Svalbard fjords. h_{BD} can be regarded as an upper bound of the depth to which wind driven turbulent mixing reaches (Randelhoff et al., 2017). The authors defined the equivalent to the mixed layer depth using the potential density anomaly of seawater ($\sigma_\theta = \rho$ – 1,000 kg/m^3), according to the equation:

$$h_{BD} = BD / \Delta \sigma_\theta \quad (10)$$

where BD is the buoyancy deficit and $\Delta\sigma_\theta$ is the density difference between the surface (mean σ_θ over 3 to 5 m) and a deeper reference layer ($\sigma_{\theta d}$). The BD was calculated as follows:

$$BD = \int_{Surface}^{60\ m} dz[\sigma_{\theta d} - \sigma_\theta(z)] \quad (11)$$

Based on visual inspection of all density profiles the background deep water density ($\sigma_{\theta d}$) was defined as the mean over the depth range of 55–65 m. If the surface density deviation $\Delta\sigma_\theta$ was larger than 0.03 kg/m^3 the profiles were considered to be influenced by freshwater. This limit was set to discern real differences in density from noise in the low resolution measurements of the SD204.

Biological activity, in terms of the balance between primary production and respiration in the surface waters, is reflected by changes in DIC according to the equation below:

$$\Delta pCO_{2,bio} = (\Delta DIC - \Delta DIC_{asf} - \Delta DIC_S)\frac{pCO_{2,pm}}{DIC_{pm}}\ (\partial \ln pCO_2/\partial \ln DIC)_{pm} \quad (12)$$

When $\Delta pCO_{2,bio}$ is positive, respiration dominates over primary production. The changes in DIC due to air-sea exchange (ΔDIC_{asf}) between observations were estimated from the air-sea flux as outlined in equation (9) without the recalculation to pCO_2 (equation (13)):

$$\Delta DIC_{asf} = \frac{\int_{t_{pm}}^{t_m} F_{asf} dt}{h_{BD}} \quad (13)$$

The impact of changes in salinity on DIC (ΔDIC_S) was calculated using equation (8b). Note that the maximum effect of biological activity on TA is in the order of the maximum change in the NO_3^- concentration (e.g., ~10 μmol/kg over the phytoplankton bloom period). For that reason, the resultant effect on pCO_2 was ignored.

To clarify seasonal patterns monthly changes in pCO_2 due to thermal forcing, changes in salinity, mixing/advection, air-sea CO_2 fluxes, and biological forcing were estimated. The parameters were interpolated at the turns of the months, and changes between observations and/or turns of the months were calculated as described above and subsequently summed within months.

2.4. Error Propagation in the Calculated Effects of the Drivers on Surface Water pCO_2

A Monte Carlo approach was used to estimate the propagated errors according to the following steps:

1. Normally distributed artificial random errors (n = 10,000) with a mean of zero and a standard deviation determined by the uncertainty of each property were added to the properties, respectively. The uncertainty is here the combined error that results from the accuracy and resolution/precision of the specific method used to determine the specific property. The documented resolution and accuracy of the CTD data are given in Appendix A (see Table A2). The precision and accuracy of TA is also given in Appendix A (see Table A2). For DIC and pCO_2 the uncertainty refers to the error estimate that is outlined in section 2.3. The uncertainty in the flux is also estimated from the uncertainties outlined in section 2.3 and can be regarded as a lower bound of the real uncertainty. The uncertainty in the temperature coefficient is difficult to assess but was set to ±0.003 as a sensitivity test. This is roughly the difference between the temperature coefficients in Table 1 and the coefficient of Takahashi et al. (1993), which means that the coefficients in Table 1 result in 3‰ larger changes in pCO_2 per degree Celsius. The uncertainties in the $\Delta TA/\Delta S$ and $\Delta DIC/\Delta S$ ratios were set to 2.5 μmol/kg per 1‰ to reflect the 4% difference between the $\Delta TA/\Delta S$ ratio and the linear relationship in Figure 2a. The uncertainty in the calculated h_{BD} was estimated by a separate Monte Carlo approach to be around ±1 m, but the main uncertainty is of course the use of h_{BD} as an approximation of the depth over which a loss or gain in CO_2 is distributed. To give a number to this uncertainty the median relationship between the ratio of h_{BD} and the depth to which wind-driven turbulent mixing reaches (h_ε) and wind work was used (Randelhoff et al., 2017, see Figure 8b). On a monthly scale the wind work in Adventfjorden is high enough for the median ratio of h_{BD} and h_ε to vary between 1 and 1.5. For that reason the ratio of 1.25 was chosen and the uncertainty in h_{BD} was approximated from the differences between all estimates of h_{BD} and $h_{BD}/1.25$, that is, in average 6 m, which gives an uncertainty of ±6 m. Note that for the iterations where h_{BD} (that ranged between 10 and 51 m)

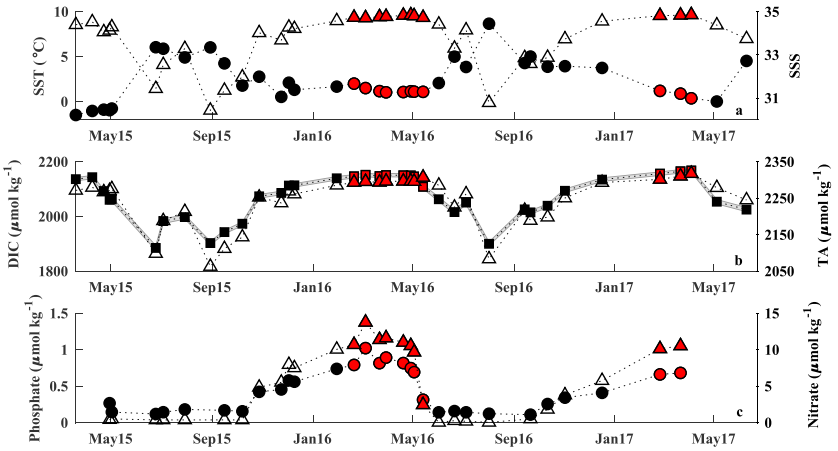

Figure 3. Time series of (a) sea surface temperature (SST, °C; dot) and sea surface salinity (SSS, open triangle), (b) total dissolved inorganic carbon (DIC, μmol/kg; filled square) with its associated estimated uncertainty (gray shade) and total alkalinity (TA, μmol/kg; open triangle), and (c) phosphate (μmol/kg; dot) and nitrate (μmol/kg; open triangle) concentrations. Red markers indicate the presence of Transformed Atlantic Water/Atlantic Water.

plus the random error were below 2 m, the sum was adjusted to 2 m to remove negative or close to zero values. This also reflects the depth from which reliable CTD measurements exist.

2. The properties plus the random errors were used to estimate $\Delta pCO_{2,T}$, $\Delta pCO_{2,S}$, $\Delta pCO_{2,mix,adv}$, $\Delta pCO_{2,asf}$, and $\Delta pCO_{2,bio}$ according to section 2.3, that is, 10,000 estimates for each term.
3. The standard deviation of the 10,000 estimates for each term was used as measure of the uncertainty.

3. Results

3.1. Hydrographic Conditions

The time series of the different parameters are shown in Figure 3. Between March 2015 and June 2017 the seasonal difference between winter and summer in SST at the IsA Station (Figure 3a) was around 7°C, that is, the maximum difference for each year, with the coldest conditions (−1.5°C) observed at the onset of the study. The two following winters were considerably warmer with temperatures averaging around 2°C. The highest observed values were 6.1°C in June 2015 and 8.7°C in August 2016, but the variability was considerably higher over the second summer.

In 2015 and early 2016 wintertime SSS was typically less than 34.6 (Figure 3a). This rather fresh water mass (ArW) was replaced in February 2016 by TAW that was also present the following winter. In June, regardless of year, SSS dropped below 34 and reached values below 31 in August. The impact of the freshening of the surface layer over the summer season was evident in the SSS throughout autumn.

The surface TA was around 2270 μmol/kg in spring 2015 and early winter 2016 (Figure 3b). These values increased to about 2,300 when TAW entered the site in February 2016. Similarly as for SSS, the addition of freshwater in the summer diluted TA with surface concentrations reaching minima of around 2,060–2,090 μmol/kg at the end of summer.

Surface DIC concentrations largely followed the observed seasonal patterns in SSS and TA, except for the drawdown of DIC that occurred in April–May before the onset of the melt season as seen in Figure 3b. Between January and April prebloom DIC concentrations reached values of around 2,140–2,170 μmol/kg with the highest values seen in 2017. The TAW had typically ~10–20 μmol/kg higher values than the fresher water mass that was observed in 2015 and early 2016. Summertime DIC concentrations dropped to around 1,900 μmol/kg in August, but the altogether lowest observed concentration (1,885 μmol/kg) was observed in June 2015.

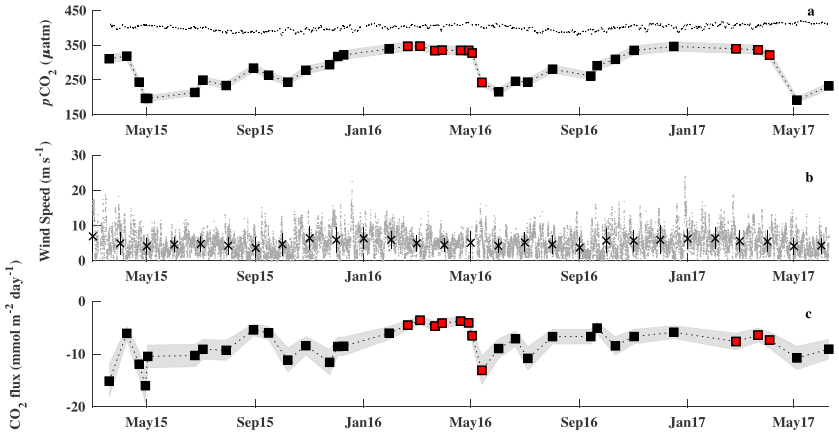

Figure 4. Time series of (a) calculated pCO_2 in air according to equation (4) for the air and vapor pressure at Longyearbyen airport using xCO_2 data from the Zeppelin mountain (hourly average, μatm; dotted black line), calculated pCO_2 in the surface water (μatm; black squares and uncertainty as indicated by gray shade), (b) hourly wind speed (m/s; gray dots) and monthly mean wind speed (m/s; black crosses with standard deviation), and (c) air-sea CO_2 flux (mmol·m^{-2}·day^{-1}; black squares and uncertainty as indicated by gray shade). Red markers indicate the presence of Transformed Atlantic Water/ Atlantic Water.

The nutrient data only extends between end of April in 2015 and March 2017 (Figure 3c). The surface concentrations of NO_3^- dropped sharply in midspring and remained close to the detection limit throughout the summer season. Late winter concentrations typically reached values of ~11 μmol/kg. PO_4^- concentrations varied from ~0.1 to 1 μmol/kg in the surface waters, following the trends observed in NO_3^-.

3.2. Surface Water pCO_2 and Air-Sea CO_2 Exchange

Between January and March pCO_2 varied from 310 to 350 μatm with higher values in 2016 and 2017 (Figure 4a). In April 2015, May 2016, and April 2017, the seawater pCO_2 dropped from the winter values mentioned above to around 200–250 μatm. These minima in pCO_2 that were more pronounced in 2015 and 2017 also coincided with low nutrient concentrations (around the detection limit for NO_3^- and 0.1–0.3 μmol/kg for PO_4^{3-}, Figure 3c). The surface water pCO_2 increased slowly over the summer and autumn months to reach winter values by the end of the year.

Atmospheric pCO_2 (Figure 4a) showed a less pronounced seasonal signal with summertime values from 380 to 395 to winter values between 400 and 415 μatm. The pCO_2 in the surface water was thereby undersaturated in CO_2 in relation to atmospheric CO_2 all year round with an air-sea pCO_2 gradient ranging between −51 and −217 μatm.

The monthly mean wind speed varied from 3.7 to 6.9 m/s (Figure 4b). The wind speed was slightly higher over the winter months compared to the summer season. The maximum wind speed of 26.5 m/s occurred during a storm event at the end of 2015, when the anemometer failed to log for a couple of hours due to the wind force.

The air-sea CO_2 fluxes varied between −4 and −16 mmol C·m^{-2}·day^{-1} (Figure 4c, negative values mean ocean CO_2 uptake), largely following the variability in surface water pCO_2; that is, the largest fluxes occurred generally when the surface water pCO_2 was at its minimum. Months with higher mean wind speed also contributed to high fluxes such as that observed in March 2015. The integrated annual fluxes were −35.8 ± 1.7 and −31.2 ± 1.8 g C·m^{-2}·year^{-1}, for the first and second annual cycles, respectively, beginning with the month of April.

3.3. Drivers of pCO_2 Variability

The different processes that drive changes in pCO_2 were investigated in terms of monthly changes following two full annual cycles, as estimated from the month of April (Figure 5). Primary production was responsible

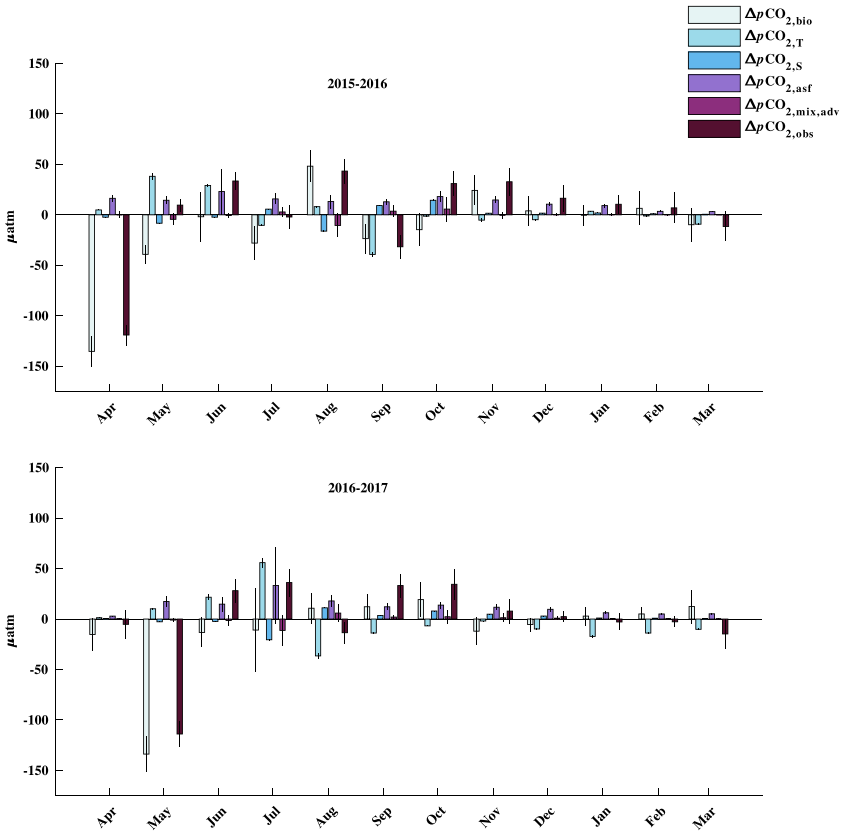

Figure 5. Monthly changes in pCO_2 (µatm) either observed ($\Delta pCO_{2,obs}$) or calculated from changes in biological activity (respiration and/or primary production, $\Delta pCO_{2,bio}$), temperature ($\Delta pCO_{2,T}$), salinity ($\Delta pCO_{2,S}$), air-sea flux ($\Delta pCO_{2,asf}$), and mixing/advection ($\Delta pCO_{2,mix,adv}$). Note that there exist no observations for the month of January in 2017. The uncertainty (black error bars) was calculated as outlined in section 2.4.

for a drop in pCO_2 of around 130–140 µatm in April 2015 and May 2016. This decrease was partly counteracted by the effect of warming, which contributed to a pCO_2 increase of ~70 µatm in May and June 2015 and nearly 90 µatm between May and July in 2016. The effect of warming was followed by cooling in late summer and autumn which decreased pCO_2. The maximum monthly changes in pCO_2 due to decreased salinity over the melt season were in the order of 20 µatm as observed in August 2015 and July 2016, which was counteracted by increases in salinity toward autumn. The magnitude of the combined effect of mixing and advection on pCO_2 was in the order of 0.1 to 10 µatm on a monthly scale. The monthly effect of air-sea CO_2 fluxes on pCO_2 was strongest in the summer months, for example, 21 µatm in June 2015 and 26 µatm in July and August 2016, when the stratification of the surface layer was more pronounced.

Between December and March, $\Delta pCO_{2,bio}$ was in average 2 ± 7 µatm. Similarly, $\Delta pCO_{2,T}$, $\Delta pCO_{2,S}$, $\Delta pCO_{2,mix,adv}$, $\Delta pCO_{2,asf}$, and $\Delta pCO_{2,obs}$ were in average -8 ± 7, 1 ± 1, 0.3 ± 0.2, 7 ± 3, and 1 ± 11 µatm, which suggests that the variation in pCO_2 and the effects of its associated drivers are small in the winter season.

On an annual scale, the biological processes resulted in a net decrease in pCO_2 of 170 and 128 µatm over the first and second annual cycles, respectively (Table 2), but the uncertainties in these estimates are large. Still,

Table 2
Net Annual Change in Surface Water pCO_2 (μatm) at the IsA Station Between April 2015, 2016, and 2017

Period	$\Delta pCO_{2,bio}$	$\Delta pCO_{2,T}$	$\Delta pCO_{2,S}$	$\Delta pCO_{2,asf}$	$\Delta pCO_{2,mix,adv}$	$\Delta pCO_{2,obs}$
2015–2016	−170 ± 37	12 ± 5	7 ± 1	155 ± 28	−2 ± 22	20 ± 14
2016–2017	−128 ± 50	−21 ± 7	7 ± 1	150 ± 43	−1 ± 21	−11 ± 15

Note. The annual changes were estimated from the observed changes ($\Delta pCO_{2,obs}$) as well as from the monthly changes outlined in section 2.3, that is, changes in biological activity ($\Delta pCO_{2,bio}$), temperature ($\Delta pCO_{2,T}$), salinity ($\Delta pCO_{2,S}$), air-sea flux ($\Delta pCO_{2,asf}$), and mixing/advection ($\Delta pCO_{2,mix,adv}$).

the net effect was negative and the annual effect of primary production on surface water pCO_2 largely exceeds the effect of respiration. The net effect of biological activity (primary production) was counteracted by air-sea CO_2 exchange that resulted in a net increase in pCO_2 of around 150 μatm for both years. The effects of temperature and salinity on surface water pCO_2 were an order of magnitude smaller. The net effect of salinity was positive over both annual cycles resulting in an increase of pCO_2 of 7 μatm for each year. The net impact of temperature on the other hand was positive over the first annual cycle by the end of which warm TAW had entered the site and negative the following year. Mixing and advection had a minimal impact on pCO_2 on an annual scale.

The relative contribution of biological activity to the total change in pCO_2, as estimated from the annual sum of the absolute valued changes, was 41% and 32% for the first and second annual cycles, respectively (Figure 6). Temperature, on the other hand, contributed with 19% and 25% of the total change in pCO_2 over the first and second annual cycles, respectively. The air-sea flux accounted for 19% of the total change. The contribution of salinity, in terms of the solubility effect on pCO_2, to the total change (7–8%) was smaller in size compared to the residual term (9–13%), but twice as large as the contribution of mixing and advection (3–4%).

4. Discussion

4.1. Variability of Air-Sea CO_2 Exchange

Spitsbergen is situated at the borders of the central Arctic Ocean and the Barents Sea and surrounded by surface waters with documented low seawater pCO_2 compared to the atmosphere (e.g., Fransson et al., 2017; Lauvset et al., 2013; Yasunaka et al., 2016). This is also the case for the IsA Station in Adventfjorden where the surface waters were undersatured in CO_2 compared to the atmosphere all year round and the air-sea pCO_2 gradient ranged between −51 and −217 μatm.

These values can be compared to air-sea pCO_2 gradients in March and September of around −30 to −140 μatm in the nearby glacial influenced fjord branch of Isfjorden, Tempelfjorden (Fransson et al., 2015), and in April and July of −70 to −200 μatm in Kongsfjorden further north (Fransson et al., 2016). The uptake potential, based on the air-sea pCO_2 gradient in these fjords, should therefore be close to comparable to that of Adventfjorden. As an example, the September air-sea pCO_2 gradient in Tempelfjorden of close to −130 to −140 μatm (Fransson et al., 2015), with SST and SSS of around 3°C and 32.2, respectively, results in fluxes of −6.3 to −6.8 mmol C·m^{-2}·day^{-1}, when using the September mean squared wind speed of 22.5 m^2/s^2 at Longyearbyen airport. These values are comparable to the calculated September fluxes at the IsA Station of −5.1 to −6.7 mmol C·m^{-2}·day^{-1} (Figure 4). However, the actual uptake in Tempelfjorden, as well as in Kongsfjorden, will be a result of the local wind distribution and on a yearly basis the length of the ice-free period will play a significant role.

Shifting the focus from the West Spitsbergen fjord systems to the surrounding areas, Fransson et al. (2017) observed air-sea pCO_2 gradients in January to June of −81 to −254 μatm (including sea ice) in the surface waters north of Svalbard (on the slope and in the Nansen Basin) and Omar et al. (2007) and Lauvset et al. (2013) give monthly mean estimates for the neighboring productive Barents Sea ranging between −10 and −100 μatm. Although comparable pCO_2 gradients, the annual CO_2 uptake rates of 31–36 g C·m^{-2}·year^{-1} found for the IsA Station are smaller than the uptake rates estimated for waters north of Svalbard (potential ice-free uptake: ~44–114 g C·m^{-2}·year^{-1}, Fransson et al., 2017) as well as for waters in the Barents Sea (46 g C·m^{-2}·year^{-1}, Nakaoka et al., 2006; 51 g C·m^{-2}·year^{-1}, Omar et al., 2007;

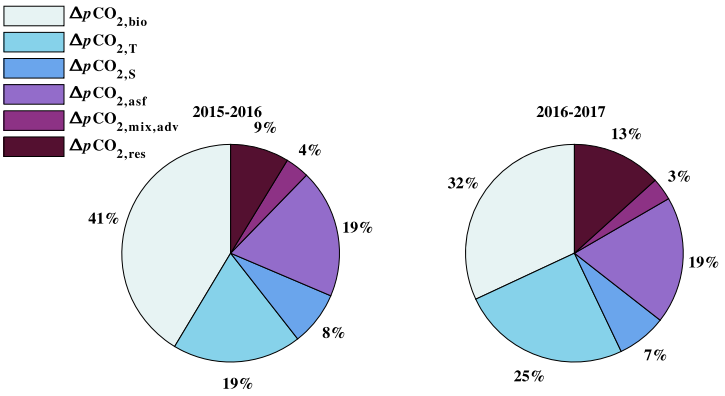

Figure 6. Pie chart over the annual sum of absolute valued monthly changes in pCO_2 due to biological activity, temperature, salinity, air-sea exchange, mixing/advection, and the residual ($\Delta pCO_{2,res}$). The latter is the change that remains when the effects of the other processes are withdrawn from the observed change.

48 g C·m^{-2}·year^{-1}, Lauvset et al., 2013; ~44 g C·m^{-2}·year^{-1}, Yasunaka et al., 2016), with a few exceptions (e.g., Land et al., 2013; Takahashi et al., 2009).

One possible reason for the observed differences in uptake rates between Adventfjorden (31–36 g C·m^{-2}·year^{-1}) and the neighboring regions (44–114 g C·m^{-2}·year^{-1}) is the gas transfer velocity both in terms of the wind speed parameterization as well as of the wind speed distribution. The estimated rates of Fransson et al. (2017) are based on comparable methods, but the studies from the Barents Sea differ from the present study. Nakaoka et al. (2006) did not specifically state which wind speed relationship their flux estimates were based on, but Lauvset et al. (2013) and Omar et al. (2007) used the wind speed relationships of Wanninkhof (1992) for long-term averaged winds of a year or more and short-term averaged winds, respectively. The latter suffered from its assumption of a Rayleigh distribution of the wind speed. Applying the two wind speed relationships for comparison to the data set from the IsA Station would increase or decrease the estimated uptake rates by around 16% for the long-term and short-term formulas, respectively. Yasunaka et al. (2016) rescaled the gas transfer coefficient of Sweeney et al. (2007) of 0.27 to 0.19 to fit the U.S. National Centers for Environmental Prediction-Department of Energy Reanalysis 2 wind speed product (NCEP-2), which applied to the present data set also would reduce the uptake rates. None of these comparisons are straightforward because of the local scale of the present study as well as the use of different wind products.

Since the different wind speed formulas did not resolve the observed differences in uptake rates between Adventfjorden and the Barents Sea, the wind speed distribution must play an important part. As an example of that, the wind speed distribution at Svalbard Airport over the first annual cycle is shown in Figure 7 together with the NCEP-2 wind distribution. The wind speed data subset for the Isfjorden region (77–79°N, 13–19°E) was provided by the NOAA/OAR/ESRL PSD, Boulder, Colorado, United States (https://www.esrl.noaa.gov/psd/data/gridded/data.ncep.reanalysis2.pressure.html). The frequency at higher wind speeds quickly drops to close to zero at Longyearbyen airport, as opposed to the more large-scale NCEP-2 wind speeds. This difference, apart from the uncertainty in the NCEP-2 product, could be a result of the local impact of the mountains that surrounds Adventfjorden and/or reflect a bias in the measured winds due to the location of the wind meter. Using an annual mean air-sea pCO_2 gradient of −108 μatm for the IsA Station and a gas transfer velocity estimated from the squared NCEP-2 wind speed and the wind speed relationship used by Yasunaka et al. (2016), the estimated annual uptake at the IsA Station would then be higher, around 57 g C·m^{-2}·year^{-1}. This implies that the surface waters of Adventfjorden have the potential to be a strong sink for atmospheric CO_2 as long as the wind distribution allows an efficient gas transfer.

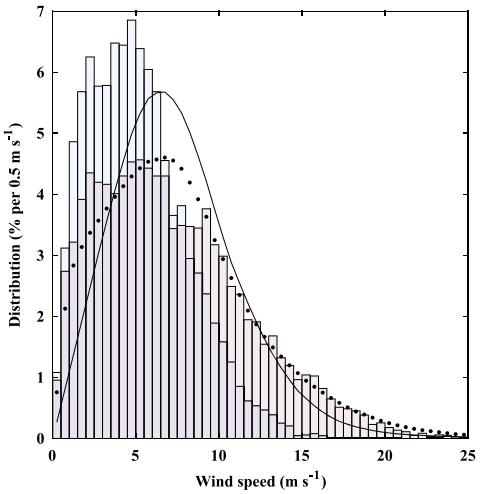

Figure 7. Histogram of the distribution of winds at Svalbard Airport (pale blue bars), and NCEP-2 over the Isfjorden area (77–79°N, 13–19°E, with a resolution of 2 ×2, pale purple bars) for the period 1 April 2015 to 1 April 2016. Solid line is the global Cross-Calibrated Multi-Platform distribution, and the dotted line is the global NCEP-2 distribution for 1990–2009 (Wanninkhof, 2014). NCEP-2 = U.S. National Centers for Environmental Prediction-Department of Energy Reanalysis 2 wind speed product.

With this in mind, the comparisons will now be extended to the glacier-influenced Greenland fjords. These studies have typically used the gas transfer velocity formula of Nightingale et al. (2000), which is comparable to that of Wanninkhof (2014) within a few percentages. Also here, the integrated uptake rates of 31–36 g C·m^{-2}·year^{-1} at the IsA Station fall in the lower range (32 g C·m^{-2}·year^{-1}, Sejr et al., 2011; 19–172 g C·m^{-2}·year^{-1}, Rysgaard et al., 2012; 37–70 g C·m^{-2}·year^{-1}, Meire et al., 2015). The estimated uptake of Sejr et al. (2011) was conducted in Young Sound and is based on a mean July–August air-sea pCO_2 gradient of −106 μatm over the sea ice-free period (94 days). This can be compared to annually integrated mean air-sea pCO_2 gradients at the IsA Station of −100 to −120 μatm. Considering that the air-sea pCO_2 gradients are comparable and the overall short period of air-sea gas exchange in Young Sound due to the extensive sea ice cover, the high annual uptake of 32 g C·m^{-2}·year^{-1} (that includes an ice formation period of 10 days with an efflux of 1.1 mmol·m^{-2}·day^{-1}) must be a result of more intense winds compared to the situation in Adventfjorden. The uptake rates in the Godthåbsfjord SW Greenland showed considerable interannual variability and the maximum annual uptake rate was more than 150 g C·m^{-2}·year^{-1} higher than the lowest (Rysgaard et al., 2012). This reflects a large interannual variability in the monthly air-sea pCO_2 gradient that ranged between −350 and 350 μatm over the whole study, but there was also interannual variability in the monthly mean wind speed. In contrast, the two annual cycles of CO_2 uptake in Adventfjorden differed with as little as 5 g C·m^{-2}·year^{-1} despite the observed shift between Arctic to Atlantic origin waters (Figure 4).

Recent changes in the atmospheric circulation (Isaksen et al., 2016) have been suggested to facilitate the intrusion of Atlantic Water onto the shelf as well as into the West Spitsbergen fjords (Nilsen et al., 2016). The difference in the CO_2 uptake rates between Arctic and Atlantic origin waters were evaluated, with the awareness that 2 years of observations are unlikely to capture the overall natural variability in the air-sea CO_2 fluxes. Prebloom and winter fluxes from March, April, and December in 2015 (Arctic conditions) were compared to prebloom values from February to April in 2016 when TAW dominated the water column ($n_{2015} = n_{2016} = 4$). The mean squared wind speed and mean atmospheric pCO_2 over the mentioned months (40.8 m^2/s^2 and 404 μatm, respectively) were used in the comparison. The fluxes of the Arctic origin waters were significantly higher and the surface water pCO_2 was significantly lower (2 mmol C·m^{-2}·day^{-1} and 24 μatm, respectively, $p = 0.001$ for both tests), as compared to those of the TAW. If the investigated periods are representative for the two water masses, especially considering that the West Spitsbergen fjords are going through some major transitions (a reduction in the sea ice cover, Muckenhuber et al., 2016; a warming of the Atlantic Water of 0.2°C per decade in Isfjorden, Pavlov et al., 2013), and if the atmospheric forcing continues to transport Atlantic Water into the fjord systems, the CO_2 uptake capacity could decrease in this region.

4.2. Impact of Drivers on pCO_2

Biological processes in terms of primary production and respiration together with temperature were the two main drivers that control surface water pCO_2 in Adventfjorden on a monthly scale (Figures 5 and 6). To validate the importance of biological processes and temperature effects on pCO_2, surface water pCO_2 was also modeled as a function of different combinations of T, S, NO_3^- using multiple linear regression (MLR) relationships (Appendix B). The linear combinations of T, S, and NO_3^- reflect not only the thermodynamic dependencies of seawater pCO_2 on T and S (e.g., Takahashi et al., 1993) but also the effects of primary production and remineralization through the Redfield stoichiometric relationship between NO_3^- and DIC (e.g., Redfield et al., 1963; Sarmiento & Gruber, 2006), which translates to changes in pCO_2. Although it should be noted that nutrients also vary to some extent due to mixing, NO_3^- and temperature had the highest predictive power of seawater pCO_2 ($R_{adj}^2 = 0.8$, Table B1).

Biological activity was likewise a key driver for surface water pCO_2 on an annual scale together with air-sea exchange that essentially counteracts the effect of primary production in spring (Table 2). The importance for biological CO_2 consumption has also been observed in the waters north of Svalbard (January–June), with a relative effect of 26% (Fransson et al., 2017), as compared to the 32–41% in Adventfjorden.

Temperature is, typically together with biological processes, a key driver of pCO_2 variability in the Global Ocean, for example, such as observed in the North Atlantic by Lüger et al. (2004), or in the subarctic North Pacific Ocean (Chierici et al., 2006), but temperature is not necessarily important in the Arctic Ocean (Chierici et al., 2011). One reason to why temperature is important in Adventfjorden could be the current lack of sea ice in large parts of the Isfjorden system (Muckenhuber et al., 2016). The lack of ice not only allows a continuous air-sea heat and gas exchange, but it also removes the impacts of different sea ice processes that may affect the surface water pCO_2. For instance, in waters north of Svalbard the relative effect of the total change in seawater fCO_2 (or pCO_2) as a result of $CaCO_3$ (ikaite) dissolution was estimated to 38% over the winter-spring period (Fransson et al., 2017).

Salinity had only a small relative effect of 7–8% on the surface water pCO_2 at the IsA Station, which reflects the rather modest seasonal difference of around 4 between winter and late summer. In comparison, the SSS drops to around 20 in the Greenland fjords (Meire et al., 2015; Rysgaard et al., 2012; Sejr et al., 2011). Meire et al. (2015) estimated that the release of glacial meltwater in the Godthåbsfjord accounted for as much as 28% of the CO_2 uptake.

So far, the discussion has ignored the effects of riverine input of nutrients and organic matter on surface water pCO_2. The main reason for this is the rather small impacts these riverine constituents have on the pCO_2 variability at the outer part of Adventfjorden. First, Wynn et al. (2007) observed NO_3^- concentrations in glacial runoff of $\leq$5 μmol/L (Midtre Lovénbreen, Ny Ålesund, Spitsbergen). For a maximum freshwater fraction (f_{fw}) of 12% as estimated from equation (14):

$$f_{fw} = \frac{S_{\text{winter}} - S}{S_{\text{winter}}} \tag{14}$$

where S = 30.4 (minimum salinity observed on 29 August 2015) and a winter reference salinity (S_{winter}) of 34.7, a meltwater NO_3^- concentration of 5 μmol/L would increase the seawater NO_3^- concentration by 0.6 μmol/L, which corresponds to 0.2 $\mu mol \cdot L^{-1} \cdot month^{-1}$ over the melt season. If this added NO_3^- was fixated into organic matter the corresponding decrease in DIC would be 1 $\mu mol \cdot L^{-1} \cdot month^{-1}$, for a classical stoichiometric Redfield ratio between carbon and nitrogen (C/N) of 6.6 (Redfield et al., 1963). The effect on surface water pCO_2 would not be discernible. Second, the riverine input of organic matter has little impact on the surface water pCO_2 since the concentration of NO_3^- remains close to the detection limit throughout the summer season ($NO_3^- < 0.4$ μmol/L). That means that any decay products of riverine organic matter will be absorbed and fixated into new organic matter with the net effect on surface water pCO_2 being zero.

5. Conclusion

Adventfjorden, similar to surrounding polar and subpolar regions, is a net annual CO_2 sink. The uptake potential, in terms of the air-sea pCO_2 gradient, is close to similar to neighboring fjords of the West Spitsbergen, to ice-covered waters north of Svalbard, and to the surface waters of the Barents Sea. The wind distribution over the fjord, as estimated from the wind meter at Svalbard Airport, is, however, shifted toward lower wind speeds. The result is a more modest annual uptake rate (31–36 g $C \cdot m^{-2} \cdot year^{-1}$) compared to most estimates in the surrounding areas.

The fluxes were significantly higher in the Arctic origin waters compared to fluxes of TAW. If Atlantic Water continues to be transported into the West Spitsbergen fjords over the coming years, as observed over recent years (Pavlov et al., 2013), the CO_2 uptake capacity could be diminished in this area. On the other hand, if the observed warming of the Atlantic Water of the West Spitsbergen Current (e.g., 0.2°C per decade, Isfjorden, Pavlov et al., 2013; 0.3°C per decade north of Svalbard, Onarheim et al., 2014) also continues, this could possibly result in an increased amount of glacial meltwater being released to the fjords. The outcome of these

potential warming and freshening effects on surface pCO_2 needs to be further evaluated. So far, on a seasonal scale, the main drivers for the observed pCO_2 variability are biological processes and to a lesser extent temperature, which likely reflect the current ice-free conditions at the IsA Station, but this may change in the coming future of climate change.

Appendix A: Data Provenance

An overview of the sampling occasions, including the CTD-devices that were used and the discrete water samples that were collected, is presented in Table A1. The documented accuracy and resolution of the different CTD-instruments are given in Table A2, together with uncertainties in the input parameters (i.e. TA, pH, T, K1 and K2) that were used in the CO2SYS software to calculate pCO_2 and DIC.

Table A1
Data Overview

Dates	CTD	Samples	TA/pH	Nutrients
19 March 2015	SD204	4	Yes	NA
8 April 2015	SD 204	8	Yes	NA
22 April 2015	SBE19+[a]	8	Yes	NA
29 April 2015	SD204	8	Yes	Yes
2 May 2015	SBE9	5	Yes	Yes
24 June 2015	SD204	8	Yes	Yes
3 July 2015	SD204	8	Yes	Yes
29 July 2015	SBE37	8	Yes	Yes
29 August 2015	SBE9	5	Yes[b]	NA
15 September 2015	SD204	5	Yes	Yes
7 October 2015	SD204	5	Yes	Yes
27 October 2015	SBE37	5	Yes	Yes
23 Nov 2015	SBE37	8	Yes	Yes
2 December 2015	SBE37	5	Yes	Yes
9 December 2015	SBE37[c]	8	Yes	Yes
29 January 2016	SBE37	5	Yes	Yes
19 February 2016	SBE19+	5	Yes	Yes
4 March 2016	SBE19+	5	Yes	Yes
21 March 2016	SBE19+	5	Yes	Yes
29 March 2016	SBE19+	5	Yes	Yes
19 April 2016	SBE19+	5	Yes	Yes
28 April 2016	SD204[d]	8	Yes	Yes
2 May 2016	SBE19+	8	Yes	Yes
13 May 2016	SBE19+	5	Yes	Yes
1 June 2016	SBE19+	5	Yes	Yes
20 June 2016	SBE19+	5	Yes	Yes
4 July 2016	SBE19+	5	Yes	Yes
1 August 2016	SBE19+	5	Yes	Yes
13 September 2016	SBE9	7	Yes[e]	NA
20 September 2016	SD204[f]	5	Yes	Yes
11 October 2016	SBE19+	5	Yes	Yes
1 November 2016	SBE19+	5	Yes	Yes
16 December 2016	SBE19+	5	Yes	Yes
24 February 2017	SD204[g]	5	Yes	Yes
21 March 2017	SD204[g]	5	Yes	Yes
3 April 2017	SD204[g]	5	Yes	NA
4 May 2017	SBE19+	5	Yes	NA
9 June 2017	SBE19+	5	Yes	NA

Note. CTD = conductivity-temperature-depth; TA = total alkalinity; NA = not applicable.
[a]Measurements were conducted 17 April 2015. [b]Fixated with $HgCl_2$ and analyzed within 6 weeks. [c]Measurements were conducted 10 December 2015. [d]Salinity corrected for an offset of −0.10. [e]Analyzed 2 days after sampling. [f]Noise in pressure measurements; i.e., pressure was modeled, salinity recalculated for the new pressure, and finally, salinity was corrected for an offset of −0.13. [g]Salinity corrected for an offset of −0.14.

Table A2
Uncertainties in Parameters Used to Calculate the Marine CO_2 System, Air-Sea CO_2 Fluxes, and Effects of Drivers on Surface Water pCO_2

Parameters	Precision/*Resolution*	Accuracy
TA (μmol/kg)	±2(±4)[a]	±2(±4)
pH	±0.001[a]	±0.005
T (°C)[b]	0.1	±0.3
T (°C)[c]	0.001[1], 0.0001[2,4], 0.0002[3]	±0.01[1], ±0.005[2], ±0.001[3], ±0.002[4]
S[c]	0.01[1]	±0.02[1](±0.1[1])
C[c] (mS/cm)	0.0005[2], 0.0004[3], 0.0001[4]	±0.005[2], ±0.003[3,4]
K_1 (%)[d]	±2.5	
K_2 (%)[d]	±4.6	

Note. TA = total alkalinity.
[a]These values are the experimental precision reported as the mean absolute difference between duplicate sample runs, with the value for the endpoint determination in parentheses. [b]The laboratory temperature was measured using a digital probe (TFX410, technical data in the table), except for March to July 2015, and July and August 2016, when a flow-through thermistor was used. [c]Temperature, salinity, and conductivity (*C*) were obtained from the following conductivity-temperature-depth devices: (1) SD204, SAIV A/S, Norway (the value in brackets represents an offset that was corrected for as noted in Table A1), (2) SBE 19+, Seabird Electronics, United States, (3) SBE 9, Seabird Electronics, United States, and (4) SBE 37 MicroCAT, Seabird Electronics, United States. [d]These values are the experimental precision ($2S_E$).

Appendix B: Multiple Linear Regression Relationships

Paragraphs have already been provided for Appendix B. Only Appendix A needed them. Please ensure Appendix B is presented correctly.

pCO_2 was modeled as a function of different combinations of *T*, *S*, NO_3^-, and PO_4^{3-} using MLR relationships and a summary of selected results is shown in Table B1. The MLRs took the following form, for example,

$$pCO_2 = a_0 + a_1\left[NO_3^-\right] + a_2T + a_3S \quad \text{(B1)}$$

where a_0 through a_3 are the regression coefficients and the NO_3^- concentration was interchanged with the PO_4^{-3} concentration. The determination of the coefficients can be improved if the predictor variables are centered, that is, subtracting the mean from each property, but the aim here is rather to investigate the importance of the individual predictors. This goal was achieved by stepwise regressions where individual predictors were omitted to investigate the resultant change in the explained variation by the original model. The interaction terms were excluded from the models. The variance inflation factor was used to investigate collinearity between the predictor variables. The best combination of predictor variables was then chosen based on the variance inflation factor results and the R_{adj}^2 of the MLR relationship.

Table B1
Summary of Selected MLR Relationships of pCO_2 as a Function of $[NO_3^-]$, SST, and SSS (n = 30)

Dependent variable	Predictor variables	VIF	Coefficients	SE	*p*	R_{adj}^2	RMSE
MLR							
pCO_2	Constant	1.9, 2.3, 3.3	173.6	221.8	0.44	0.796	± 22.7
	$[NO_3^-]$		10.8	1.2	$3.1{\cdot}10^{-9}$		
	SST		8.8	3.0	$6.1{\cdot}10^{-3}$		
	SSS		1.1	6.5	0.86		
pCO_2	Constant	1.4, 1.4	212.1	10.4	$5.8{\cdot}10^{-18}$	0.803	± 22.3
	$[NO_3^-]$		10.9	1.0	$2.7{\cdot}10^{-11}$		
	SST		8.5	2.2	$6.9{\cdot}10^{-4}$		
pCO_2	Constant	1.9, 1.9	620.2	186.1	$2.5{\cdot}10^{-3}$	0.736	± 25.8
	$[NO_3^-]$		10.9	1.4	$2.3{\cdot}10^{-8}$		
	SSS		−11.4	5.6	$5.3{\cdot}10^{-2}$		
SLR							
pCO_2	Constant		244.5	7.3	$4.6{\cdot}10^{-24}$	0.707	± 27.2
	$[NO_3^-]$		8.9	1.1	$3.6{\cdot}10^{-9}$		
$pCO_{2,T\,=\,2.4°C}$	Constant		227.7	5.5	$1.3{\cdot}10^{-26}$	0.887	± 20.4
	$[NO_3^-]$		12.0	0.8	$5.4{\cdot}10^{-15}$		

Note. SST = sea surface temperature; SSS = sea surface salinity; MLR = multiple linear regression; RMSE = root-mean-square error; SLR = simple linear regression.

Acknowledgments
The fieldwork was mainly funded by Arctic Field grant (RiS: 10127, 10404, and 10662), which is given by the Research Council of Norway, with additional support from course activities at the University Centre in Svalbard (UNIS). Metadata is available at the RiS portal at www.researchinsvalbard.no. Data will be available within a year after publication at the Norwegian Marine Data Centre (NMDC), until then contact the corresponding author. CO_2 atmospheric data are available from the EBAS database: http://ebas.nilu.no with annual updates. We thank especially M. Porcires and L.-F. Stangeland, and also the whole logistic department at UNIS, for technical and logistic support. We also thank the marine researchers at the Department of Arctic Biology at UNIS for collaboration and support with the fieldwork. The study was also supported by the Ocean Acidification flagship within the FRAM-High North Centre for Climate and the Environment, Norway (A. Fransson and M. Chierici). The atmospheric xCO_2 data were supported by the Norwegian Research Council project Signals from the Arctic Ocean in the Atmosphere-SOCA. Finally, we give thanks to the Norwegian Meteorological Institute for the data from Svalbard Airport.

References

Andersson, A., Falck, E., Sjöblom, A., Kljun, N., Sahlée, E., Omar, A. M., & Rutgersson, A. (2017). Air-sea gas transfer in high Arctic fjords. *Geophysical Research Letters*, *44*, 2519–2526. https://doi.org/10.1002/2016GL072373

Bates, N. R., & Mathis, J. T. (2009). The Arctic Ocean marine carbon cycle: Evaluation of air-sea CO_2 exchanges, ocean acidification impacts and potential feedbacks. *Biogeosciences*, *6*(11), 2433–2459. https://doi.org/10.5194/bg-6-2433-2009

Chen, B., Cai, W.-J., & Chen, L. (2015). The marine carbonate system of the Arctic Ocean: Assessment of internal consistency and sampling considerations, summer 2010. *Marine Chemistry*, *176*, 174–188. https://doi.org/10.1016/j.marchem.2015.09.007

Chierici, M., Fransson, A., & Anderson, L. G. (1999). Influence of *m*-cresol purple indicator additions on the pH of seawater samples: Correction factors evaluated from a chemical speciation model. *Marine Chemistry*, *65*(3-4), 281–290. https://doi.org/10.1016/S0304-4203(99)00020-1

Chierici, M., Fransson, A., Lansard, B., Miller, L. A., Mucci, A., Shadwick, E., et al. (2011). The impact of biogeochemical processes and environmental factors on the calcium carbonate saturation state in the Circumpolar Flaw Lead in the Amundsen Gulf, Arctic Ocean. *Journal of Geophysical Research*, *116*, C00G09. https://doi.org/10.1029/2011JC007184

Chierici, M., Fransson, A., & Nojiri, Y. (2006). Biogeochemical processes as drivers of surface fCO_2 in contrasting provinces in the subarctic North Pacific Ocean. *Global Biogeochemical Cycles*, *20*, GB1009. https://doi.org/10.1029/2004GB002356

Clayton, T. D., & Byrne, R. H. (1993). Spectrophotometric seawater pH measurements: Total hydrogen ion concentration scale calibration of m-cresol purple and at-sea results. *Deep Sea Research, Part I*, *40*(10), 2115–2129. https://doi.org/10.1016/0967-0637(93)90048-8

Cottier, F. R., Tverberg, V., Inall, M. E., Svendsen, H., Nilsen, F., & Griffiths, C. (2005). Water mass modification in an Arctic fjord through crossshelf exchange: The seasonal hydrography of Kongsfjorden, Svalbard. *Journal of Geophysical Research*, *110*, C12005. https://doi.org/10.1029/2004JC002757

Dickson, A. G. (1990). Standard potential of the reaction: AgCl (s) + $1/2H_2$ (g) = Ag (s) + HCl (aq), and the standard acidity constant of the ion HSO_4^- in synthetic sea water from 273.15 to 318.15 K. *The Journal of Chemical Thermodynamics*, *22*, 113–127. https://doi.org/10.1016/0021-9614(90)90074-Z

Dickson, A. G., & Millero, F. J. (1987). A comparison of the equilibrium constants for the dissociation of carbonic acid in seawater media. *Deep Sea Research Part A*, *34*(10), 1733–1743. https://doi.org/10.1016/0198-0149(87)90021-5

Department of Energy (1994). In A. G. Dickson, & C. Goyet (Eds.), *Handbook of methods for the determination of the parameters of the oceanic carbon dioxide system (version 2)*. Oak Ridge, Tennessee: ORNL/CDIAC-74, CDIAC.

Else, B. G. T., Galley, R. J., Lansard, B., Barber, D. G., Brown, K., Miller, L. A., et al. (2013). Further observations of a decreasing atmospheric CO_2 uptake capacity in the Canada Basin (Arctic Ocean) due to sea ice loss. *Geophysical Research Letters*, *40*, 1132–1137. https://doi.org/10.1002/grl.50268

Else, B. G. T., Papakyriakou, T. N., Galley, R. J., Mucci, A., Gosselin, M., Miller, L. A., et al. (2012). Annual cycles of pCO_{2sw} in the southeastern Beaufort Sea: New understandings of air–sea CO_2 exchange in Arctic polynya regions. *Journal of Geophysical Research*, *117*, C00G13. https://doi.org/10.1029/2011JC007346

Evans, W., Mathis, J. T., Cross, J. N., Bates, N. R., Frey, K. E., Else, B. G. T., et al. (2015). Sea-air CO_2 exchange in the western Arctic coastal ocean. *Global Biogeochemical Cycles*, *29*, 1190–1209. https://doi.org/10.1002/2015GB005153

Fransson, A., Chierici, M., Hop, H., Findlay, H. S., Kristiansen, S., & Wold, A. (2016). Late winter-to-summer change in ocean acidification state in Kongsfjorden, with implications for calcifying organisms. *Polar Biology*, *39*(10), 1841–1857. https://doi.org/10.1007/s00300-016-1955-5

Fransson, A., Chierici, M., Miller, L. A., Carnat, G., Shadwick, E., Thomas, H., et al. (2013). Impact of sea-ice processes on the carbonate system and ocean acidification at the ice-water interface of the Amundsen Gulf, Arctic Ocean. *Journal of Geophysical Research: Oceans*, *118*, 7001–7023. https://doi.org/10.1002/2013JC009164

Fransson, A., Chierici, M., Nomura, D., Granskog, M. A., Kristiansen, S., Martma, T., & Nehrke, G. (2015). Effect of glacial drainage water on the CO_2 system and ocean acidification state in an Arctic tidewater-glacier fjord during two contrasting years. *Journal of Geophysical Research: Oceans*, *120*. https://doi.org/10.1002/2014JC010320, 2413–2429.

Fransson, A., Chierici, M., Skjelvan, I., Olsen, A., Assmy, P., Peterson, A. K., et al. (2017). Effects of sea-ice and biogeochemical processes and storms on under-ice water fCO_2 during the winter-spring transition in the high Arctic Ocean: Implications for sea-air CO_2 fluxes. *Journal of Geophysical Research: Oceans*, *122*, 5566–5587. https://doi.org/10.1002/2016JC012478

Isaksen, K., Nordli, Ø., Førland, E. J., Lupikasza, E., Eastwood, S., & Niedźwiedź, T. (2016). Recent warming on Spitsbergen—Influence of the atmospheric circulation and sea ice cover. *Journal of Geophysical Research: Atmospheres*, *121*, 11,913–11,931. https://doi.org/10.1002/2016JD025606

Jutterström, S., & Anderson, L. G. (2010). Uptake of CO_2 by the Arctic Ocean in a changing climate. *Marine Chemistry*, *122*(1-4), 96–104. https://doi.org/10.1016/j.marchem.2010.07.002

Land, P. E., Shutler, J. D., Cowling, R. D., Woolf, D. K., Walker, P., Findlay, H. S., et al. (2013). Climate change impacts on sea-air fluxes of CO_2 in three Arctic seas: A sensitivity study using Earth observation. *Biogeosciences*, *10*, 8109–8128. https://doi.org/10.5194/bg-10-8109-2013

Lauvset, S. K., Chierici, M., Counillon, F., Omar, A., Nondal, G., Johannessen, T., & Olsen, A. (2013). Annual and seasonal fCO_2 and air-sea CO_2 fluxes in the Barents Sea. *Journal of Marine Systems*, *113-114*, 62–74. https://doi.org/10.1016/j.jmarsys.2012.12.011

Lewis, E., & Wallace, D. W. R. (1998). *Program developed for CO_2 system calculations, ORNL/CDIAC-105*, CDIAC. Oak Ridge, Tennessee: Oak Ridge Natl. La.b.

Lueker, T. J., Dickson, A. G., & Keeling, C. D. (2000). Ocean pCO_2 calculated from dissolved inorganic carbon, alkalinity, and equations for K_1 and K_2: Validation based on laboratory measurements of CO_2 in gas and seawater at equilibrium. *Marine Chemistry*, *70*(1–3), 105–119. https://doi.org/10.1016/S0304-4203(00)00022-0

Lüger, H., Wallace, D. W. R., Körtzinger, A., & Nojiri, Y. (2004). The pCO_2 variability in the midlatitude North Atlantic Ocean during a full annual cycle. *Global Biogeochemical Cycles*, *18*, GB3023. https://doi.org/10.1029/2003GB002200

Mehrbach, C., Culberson, C. H., Hawley, J. E., & Pytkowicz, R. M. (1973). Measurement of the apparent dissociation constants of carbonic acid in seawater at atmospheric pressure. *Limnology and Oceanography*, *18*, 897–907. https://doi.org/10.4319/lo.1973.18.6.0897

Meire, L., Søgaard, D. H., Mortensen, J., Meysman, F. J. R., Soetaert, K., Arendt, K. E., et al. (2015). Glacial meltwater and primary production are drivers of strong CO_2 uptake in fjord and coastal waters adjacent to the Greenland Ice Sheet. *Biogeosciences*, *12*(8), 2347–2363. https://doi.org/10.5194/bg-12-2347-2015

Millero, F. J. (1979). The thermodynamics of the carbonate system in seawater. *Geochimica et Cosmochimica Acta*, *43*(10), 1651–1661. https://doi.org/10.1016/0016-7037(79)90184-4

Muckenhuber, S., Nilsen, F., Korosov, A., & Sandven, S. (2016). Sea ice cover in Isfjorden and Hornsund, Svalbard (2000-2014) from remote sensing data. *The Cryosphere*, *10*(1), 149–158. https://doi.org/10.5194/tc-10-149-2016

Nakaoka, S.-I., Aoki, S., Nakazawa, T., Hashida, G., Morimoto, S., Yamanouchi, T., & Yoshikawa-Inoue, H. (2006). Temporal and spatial variations of oceanic pCO_2 and air-sea CO_2 flux in the Greenland Sea and the Barents Sea. *Tellus Series B: Chemical and Physical Meteorology*, *58*(2), 148–161. https://doi.org/10.1111/j.1600-0889.2006.00178.x

Nightingale, P. D., Malin, G., Law, C. S., Watson, A. J., Liss, P. S., Liddicoat, M. I., et al. (2000). In situ evaluation of the air–sea gas exchange parameterizations using novel conservative and volatile tracers. *Global Biogeochemical Cycles*, *14*(1), 373–387. https://doi.org/10.1029/1999GB900091

Nilsen, F., Cottier, F., Skogseth, R., & Mattsson, S. (2008). Fjord-shelf exchanges controlled by ice and brine production: The interannual variation of Atlantic Water in Isfjorden, Svalbard. *Continental Shelf Research*, *28*(14), 1838–1853. https://doi.org/10.1016/j.csr.2008.04.015

Nilsen, F., Skogseth, R., Vaardal-Lunde, J., & Inall, M. (2016). A simple shelf circulation model: Intrusion of Atlantic Water on the West Spitsbergen Shelf. *Journal of Physical Oceanography*, *46*(4), 1209–1230. https://doi.org/10.1175/JPO-D-15-0058.1

Omar, A. M., Johannessen, T., Olsen, A., Kaltin, S., & Rey, F. (2007). Seasonal and interannual variability of the air-sea CO_2 flux in the Atlantic sector of the Barents Sea. *Marine Chemistry*, *104*(3-4), 203–213. https://doi.org/10.1016/j.marchem.2006.11.002

Onarheim, I. H., Smedsrud, L. H., Ingvaldsen, R. B., & Nilsen, F. (2014). Loss of sea ice during winter north of Svalbard. *Tellus Series A*, *66*(1), 23933. https://doi.org/10.3402/tellusa.v66.23933

Pavlov, A. K., Tverberg, V., Ivanov, B. V., Nilsen, F., Falk-Petersen, S., & Granskog, M. A. (2013). Warming of Atlantic water in two West Spitsbergen fjords over the last century (1912-2009). *Polar Research*, *32*, 11206. https://doi.org/10.3402/polar.v32i0.1

Pipko, I. I., Semiletov, I. P., Pugach, S. P., Wåhlström, I., & Anderson, L. G. (2011). Interannual variability of air-sea CO_2 fluxes and carbon system in the East Siberian Sea. *Biogeosciences*, *8*(7), 1987–2007. https://doi.org/10.5194/bg-8-1987-2011

Randelhoff, A., Fer, I., & Sundfjord, A. (2017). Turbulent upper-ocean mixing affected by meltwater layers during Arctic summer. *Journal of Physical Oceanography*, *47*(4), 835–853. https://doi.org/10.1175/JPO-D-16-0200.1

Redfield, A. C., Ketchum, B. H., & Richards, F. A. (1963). The influence of organisms on the composition of sea-water. In M. N. Hill (Ed.), *The sea: Ideas and observations on the progress in the study of the seas* (Vol. 2, pp. 26–77). New York: Interscience.

Rysgaard, S., Mortensen, J., Juul-Pedersen, T., Sørensen, L. L., Lennert, K., Søgaard, D. H., et al. (2012). High air–sea CO_2 uptake rates in nearshore and shelf areas of Southern Greenland: Temporal and spatial variability. *Marine Chemistry*, *128-129*, 26–33. https://doi.org/10.1016/j.marchem.2011.11.002

Sarmiento, J. L., & Gruber, N. (2006). *Ocean biogeochemical dynamics*. Princeton, NJ, USA: Princeton University Press.

Sejr, M. K., Krause-Jensen, D., Rysgaard, S., Sørensen, L. L., Christensen, P. B., & Glud, R. N. (2011). Air-sea flux of CO_2 in arctic coastal waters influenced by glacial melt water and sea ice. *Tellus Series B*, *63*(5), 815–822. https://doi.org/10.1111/j.1600-0889.2011.00540.x

Semiletov, I. P., Pipko, I. I., Repina, I., & Shakhova, N. E. (2007). Carbonate chemistry dynamics and carbon dioxide fluxes across the atmosphere-ice-water interfaces in the Arctic Ocean: Pacific sector of the Arctic. *Journal of Marine Systems*, *66*(1–4), 204–226. https://doi.org/10.1016/j.jmarsys.2006.05.012

Svendsen, H., Beszczynska-Møller, A., Hagen, J. O., Lefauconnier, B., Tverberg, V., Gerland, S., et al. (2002). The physical environment of Kongsfjorden-Krossfjorden, an Arctic fjord system in Svalbard. *Polar Research*, *21*(1), 133–166.

Sweeney, C., Gloor, E., Jacobson, A. R., Key, R. M., McKinley, G., Sarmiento, J. L., & Wanninkhof, R. (2007). Constraining global air-sea gas exchange for CO_2 with recent bomb ^{14}C measurements. *Global Biogeochemical Cycles*, *21*, GB2015. https://doi.org/10.1029/2006GB002784

Takahashi, T., Olafsson, J., Goddard, J. G., Chipman, D. W., & Sutherland, S. C. (1993). Seasonal variation of CO_2 and nutrients in the high latitude surface oceans: A comparative study. *Global Biogeochemical Cycles*, *7*(4), 843–878. https://doi.org/10.1029/93GB02263

Takahashi, T., Sutherland, S. C., Wanninkhof, R., Sweeney, C., Feely, R. A., Chipman, D. W., et al. (2009). Climatological mean and decadal change in surface ocean pCO_2, and net sea–air CO_2 flux over the global oceans. *Deep Sea Research Part II*, *56*(8–10), 554–577. https://doi.org/10.1016/j.dsr2.2008.12.009

Uppström, L. R. (1974). The boron/chlorinity ratio of deep-sea water from the Pacific Ocean. *Deep Sea Research and Oceanographic Abstracts*, *21*(2), 161–162. https://doi.org/10.1016/0011-7471(74)90074-6

van Heuven, S., Pierrot, D., Rae, J. W. B., Lewis, E., & Wallace, D. W. R. (2011). MATLAB program developed for CO_2 system calculations, rep. ORNL/CDIAC-105b, carbon dioxide Inf. Anal. Cent., Oak Ridge, Tenn. https://doi.org/10.3334/CDIAC/otg.CO2SYS_MATLAB_v1.1

Wanninkhof, R. (2014). Relationship between wind speed and gas exchange over the ocean revisited. *Limnology and Oceanography: Methods*, *12*(6), 351–362. https://doi.org/10.4319/lom.2014.12.351

Wanninkhof, R. H. (1992). Relationship between wind speed and gas exchange over the ocean. *Journal of Geophysical Research*, *97*(C5), 7373–7382. https://doi.org/10.1029/92JC00188

Wanninkhof, R. H., Asher, W. E., Ho, D. T., Sweeney, C., & McGillis, W. R. (2009). Advances in quantifying air-sea gas exchange and environmental forcing. *Annual Review of Marine Science*, *1*(1), 213–244. https://doi.org/10.1146/annurev.marine.010908.163742

Weiss, R. F. (1974). Carbon dioxide in water and seawater: The solubility of a non-ideal gas. *Marine Chemistry*, *2*(3), 203–215. https://doi.org/10.1016/0304-4203(74)90015-2

Woosley, R. J., Millero, F. J., & Takahashi, T. (2017). Internal consistency of the inorganic carbon system in the Arctic Ocean. *Limnology and Oceanography: Methods*, *15*(10), 887–896. https://doi.org/10.1002/lom3.10208

World Meteorological Organization (2014). *Guide to Meteorological Instruments and Methods of Observation (WMO-No 8)*. Geneva, Switzerland: World Meteorological Organization.

Wynn, P. M., Hodson, A. J., Heaton, T. H. E., & Chenery, S. R. (2007). Nitrate production beneath High Arctic glacier, Svalbard. *Chemical Geology*, *244*(1–2), 88–102. https://doi.org/10.1016/j.chemgeo.2007.06.008

Yasunaka, S., Murata, A., Watanabe, E., Chierici, M., Fransson, A., van Heuven, S., et al. (2016). Mapping of the air-sea CO_2 flux in the Arctic Ocean and its adjacent seas: Basin-wide distribution and seasonal to interannual variability. *Polar Science*, *10*(3), 323–334. https://doi.org/10.1016/j.polar.2016.03.006

Graphic design: Communication Division, UiB / Print: Skipnes Kommunikasjon AS

uib.no

ISBN: 978-82-308-3552-4